MAREES TERRESTRES

BULLETIN D'INFORMATIONS

INTERNATIONAL CENTER FOR EARTH TIDES
CENTRE INTERNATIONAL DES MAREES TERRESTRES

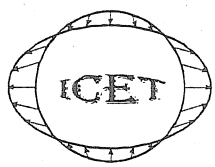

Federation of Astronomical and Geophysical Data Analysis Services
(FAGS)

International Association of Geodesy - International Gravity Field Service
(IAG – IGFS)

Publié avec le soutien de l'Observatoire Royal de Belgique

BIM
1 3 6

15 AOÛT 2002

Editeur: Dr. Bernard DUCARME
Observatoire Royal de Belgique
Avenue Circulaire 3
B-1180 Bruxelles

BIM 136

15 août 2002

Meeting of the ETC-Working Group 7 on Analysis of Environmental Data

Preliminary Results of the Free Core Nutation Eigenperiod Obtained by Stacking SG Observations at GGP Stations*

He-Ping Sun[1)*], Bernard Ducarme[2)], Jian-Qiao Xu[1)]

[1)] Institute of Geodesy and Geophysics, Chinese Academy of Sciences
54 Xu Dong road, 430077 Wuhan, China, email: *heping@asch.whigg.ac.cn*
[2)] Observatoire Royal de Belgique
Av. Circulaire 3, B-1180 Brussels, email: *b.ducarme@ksb-orb.oma.be*

Abstract

The tidal gravity results obtained from total 92 years at 19 Global Geodynamics Projects (GGP) stations (after loading correction with 6 different ocean models) are stacked in order to determine the free core nutation resonant parameters. The eigenperiod as of 429.9 sidereal days (sd) with error range (427.2, 432.7 sd) is obtained that agrees with the recent models as 429.5 sd (Dehant et al 1999) and 430.04 sd (Mathews et al, 2001).

1 Introduction

Since Jeffreys mentioned in 1957 the frequency dependents of the tidal amplitude factors in the diurnal wave band, many studies have been developed in theoretical and experimental aspects. Considering that the Earth occupies a rotating, slightly elliptical deformable core-mantle boundary, the dynamic influence of the liquid core leads to a rotation eigenmode associated with the wobble with respect to the mantle, it is the free core nutation (FCN). Based on the angular momentum equations, the FCN eigenperiod and quality factor can be theoretically computed by using a numerical integration technique (Wahr and Sasao, 1981, Mathews et al 2001). The researches show that the resonance of the liquid core will enhance wave amplitudes as P1, K1, ψ1 and φ1, therefore it is possible for us to retrieve the FCN resonant parameters from diurnal tidal gravity.

The determined eigenperiods in the previous studies are about 10% less than those in theoretical prediction (Wahr et al 1981). They are different (1) when using the data from various stations, (2) when using various global ocean tidal models and (3) when using different kind of observations. More than 19 stations around the world, equipped with superconducting gravimeters (SGs), are now taking part in the Global Geodynamics Projects (GGP). By using tidal gravity observations at GGP stations for the length of totally 92 years, the FCN parameters will be determined by using a stacking technique in this paper. The discrepancies of the resonance parameters from different stations when using various ocean models are investigated.

2 Tidal gravity observations at GGP network

The tidal gravity observations recorded from SGs are from stations Bandung (Indonisia), Brussels (Belgium), Boulder (American), Brasimone (Italy), Cantley (Canada), Canberra (Australia), Esashi (Japan), Kyoto (Japan), Matsushiro (Japan), Membach (Belgium), Metsahovi (Finland), Moxa (Germany), Potsdam (Germany), Strasbourg (France), Sutherland (South African), Syowa (South Pole), Vienna (Austria), Wettzell (Germany), Wuhan (China). The tidal gravity data

---

* Correspondence: He-Ping Sun, email: heping@asch.whigg.ac.cn
* Supported jointly by Nature Science Foundation of China (49925411 and 40074018) , Chinese Academy of Sciences (KZCS2-106) and the bilateral scientific and technical agreements between Belgium and China (project "SG observations and Geodynamics", BL/33/C17).

recorded from LCR-ET tidal gravimeter at station Pecny (Czech Republic) are also adopted since their quality. The 3 series at Moxa (1st series is from lower sphere, 2nd series is from upper sphere, and 3rd series is from stacking data of lower and upper spheres), 2 series at Strasbourg (old and new series), 3 series at Sutherland (same as the sation Moxa) and 4 series at Wetzell (one series from old period and other 3 series are same as Moxa) are included (Ducarme et al, 2002).

By using a remove restore technique, the minute tidal gravity samplings are pre-processed using a Tsoft technique (Vauterin, 1998) in the International Centre for Earth Tides (ICET). The hourly samplings are obtained after applying for a filtering technique, the tidal parameters and their RMS are determined by using Eterna 3.4 (Wenzel 1996). The atmospheric pressure signals are removed by using the regression coefficients between gravity residuals and station pressure.

The ocean tidal signals should be carefully removed before explanation of the results in geodynamics (Sato et al, 1994, Sun et al, 2002). Previous studies show that the correlation between the predicted load vectors and the observed ones is up to 90% (Melchior and Francis 1996, Sun, 2002). Based on 6 ocean models (Scw80, Csr3.0, Fes95.2, Tpxo2, Csr4.0 and Ori96), the load vectors are computed using a standard procedure (Agnew, 1997). The loading vectors for small waves $\psi 1$ and $\varphi 1$ are obtained by using an interpolation technique in which we considered the ocean resonance phenomena (Wahr and Sasao, 1981).

The main wave tidal gravity parameters with frequency at core resonance (P1, K1, $\psi 1$ and $\varphi 1$) before (δ, $\Delta\varphi$) and after (δ', $\Delta\varphi'$) loading correction (Csr4.0) are given in table 1. The discrepancy of these corrected amplitude factors with respect to theoretical values (Dehant et al., 1999) and experimental models (Sun et al, 2002) is investigated. The numerical results show the corrected results are much approach to the theoretical values, this signifies the effectiveness of the loading correction for both principle and weak tidal components (Sun et al 2002).

3 Numerical results and discussions

A similar treatment in determining the FCN parameters same as the one in previous studies as Defraigne et al. (1994) and Xu et al. (2001) is used. The fitting equations are deduced by modelling the observed complex diurnal tidal gravity parameter to theoretical ones with consideration of removing the signals of wave O1. After oceanic loading correction, the eigenperiod T_{FCN} ranges to be from 415 to 440 sd, except for the stations Sutherland (468.3 sd) and Syowa (464.5 sd). It shows that the high inner data quality is important in the determination of the FCN eigenperiod. The large discrepancy for stations Sutherland and Syowa relates to the un-accuracy of the ocean tidal models. By stacking the tidal observations separately from various regions, we obtained T_{FCN} as 427.5 sd with error range (418.6, 436.8 sd) for 4 stations in Asia, 427.1 sd with error range (410.8, 444.8 sd) for 9 stations in Europe, 426.4 sd with error range (420.6, 432.3 sd,) for 2 stations in Northern American and 440.9 sd with error range (423.5, 459.7 sd) for 4 stations in Southern hemisphere.

Stacking tidal gravity observations obtained from 20 GGP stations, the T_{FCN} as of 429.9 sd with error range (427.2, 432.7 sd) is obtained. It corresponds well to those in previous researches as 433.6 sd with error range (433.1, 434.1 sd, Defraigne et al 1994) and 429.0 sd with error range (424.3, 433.7 sd, Xu et al, 2001). They correspond also to those deduced from the VLBI as 429.5 sd (Dehant et al 1999) and 430.04 sd when considering the electro-magnetic force coupling at mantle-core boundary (Mathews et al, 2002). As the theoretical prediction of the T_{FCN} is as of 455.8 to 467.4 sd (Wahr, 1981, Mathews et al, 1991), the convinced explanation to the T_{FCN} discrepancy of 30 sd, is the dynamic ellipticity of the fluid core may be about 4.8% larger than the hydrostatic one.

The quality factor relates to the damping properties of the Earth, such as the viscosity of the mantle, the tidal friction in the ocean bottom, the electro-magnetic and viscous coupling between the core and mantle. It mainly depends on the phase differences in tidal gravity observations, it is found that the quality factors differ from one station to another, and from one ocean model to another, the discrepancy is quite large. However, the discrepancy of the T_{FCN} when using various ocean models is about 2.0% for most stations. The eigenperiod to inverse quality factors is given in figures 1. It is found that the results when stacking tidal gravity observations corrected with loading vectors averaged with 6 ocean models are situated at the figure center. It proves that the stacking technique can be used to reduce effectively the local influence of the ocean tides, atmospheric pressure, underground water level change, and other station environmental perturbations.

4 Preliminary conclusions

Based on the numerical results and discussions, we conclude: the high quality observations are important in the determination of the FCN parameters. The ocean tides are one of the main perturbations, the discrepancy of the T_{FCN} when using various ocean models is about 2.0%. The determined T_{FCN} is as 429.9 sd with error ±0.65% when stacking the tidal gravity observations from 19 GGP stations, it is in good agreement with those determined from recent theoretical studies.

Acknowledgements

The authors are grateful to D. Crossley, GGP Chairman, and all instrumental managers at stations, Bandung, Brussels, Boulder, Brasimone, Cantley, Canberra, Esashi, Kyoto, Matsushiro, Membach, Metsahovi, Moxa, Potsdam, Strasbourg, Sutherland, Syowa, Vienna, Wettzell, Wuhan and Pecny. The authors wishes to express their thanks to M. Hendrickx and L. Vandercoilden from Royal Observatory of Belgium, who maintaining the GGP data sets.

References

[1] Agnew DC, A program for computing ocean-tide loading, J. Geophysical Research, 1997, 102(B3): 5109-5110.

[2] Defraigne P, Dehant V, Hinderer J. Staking gravity tide measurements and nutation observations in order to determine the complex eigenfrequency of nearly diurnal free wobble. J. Geophys. Res., 1994, 99 (B5): 9203–9213.

[3] Dehant, V., Defraigne, P. and Wahr, J. (1999): Tides for a convective Earth, J. Geophys. Res., 104, B1, 1035–1058.

[4] Ducarme B, Sun H.P and Xu JQ, New investigation of tidal gravity results from the GGP Network, 2002,

[5] Mathews P.M. (2001): Love numbers and gravimetric factor for diurnal tides. Journal of the Deodetic Society of Japan, 2001, 47(1), 231–236.

[6] Melchior P and Francis O. Comparison of recent ocean tide models using ground-based tidal gravity measurements. Marine Geodesy, 1996, 19: 291–330

[7] Sato T, Tamura Y, Higashi T, Takemoto S, Nakagawa I, Morimoto N, Fukuda Y,Segawa J and Seama J, 1994. Resonance parameters of the free core nutation measured from three superconducting gravimeters in Japan, J. Geomag. Geoelectr., 46, 571–586.

[8] Sun He-Ping, Hou-Tze Hsu, Gerhard Jentzsch, Jian-Qiao Xu, Tidal gravity observations obtained with a superconducting gravimeter at Wuhan/China and its application to geodynamics, Journal of Geodynamics, 2002, 33(1-2): 187–198.

[9] Sun He-Ping, Xu Jian-Qiao and Ducarme Bernard. Experimental earth tidal models of the core resonance obtained by stacking tidal gravity observations from the GGP Stations, GGP work shop, Jena, March 11–15, 2002.

[10] Wahr J M, Sasao T. A diurnal resonance in the ocean tide and in the Earth's load response duo to the resonant free 'core nutation'. Geophys. J. R. astr. Soc.. 1981, 64: 747–765.

[11] Wenzel, H.G.(1996): The nanogal software: data processing package ETERNA 3.3, Bull. Inf. Marées Terrestres, 124, 9425–9439.

[12] Xu Jian-Qiao, Sun He-Ping and Luo Shao-Cong. Investigation of the Earth's free core nutation by using global tidal gravity observations with superconducting gravimeters. Science in China, 2001, 31(9): 719–726 (in Chinese).

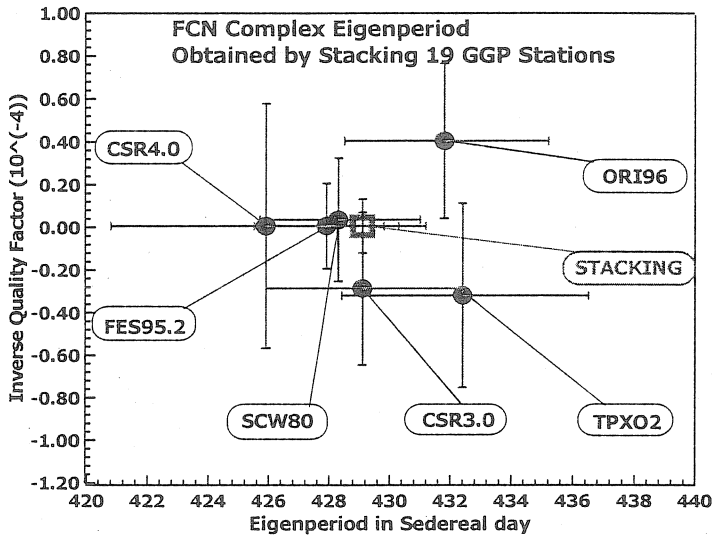

Figure 1 Comparison of the resonant parameters when using various ocean models

Table 1 Main tidal wave amplitude factors before and after ocean loading correction (Csr4.0)

	P1 wave				K1 wave				ψ1 wave				φ1 wave			
	observed		corrected		observed		corrected		observed		corrected		observed		corrected	
station	δ	Δφ(°)	δ′	Δφ′(°)	δ	Δφ(°)	δ′	Δφ′(°)	δ	Δφ(°)	δ′	Δφ′(°)	δ	Δφ(°)	δ′	Δφ′(°)
Bandung	1.1685	9.87	1.1377	-0.45	1.1641	11.02	1.1215	0.34	1.6061	-1.73	1.6041	-7.34	1.2145	6.19	1.1903	-3.10
Brussels	1.1524	0.15	1.1541	-0.20	1.1401	0.25	1.1406	-0.05	1.2365	-0.47	1.2372	-0.69	1.1746	0.05	1.1752	-0.23
Boulder	1.1659	1.27	1.1501	0.09	1.1540	1.30	1.1369	0.06	1.2675	2.08	1.2547	1.30	1.1798	2.61	1.1632	1.59
Brasimone	1.1453	0.20	1.1466	-0.16	1.1329	0.22	1.1333	-0.11	1.3132	3.60	1.3134	3.37	1.1708	-0.32	1.1715	-0.65
Cantley	1.1608	0.48	1.1545	-0.03	1.1480	0.57	1.1405	0.03	1.2815	-0.46	1.2767	-0.80	1.1810	0.75	1.1749	0.31
Canberra	1.1528	-0.82	1.1561	0.03	1.1367	-0.84	1.1400	0.08	1.2460	0.77	1.2503	1.37	1.1661	-0.99	1.1721	-0.17
Esashi	1.2131	0.31	1.1515	-0.16	1.2007	0.31	1.1406	-0.11	1.3163	-1.10	1.2719	-1.40	1.2395	0.64	1.1839	0.37
Kyoto	1.2002	-0.08	1.1477	0.09	1.1870	-0.20	1.1360	0.01	1.4702	5.70	1.4328	5.99	1.1651	0.61	1.1177	0.89
Matsushiro	1.1947	-0.06	1.1450	-0.10	1.1838	-0.08	1.1354	-0.10	1.2587	0.18	1.2226	0.20	1.2065	-0.48	1.1612	-0.46
Membach	1.1496	0.24	1.1507	-0.08	1.1373	0.28	1.1374	0.01	1.2821	1.00	1.2823	0.81	1.1626	0.63	1.1628	0.37
Metsahovi	1.1548	0.05	1.1592	0.09	1.1407	0.07	1.1443	0.25	1.2553	1.00	1.2580	1.11	1.1764	-0.51	1.1795	-0.33
Moxa	1.1491	0.21	1.1503	-0.04	1.1363	0.24	1.1366	0.05	1.2646	0.09	1.2650	-0.06	1.1699	0.16	1.1704	-0.03
Pecny	1.1512	0.18	1.1525	-0.04	1.1364	0.15	1.1370	-0.02	1.2629	3.66	1.2634	3.53	1.1670	0.88	1.1678	0.71
Potsdam	1.1504	0.16	1.1515	-0.06	1.1374	0.26	1.1377	0.11	1.2582	0.69	1.2586	0.57	1.1777	-0.14	1.1783	-0.29
Strasbourg	1.1497	0.18	1.1506	-0.13	1.1370	0.23	1.1368	-0.02	1.2679	-0.56	1.2680	-0.74	1.1675	0.78	1.1674	0.53
Sutherland	1.1510	-0.54	1.1498	-0.11	1.1355	-0.51	1.1363	-0.12	1.2198	-0.80	1.2205	-0.49	1.1729	-1.00	1.1742	-0.58
Syowa	1.2144	0.16	1.1546	-0.37	1.1992	0.19	1.1457	-0.41	1.2798	1.39	1.2435	1.11	1.2021	0.13	1.1606	-0.24
Vienna	1.1472	0.15	1.1490	-0.08	1.1339	0.19	1.1351	0.01	1.2781	0.71	1.2792	0.58	1.1692	0.16	1.1706	-0.02
Wettzell	1.1492	0.28	1.1505	0.03	1.1353	0.34	1.1358	0.15	1.2659	-0.79	1.2665	-0.94	1.1671	0.32	1.1678	0.12
Wuhan	1.1663	-0.43	1.1519	-0.01	1.1531	-0.47	1.1403	-0.03	1.2711	-1.43	1.2612	-1.16	1.1912	0.17	1.1792	0.54

Experimental Earth Tidal Models of the Core Resonance Obtained by Stacking Tidal Gravity Observations from GGP Stations

He-Ping Sun*, Jian-Qiao Xu*, Bernard Ducarme**

*Institute of Geodesy and Geophysics, Chinese Academy of Sciences
54 Xu Dong road, 430077 Wuhan, China, email: heping@asch.whigg.ac.cn
**Observatoire Royal de Belgique, Av. Circulaire 3, B-1180 Brussels,
email: b.ducarme@ksb-orb.oma.be

Abstract

By stacking tidal gravity observations obtained by superconducting gravimeters in 20 GGP stations, the resonant parameters of the free core nutation are determined and 3 experimental tidal gravity models in diurnal band are constructed. It is found that our experimental models are in good agreement with those obtained in previous studies (Dehant et al 1999) and (Mathews et al, 2002).

1 Introduction

In recent years, many studies are developed in theoretical modelling and practical detection on the free core nutation (FCN) phenomena of the Earth. Based on the angular momentum equations, the eigenperiod can be theoretically computed by using analytical or numerical integration techniques, it is in the range from 455.8 to 467.4 sidereal days (sd) depending on Earth's model adopted (Wahr, 1981, Wahr and Bergen, 1986, Mathews et al 1991). The researches show that ground based observations as gravity, tilt, strain, water tube and VLBI, can be influenced by the FCN. In the diurnal tidal observations, the amplitudes of the P1, K1, ψ1 and φ1 wave, are enhanced due to the core resonance. By using ground based high precision tidal gravity observations recorded with superconducting gravimeters (SGs) at the GGP network, the tidal parameters will be determined with considering pressure and ocean loading corrections. Then the resonant parameters of the Earth will be determined. The experimental tidal gravity models will be constructed when rejecting some bad tidal parameters due to the high noise level in this paper.

2 Data preparation

In our researches, 28 series of the tidal gravity observations recorded from SGs at 20 stations in total 92.086 years are used. The minute samplings are pre-processed using a Tsoft technique (Vauterin, 1998) at the International Centre for Earth Tides (ICET). The hourly sampling are obtained by using a remove restore technique and then processed by using Eterna technique. The details of the data length, atmospheric pressure admittances and the standard deviations can be found in Sun (Sun et al, 2002). As the selected data length for all stations is longer than one year, it is possible to separate accurately 13 wave groups in the diurnal wave band including some small waves as ψ_1 and φ_1 in which their frequency are close to the resonant one of the Earth's liquid core. In order to check against the values predicted by recent models of the response of the Earth to the

---

*Correspondence: He-Ping Sun, email: heping@asch.whigg.ac.cn
*Supported jointly by Nature Science Foundation of China (49925411 and 40174022), Chinese Academy of Sciences (KZCS2-106) and the bilateral scientific and technical agreements between Belgium and China (project "SG observations and Geodynamics", BL/33/C17).

tidal forces, it is necessary for us to remove for the first step the influence of the atmospheric pressure and oceanic tides.

The influence of the atmospheric pressure is corrected by using the regression coefficients between gravity residual and change in station pressure. The global ocean models used in this study include the old Scw80, and the most recent ones developed by the analysis of the precise measurements from the Topex/Poseidon altimeters, and those result from parallel developments in numerical tidal modelling and data assimilation, such as the Csr3.0 (Eanes), Fes95.2 (Grenoble), TPXO2 (Egbert), CSR4.0 and Ori96 (Matsumoto) models.

Based on the global ocean models and model Earth Green's functions (Farrell 1972), the loading vectors are computed using a standard procedure (Agnew 1997, Sun 1992). Since the tidal load vectors are directly proportional to the wave amplitude in the exciting tidal potential and the phase change exhibits a regular behaviour with respect to the frequency shift, it is easy to interpolate the load vectors for weak components as ψ1 and φ1. However, during the interpolation process, it is necessary for us to take into account the influence of the core resonance phenomena on oceanic tides (Wahr and Sasao, 1981, Matheow 2001). The loading vectors for 9 additional small components as σ1, ρ1, NO1, π1, ψ1, φ1, θ1, J1 and OO1 in diurnal wave band are obtained. The efficiency of the loading correction for both principal and small tidal components is confirmed (Sun et al, 2002).

3 Calculation techniques

The complex amplitude factor of a diurnal tidal wave with frequency σ can be theoretically computed as (Defraigne et al 1994)

$$\delta_{th}(\sigma) = \delta_0 + \bar{A}/(\sigma - \bar{\sigma}_{FCN}), \tag{1}$$

with

$$\delta_0 = 1 + h_0 - \tfrac{3}{2}k_0, \qquad \bar{A} = -(A/A_m)(h_1 - \tfrac{3}{2}k_1)(\alpha - q_0 h^c/2)\Omega, \tag{2}$$

where δ_0 is the amplitude factor combined from the classical Love numbers h_0 and k_0, the $\bar{\sigma}_{FCN}$ is the eigenfrequency of the FCN, $\bar{A}$ is the resonance strength related to the geometric shape of the Earth and the rheology properties of the Earth's mantle. h_1 and k_1 are the internal pressure Love numbers, h^c is the secular Love number. A and A_m are the equatorial moments of inertia of the entire Earth and the solid mantle, α is the dynamic ellipticity of the Earth, q_0 ratio of the centrifugal force to gravity on the equator and Ω is the sidereal frequency of the Earth's rotation. For an inelastic Earth model, $\bar{A}$ and $\bar{\sigma}_{FCN}$ should be described as a complex

$$\bar{A} = A_r + iA_i, \qquad \bar{\sigma}_{FCN} = \sigma_r + i\sigma_i. \tag{3}$$

The eigenperiod of the FCN is then $T_{FCN} = \Omega/(\sigma_r + \Omega)$ and the quality factor is $Q = \sigma_r/(2\sigma_i)$. Considering the frequency of the wave O_1 is far away from the one of the FCN, it can be referred as a reference. The similar treatment in determination of the FCN parameters as in the previous studies is used (Neuberg et al,1987, Defraigne et al, 1994 and Xu et al, 1999). The data from various stations are stacked in order to reduce the systematic discrepancy and local environmental disturbance. When removing the signals of wave O_1, the fitting equations can be deduced by modelling the observed parameters to theoretical ones in expression (1)

$$\delta(\sigma, j) - \delta(O_1, j) = \frac{A_r + iA_i}{\sigma - (\sigma_r + i\sigma_i)} - \frac{A_r + iA_i}{\sigma(O_1) - (\sigma_r + i\sigma_i)} \tag{4}$$

where j stands for the station series number. To solve the above equation, Marquadt's algorithm of linearized iteration and modification is used (Xu et al, 2001).

4 Numerical results and discussions

The tidal gravity parameters are corrected by using loading vectors averaged from 6 different global ocean models for waves O1, P1, K1, ψ1 and φ1. In order to check globally the core resonance phenomena, by stacking all tidal gravity observations from the GGP network, the eigenperiods of the core resonance T_{FCN} are obtained for three different cases, they are (1) 429.9 sd with error range (427.2, 432.7 sd) when staking tidal gravity observations obtained at 19 GGP stations with rejecting the stations BA and CB since the high noise level (the abridge of the station name can be found in Sun (Sun et al 2002); (2) 429.1 sd with error range (428.0, 430.3) when staking tidal gravity observations obtained at 22 series from 20 GGP stations (two series from stations ST and WE, with rejecting some special bad waves as K1 (SY), O1 (SY, WE), P1 (SY), ψ1 (BA, BR, KY, MA, PC, SU), φ1 (BA, BO, KY); and (3) 429.7 sd with error range (426.8, 432.6) when using the procedure same as (2) with taking into account the signal to noise ratio by normalizing the standard deviations of the waves using the theoretical amplitudes of the corresponding waves.

It is found our results to be in good agreement with those deduced from the VLBI as 429.5 sd (Dehant et al 1999) and 430.04 sd (Mathews et al, 2002), the discrepancy is about 0.4%. They correspond also to those in previous experimental researches (Herring et al 1986, Neuberg 1987, Defraigne et al 1994 and Xu et al 2001). However, they are much less than the one in theoretical calculation as of about 460 sd (Wahr and Sasao, 1981). The unique convinced explanation to the T_{FCN} discrepancy of 30 sd is the dynamic ellipticity of the fluid core may to be about 4.8% larger than the hydrostatic one (Sun et al 2002).

Based on above three cases, three experimental Earth tidal models of the core resonance (SXD1, SXD2 and SXD3) are constructed based on formula (1). It is found that the largest discrepancy among the models of SXD1, SXD2 and SXD3 is less than 0.1% (table 1 and figure 1). The comparison of our results with those given by Mathews is also made (figure 2). It is found that the discrepancy is about 0.56% between MATH and SXD1, 0.25% between MATH and SXD2 and 0.33% between MATH and SXD3. The DDW tidal gravity models are also listed in table 1 in order to compare easily. The results in table1 and figures 1 and 2 demonstrate our 3 experimental models are in same level, they are close to the theoretical ones. It seems that the best fitting model is the one of SXD2 since the effectiveness of rejecting some bad waves, and comparing to the Mathew's model, the discrepancy is lowest one.

6 Conclusions

Based on the numerical results, we conclude the high quality observations are important in the determination of the FCN parameters, Our experimental models are in good agreement with those obtained in theoretical computations (Dehant et al 1999) and (Mathews et al, 2002).

Acknowledgements

The authors are grateful to D. Crossley, GGP Chairman, and all instrumental managers at stations, Bandung/Indonisia, Brussels/Belgium, Boulder/USA, Brasimone/Italy, Cantley/Canada, Canberra/Australia, Esashi/Japan, Kyoto/Japan, Matsushiro/Japan, Membach/Belgium, Metsahovi/Finland, Moxa/Germany,

Potsdam/Germany, Strasbourg/France, Sutherland/South African, Syowa/South Pole, Vienna/Austria, Wettzell/ Germany, Wuhan/China and Pecny/Czech Republic. The authors wishes to express their thanks to M. Hendrickx and L. Vandercoilden from Royal Observatory of Belgium, who maintaining the GGP data sets at ICET and checking carefully all the income data.

References

[1] Defraigne P, Dehant V, Hinderer J. Staking gravity tide measurements and nutation observations in order to determine the complex eigenfrequency of nearly diurnal free wobble. J. Geophys. Res., 1994, 99 (B5): 9203–9213

[2] Dehant, V, Defraigne P. and Wahr J. Tides for a convective Earth, J. Geophys. Res., 1999, 104, B1, 1035–1058.

[3] Ducarme Bernard, Sun He-Ping and Xu Jian-Qiao. New investigation of tidal gravity results from the GGP Network, GGP work shop, Jena, March 11–15, 2002.

[4] Herring T A, Gwinn C R, Shapiro II. Geodesy by Radio Interferometry: Studies of the Forced Nutations of the earth 1. Data Analysis. J. Geophys. Res.. 1986, 91(B5): 4745–4754

[5] IERS Standards, IERS technical note, Observatoire de Paries, 1992(13): 1–20

[6] Mathews, P.M. (2001): Love numbers and gravimetric factor for diurnal tides. Journal of the Geodetic Society of Japan, 2001, 47(1), 231–236.

[7] Sato T. Fluid core resonances measured by quartz tube extensometers at the Esashi Earth tide station. In: Kakkuri J. ed. Pro. 11th Int. Sympos. On Earth Tides, Stuttgart, 1991: 573–582

[8] Sun He-Ping. Comprehensive researches for the effect of the ocean loading on gravity observations in the Western Pacific Area, Bulletin d'informations de Marées Terrestres, 1992, 113: 8271–8292.

[9] Sun He-Ping, Ducarme Bernard and Xu Jian-Qiao, Determination of the Free Core Nutation Parameters by Stacking Tidal Gravity Measurements from GGP Stations, GGP work shop, Jena, March 11–15, 2002.

[10] Sun He-Ping, Xu Hou-Ze, Jentzsch G, Xu Jian-Qiao, Tidal gravity observations obtained with a superconducting gravimeter at Wuhan/China and its application to geodynamics, Journal of Geodynamics, 2002, 33(1-2): 187–198

[11] Wahr J M, Sasao T. A diurnal resonance in the ocean tide and in the Earth's load response duo to the resonant free 'core nutation'. Geophys. J. R. astr. Soc.. 1981, 64: 747–765

[12] Wenzel, H.G. The nanogal software: data processing package ETERNA 3.3, Bull. Inf. Marées Terrestres, 1996, 124, 9425–9439.

[13] Xu Jian-Qiao, Sun He-Ping and Luo Shao-Cong. Investigation of the Earth's free core nutation by using global tidal gravity observations with superconducting gravimeters. Science in China, 2001, 31(9): 719–726 (in Chinese).

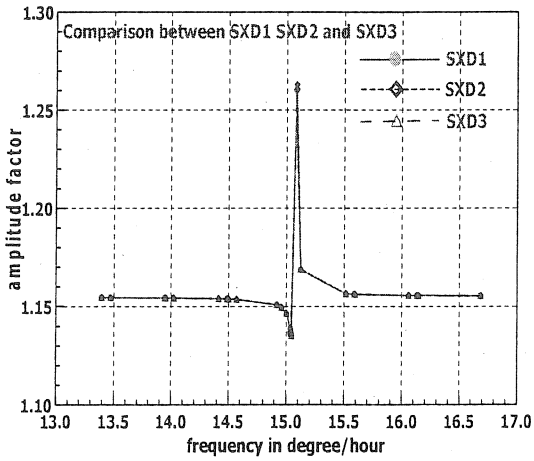

Figure 1 Comparison among the SXD models

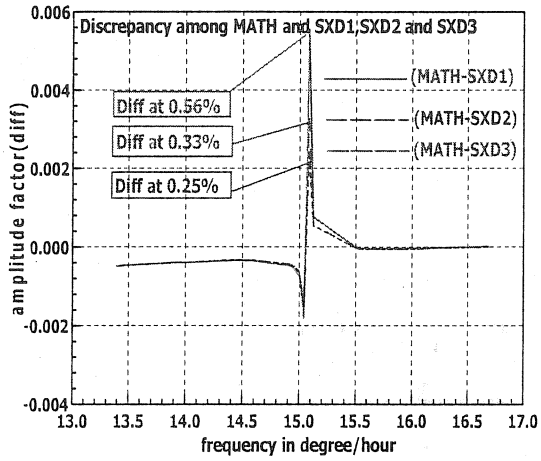

Figure 2 Comparison of SXD models with the Mathew's one

Table 1 Comparison of the tidal gravity models in the diurnal wave band

Wave argument		Frequency	name	DDW1	DDW2	MATH	SXD1	SXD2	SXD3
1-4 0 3 0 0	115.855	12.30991148	308	1.15254	1.15400		1.15473	1.15474	1.15474
1-4 2 1 0 0	117.655	12.38276513	SGQ1	1.15256	1.15402	1.15403	1.15473	1.15473	1.15473
1-3 0 1 0 0	125.655	12.84964437	noname	1.15269	1.15415		1.15468	1.15468	1.15468
1-3 0 2-1 0	125.745	12.85207978	2Q1x	1.15269	1.15415		1.15468	1.15468	1.15468
1-3 0 2 0 0	125.755	12.85428619	2Q1	1.15269	1.15415	1.15409	1.15468	1.15468	1.15468
1-3 2 0-1 0	127.545	12.92493343	SG1x	1.15271	1.15417		1.15467	1.15467	1.15467
1-3 2 0 0 0	127.555	12.92713984	SIG1	1.15271	1.15417	1.15410	1.15467	1.15467	1.15467
1-2 0 0-1 0	135.545	13.39181267	noname	1.15279	1.15425		1.15459	1.15459	1.15459
1-2 0 0 0 0	135.555	13.39401908	noname	1.15279	1.15425		1.15458	1.15459	1.15459
1-2 0 1-1 0	135.645	13.39645449	Q1x	1.15279	1.15425	1.15410	1.15458	1.15459	1.15459
1-2 0 1 0 0	135.655	13.39866089	Q1	1.15280	1.15425	1.15410	1.15458	1.15459	1.15459
1-2 2-1 0 0	137.455	13.47151455	RHO1	1.15280	1.15426	1.15410	1.15457	1.15457	1.15457
1-1 0 0-1 0	145.545	13.94082919	O1x	1.15279	1.15424	1.15401	1.15440	1.15440	1.15440
1-1 0 0 0 0	145.555	13.94303560	O1	1.15279	1.15424	1.15401	1.15440	1.15440	1.15440
1-1 0 1 0 0	135.655	13.94767741	noname	1.15279	1.15424		1.15440	1.15440	1.15440
1-1 0 2 0 0	145.755	13.95231923	2NO1	1.15279	1.15424		1.15440	1.15440	1.15440
1-1 2 0 0 0	147.555	14.02517288	TAU1	1.15278	1.15422	1.15397	1.15436	1.15436	1.15436
1 0-2 1 0 0	153.655	14.41455665	NTAU	1.15252	1.15396	1.15366	1.15400	1.15399	1.15399
1 0 0-1-1 0	155.445	14.48520390	LK1x	1.15242	1.15386		1.15388	1.15387	1.15387
1 0 0-1 0 0	155.455	14.48741031	LK1	1.15242	1.15385	1.15354	1.15388	1.15387	1.15387
1 0 0 0-1 0	155.545	14.48984571	noname	1.15242	1.15385		1.15387	1.15386	1.15386
1 0 0 0 0 0	155.555	14.49205212	noname	1.15241	1.15385		1.15387	1.15386	1.15386
1 0 0 0 1 0	155.565	14.49425853	noname	1.15241	1.15384		1.15386	1.15386	1.15386
1 0 0 1 0 0	155.655	14.49669393	NO1	1.15240	1.15384	1.15351	1.15386	1.15385	1.15385
1 0 0 1 1 0	155.665	14.49890034	NO1x	1.15240	1.15383	1.15351	1.15386	1.15385	1.15385
1 0 2-1 0 0	157.455	14.56954759	CHI1	1.15226	1.15369	1.15336	1.15370	1.15369	1.15369
1 1-3 0 0 1	162.556	14.91786468	PI1	1.14933	1.15072	1.15043	1.15091	1.15087	1.15087
1 1-2 0-1 0	163.545	14.95672495	P1x	1.14788	1.14927	1.14903	1.14959	1.14953	1.14953
1 1-2 0 0 0	163.555	14.95893136	P1	1.14777	1.14916	1.14892	1.14949	1.14943	1.14942
1 1-1 0 0 1	164.556	15.00000196	S1	1.14446	1.14589	1.14578	1.14654	1.14643	1.14643
1 1 0-1 0 0	165.455	15.03642683	noname	1.13543	1.13728		1.13879	1.13860	1.13858
1 1 0 0-1 0	165.545	15.03886223	K1x-	1.13416	1.13610	1.13610	1.13773	1.13753	1.13751
1 1 0 0 0 0	165.555	15.04106864	K1	1.13284	1.13489	1.13494	1.13664	1.13643	1.13641
1 1 0 0 1 0	165.565	15.04327505	K1x+	1.13133	1.13352	1.13361	1.13541	1.13518	1.13516
1 1 1 0 0-1	166.554	15.08213532	PSI1	1.23736	1.26978	1.26548	1.25993	1.26302	1.26217
1 1 2 0 0 0	167.555	15.12320592	PHI1	1.16776	1.17029	1.16932	1.16856	1.16878	1.16876
1 2-2 1 0 0	173.655	15.51258969	TET1	1.15551	1.15703	1.15641	1.15643	1.15646	1.15646
1 2 0-1 0 0	175.455	15.58544335	J1	1.15531	1.15682	1.15619	1.15622	1.15625	1.15625
1 2 0-1 1 0	175.465	15.58764975	J1x	1.15530	1.15682	1.15618	1.15622	1.15624	1.15624
1 2 0 0 0 0	175.555	15.59008516	noname	1.15530	1.15681		1.15621	1.15624	1.15624
1 2 0 0 1 0	175.565	15.59229157	noname	1.15529	1.15681		1.15621	1.15623	1.15623
1 3-2 0 0 0	183.555	16.05696440	SO1	1.15482	1.15631	1.15559	1.15562	1.15564	1.15564
1 3 0-2 0 0	185.355	16.12981805	2J1	1.15479	1.15628		1.15557	1.15559	1.15559
1 3 0-1 0 0	185.455	16.13445987	noname	1.15479	1.15628		1.15557	1.15559	1.15559
1 3 0 0 0 0	185.555	16.13910168	OO1	1.15479	1.15628	1.15555	1.15557	1.15559	1.15559
1 3 0 0 1 0	185.565	16.14130809	OO1x	1.15479	1.15628	1.15555	1.15557	1.15558	1.15558
1 4 0-1 0 0	195.455	16.68347639	NU1	1.15474	1.15623	1.15538	1.15536	1.15538	1.15538
1 4 0-1 1 0	195.465	16.68568279	NU1x	1.15474	1.15623		1.15536	1.15538	1.15538

Note: DDW1: tidal model in hydro static Earth hypotheses given by Dehant-Defraign-Wahr (1999);
DDW2: tidal static in non-hydro static Earth hypotheses given by Dehant-Defraign-Wahr (1999);
MATH: tidal model obtained by Mathews (2001);
SXD1: experimental tidal models given by Sun-Xu-Ducarme in this paper (2002);
SXD2: experimental tidal models given by Sun-Xu-Ducarme in this paper (2002);
SXD3: experimental tidal models given by Sun-Xu-Ducarme in this paper (2002);

GGP Ground Truth for Satellite Gravity Missions

by

David Crossley[1] and Jacques Hinderer[2]

[1]Earth and Atmospheric Sciences, Saint Louis University,
[2]Institut de Physique du Globe / EOST Strasbourg, France
crossley@eas.slu.edu

Abstract

The launch of the satellite GRACE heralds a new era of high precision, time-varying, satellite measurements of the Earth's gravity field. An important aspect of the mission is to consider how the predicted high-accuracy gravity data might be validated. Two kinds of validation have been proposed; the first is internal, whereby the data are modeled for self – consistency to verify the internal accuracy of the spherical harmonic coefficients. The second is external validation using data from independent measurements, for example ocean bottom pressure gauges or continental land surface gravity measurements. Here we consider the latter possibility using the European sub-array of the Global Geodynamics Project (GGP) as 'ground truth' for comparison with GRACE. As a pilot study, we use 190 days of 1-hour data from the beginning of GGP (1 July 1997), at 8 European stations. We remove local tides, polar motion and local air pressure and filter the data to 6-hour samples and find that there are large variations between some stations, but also some stations show high correlations over periods of several weeks. For each time sample, the 8 stations are used to interpolate a minimum curvature (gridded) surface that extends over the geographical region. Although promising, no conclusions can yet be made on the accuracy that might be achieved in future comparisons with GRACE.

Introduction

In preparation for the new generation of satellite gravity missions, Wahr et al. (1998) published an analysis of the expected accuracy of GRACE data. In it they carefully simulated the corrections required to interpret the new data for small time-varying signals such as variations in continental water storage. This was one of the papers that prompted us first to think about the possibility of combining satellite data and ground-based data from the Global Geodynamics Project (GGP). The GGP superconducting gravimeter (SG) network is far too sparse geographically to be suitable as a global gravity field, but there are sub-arrays of instruments, particularly in Asia and Europe, that warrant closer consideration. A preliminary look at the data was presented at the last IUGG meeting (Crossley and Hinderer, 1999).

Here we complete this initial study and develop a method to produce surface maps of the gravity over central Europe. Further developments have since been reported by us at the recent EGS meeting (Crossley et al., 2002) and a more detailed publication is in preparation.

Review of GRACE Mission

The GRACE (Gravity Recovery and Climate Experiment) is a joint venture of NASA (USA), DLR (Germany), UTCSR (Texas), and GFZ (Potsdam). The spacecraft was launched on

March 16, 2002 from Pletesk Cosmodrome in Russia. The orbit is almost polar and has an initial altitude of about 485 km, giving a short orbital period of 1.5 hr. There are two satellites 250 km apart, linked to each other by microwave and to other satellites and ground-based stations by GPS positioning.

Satellite gravity missions traditionally have targeted the largest sources of variability in the Earth's gravity field: atmospheric mass redistribution, long period ocean and solid Earth tides, post glacial rebound, large scale vertical tectonics, and changes in Arctic / Antarctic ice volumes. With the very high accuracy anticipated of GRACE data, it is hoped that other effects can be determined, i.e. changes in continental water storage, the variability of ocean bottom pressure, and the redistribution of snow and ice. These changes will be monitored down to ground distances of 100-200 km and intervals of 2-4 weeks.

The methodology follows the following sequence (for details, see Wahr et al., 1998):

- assume a density change $\Delta\rho$ in a layer of thickness H (10 -15 km) surrounding the Earth's surface (i.e. the lower atmosphere and upper hydrosphere).
- convert $\Delta\rho$ to a surface density distribution $\Delta\sigma$ by integrating over H.
- expand $\Delta\sigma$ in spherical harmonics, with coefficients ($\hat{C}_\ell^m$, $\hat{S}_\ell^m$)
- relate these harmonics to the harmonics (C_ℓ^m , S_ℓ^m) of the gravity field, determined from the satellite orbit, approximately every 14 days.
- deduce $\Delta\sigma$ from ($\hat{C}_\ell^m$, $\hat{S}_\ell^m$), and thus infer $\Delta\rho$ by assuming H.

Note that in $\Delta\sigma$ we cannot distinguish between the type of source, e.g. water, ice, or snow. It is also evident that the GRACE data will be time-aliased if there is any unmodeled variation of gravity on time scales less than 2 weeks (as seems probable for the atmosphere and oceans).

One of the examples considered by Wahr et al., is for Manaus, Brazil, in the Amazon River Basin. The accuracy of the GRACE recovery should be equivalent to 2 mm of water at wavelengths longer than 400 km. The errors rise rapidly; from about 10 cm water equivalent at 200 km to more than 100 cm at 100 km. This suggests that to be competitive and useful, ground-based gravity measurements will have to satisfy two criteria (a) to cover wavelengths between 100 and 1000 km and (b) reach accuracies of less than 0.4 μgal at wavelengths between 200 and 300 km. If both conditions are satisfied, then the errors of ground-based gravity and projected satellite gravity will overlap, and we can claim that ground-based (in this case GGP) gravity can be used to 'validate' satellite measurements.

European GGP Data Sets

The stations used in this study are shown in Figure 1; they are BR (Brasimone), BE (Brussels), MB (Membach), ME (Metsahovi), PO (Potsdam), ST (Strasbourg), VI (Vienna), and WE (Wettzell). Most of these are relatively evenly spaced in the middle of the European landmass, while Metsahovi is somewhat isolated at a distance from the others. Some stations are no longer operating; BE has been retired and PO was moved to Sutherland, South Africa. Also the instrument at Wettzell has been replaced with a newer model and a new station, Moxa, was started in 2000.

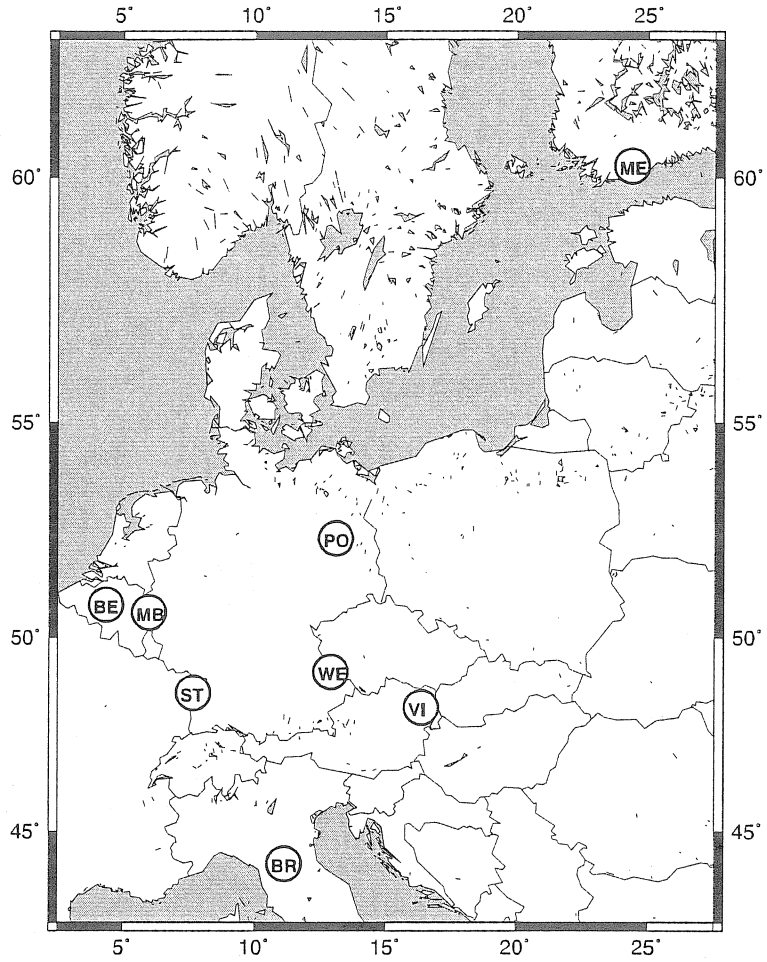

Figure 1. GGP stations from July 1997 – January 1998.

The distribution, or spacing, of the 8 stations taken in pairs, is plotted as a histogram in Figure 2. The distance range of 200 – 1000 km is well covered, but the inclusion of a single distant station (ME) extends the coverage up to 2000 km. Bernard Ducarme (personal communication, 1999), supplied the original series through the International Center for Earth Tides (ICET). They had been corrected for major problems and decimated to 1 hour (Figure 3).

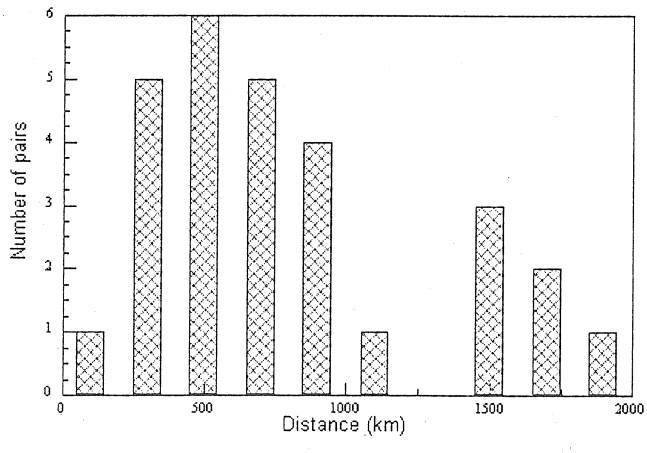

Figure 2. Station distribution, by pairs.

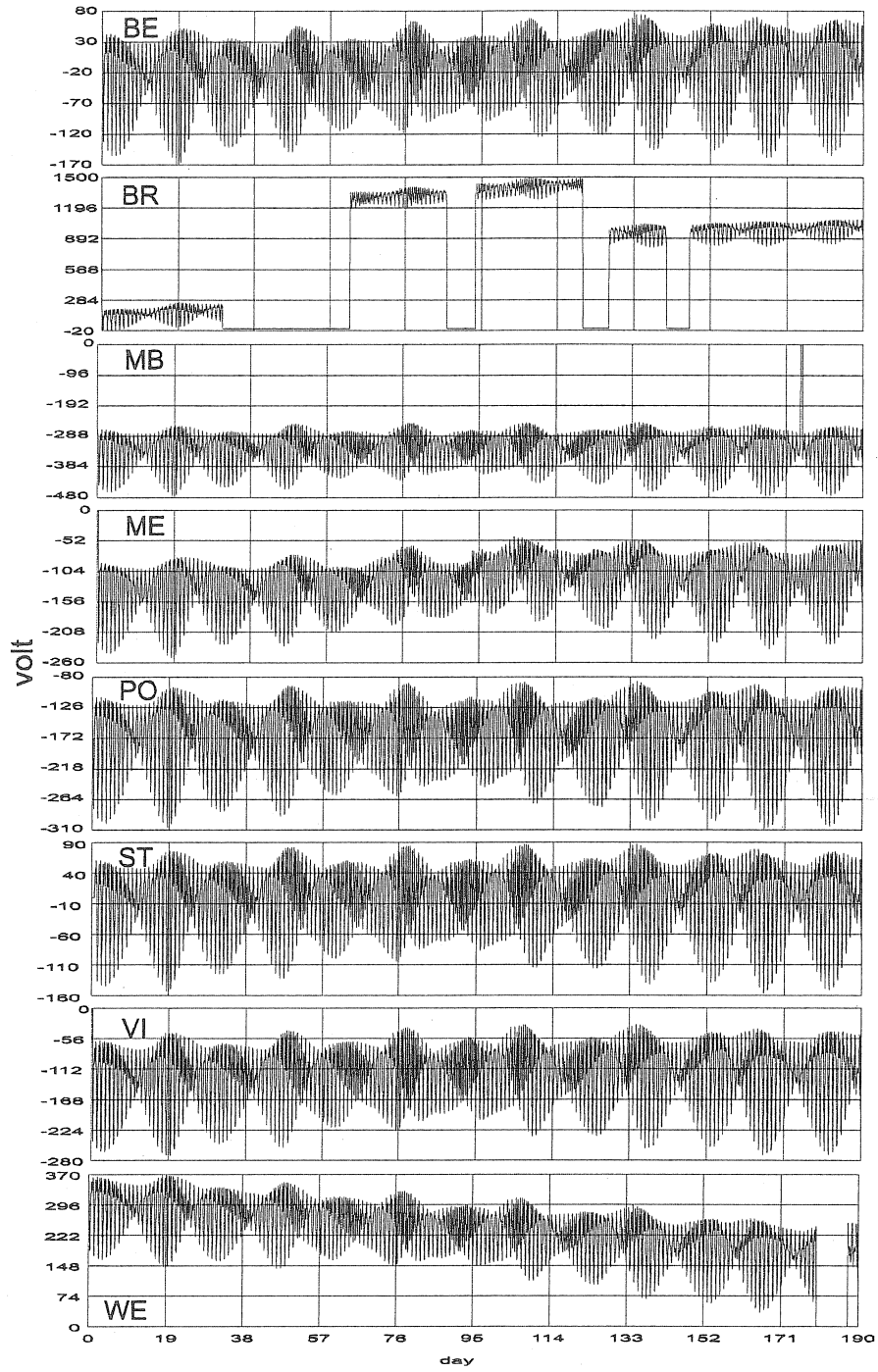

Figure 3. Initial 1-hour gravity data for 8 GGP stations, July 1997 – January 1998.

The first step is to remove a synthetic, or modeled, tide from each station. We do this using local tidal gravimetric factors (δ,κ) obtained from independent analyses for all waves with periods up to, and including, a month. For semi-annual and longer periods we use nominal values of (1.16, 0) to avoid minimizing the residual annual signals. We also remove the effect of local atmospheric pressure using a nominal admittance of –0.3 μgal mbar^{-1}. The residual series are displayed in Figure 4. It is clear that two stations, Brasimone and Wettzell, have special problems: BR has large data gaps and offsets and WE has a large negative drift that appears almost linear.

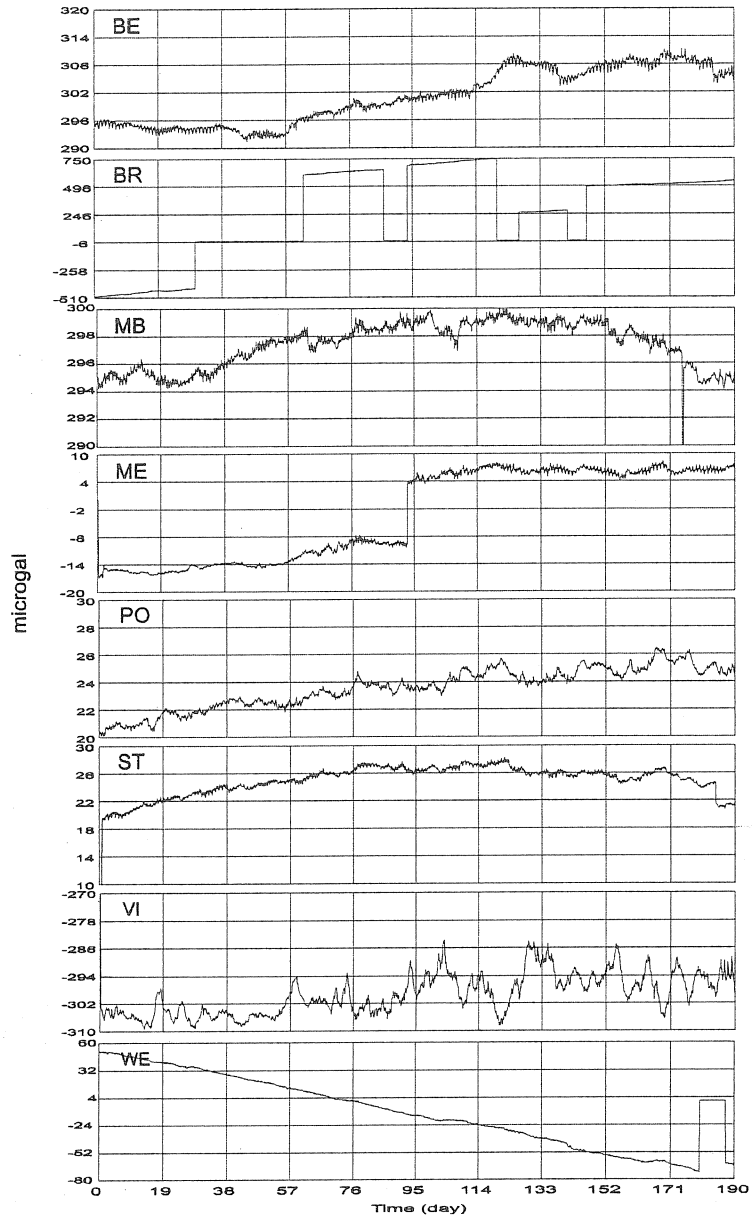

Figure 4. Gravity residuals after removal of tides and local pressure.

For both stations BR and WE, we fit simultaneously a linear drift function and a series of offsets at fixed time locations; this is done iteratively to arrive at the correcting functions shown in Figure 5. None of the other stations had drifts removed, but the other offsets in Figure 4 were corrected. IERS-derived polar motion was also subtracted from each data set. The final 1-hour residuals are shown below in Figure 6.

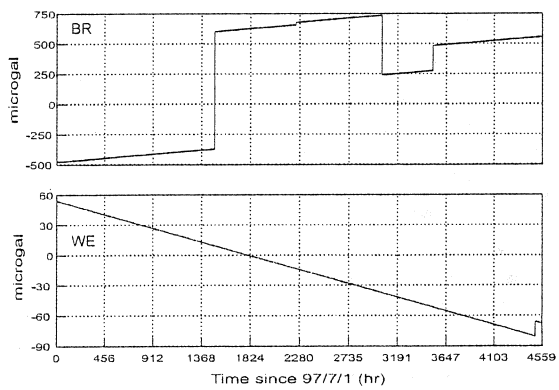

Figure 5. Corrections removed from 2 stations.

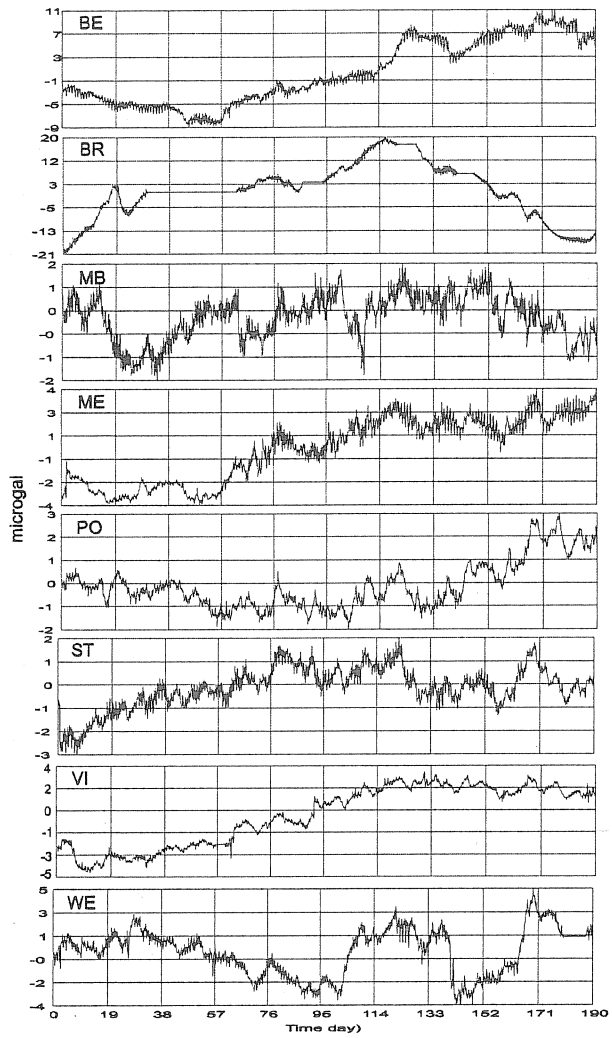

Figure 6. Gravity residuals after removal of offsets and polar motion.

We now decimate the series to 6 hour samples using a filter with a cut-off period of 1 day (this is legal), thus removing the small residual tidal fluctuations (Figure 7). The 6-hour sampling was chosen because we intend to do a second step of adding global pressure effects from 6-hour meteorological data (but this is not done here).

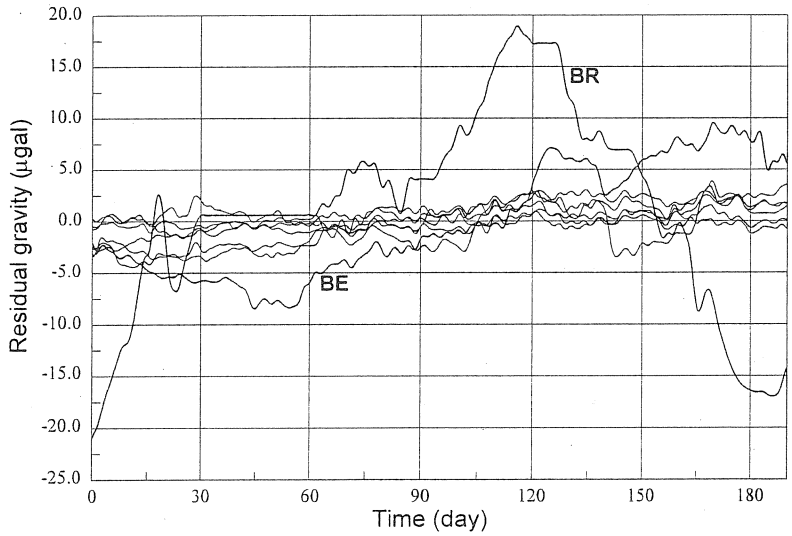

Figure 7. Filtered gravity residuals superimposed

Thes residuals in Figure 7 are displayed at the same scale and we can see that 2 stations, BE and BR, account for the largest variability in the data. This is clear in Figure 8 where the root mean square values of the residuals are shown together. We refer to the stations VI, ME, WE, ST, PO and MB as as the 6 'best stations'. This division is clearly consistent with what we know of the stations themselves. Station BE was one of the first stations to be installed and it has experienced a variety of problems during its long installation at the Royal Observatory in Brussels. The long term gravity residuals are probably less reliable than at most of the other stations. Also, as mentioned above, station BR had many problems due to the data gaps, drift and offsets that are not completely correctable after the fact. Therefore we do not have a lot of confidence in the BR residuals in Figure 6.

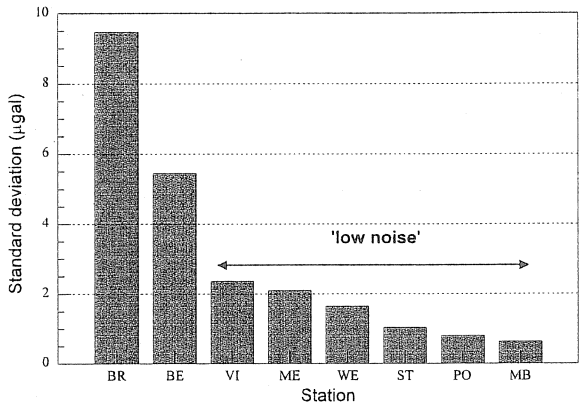

Figure 8. Station variability

If therefore we restrict attention to the 6 'low-noise' stations, we can plot their residuals on a scale of –5 to +4 μgal (Figure 9). Stations WE and ME now show greater variability than the other central stations MB, PO, ST, and VI.

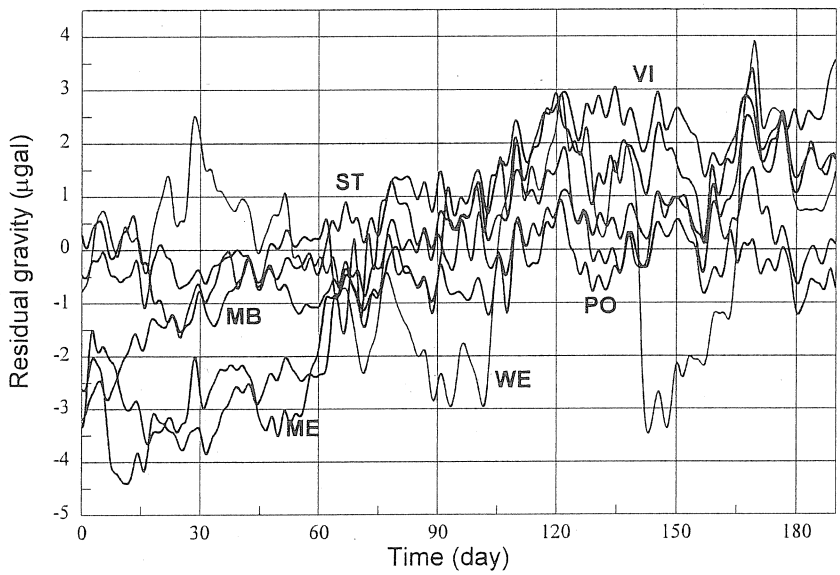

Figure 9. Six best stations, July 97 – Jan 98.

Despite the clear variability between sites, there are also significant similarities. For example, if we consider the data between days 70 and 100 (a month), and remove the local means for this month from each station, the coherence in the residuals can be quite striking (Figure 10). These stations reflect common variations with periods of several days, and this coherence persists for several weeks. The origin of these coherent signals is not known at this time, but the atmosphere must be considered the most likely source.

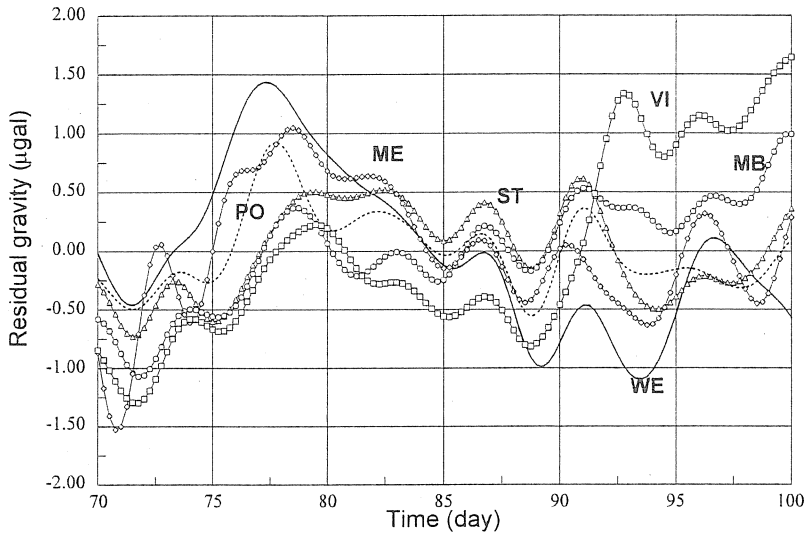

Figure 10. Six best stations over 1 month, local means removed.

Discussion and Conclusions

In the oral presentation of this paper, the data was taken one stage further. For each 1 day interval, the residuals at each station were interpolated to a uniform grid using a minimum curvature algorithm. This surface was then color coded and presented as an animation of bitmap images in the form of a movie. Space does not permit this movie to be show here, but it gives an idea of the time evolution of each station's gravity. Many things are yet to be done:

(1) Smooth the gravity surface to simulate the wavelengths that GRACE would be able to see in the European network of 8 stations. Smoothing can be as simple as fitting a polynomial surface, or as complicated as generating spherical harmonic coefficients and the pretending GRACE is trying to see this surface from 485 km.
(2) Remove instrument drift at all the stations, in addition to the 2 stations in Figure 5.
(3) Include the effect of global atmospheric pressure changes, in addition to the local correction.
(4) Consider other local signals, such as hydrology, that might not be seen by GRACE.
(5) Compare GGP data from 2000-2002 with actual gravity field models from CHAMP, which is now producing similar data to GRACE, but at a lower accuracy.

Our conclusion is necessarily tentative, but we believe that there are some promising features of GGP data that may be relevant to GRACE once a more sophisticated analysis is done.

Acknowledgments

We thank the various SG station operators for making the data available through GGP. This research was supported by CNRS; it is EOST contribution No. 2002-16-7516.

References

Crossley, D. J., and J. Hinderer, 1999. Global gravity campaigns - from the ground (GGP) to the sky (GRACE), *IUGG XXII General Assembly,* Abstract Volume A, p71-72.

Crossley, D., J. Hinderer, M. Llubes and N. Florsch, 2002. The potential use of ground gravity measurements to validate GRACE data, EGS Annual Congress, Abstract A04032, p 115.

Wahr, J., M. Molenaar, and F. Bryan. 1998. Time variability of the Earth's gravity field: hydrological and oceanic effects and their possible detection using GRACE, *J. Geophys. Res.*, **103** (B12), 30,205-30,229.

CONFRONTING SUPERCONDUCTING AND ABSOLUTE GRAVITY MEASUREMENTS WITH MODELS

T. F. Baker, M. S. Bos[1] and S. D. P. Williams
Proudman Oceanographic Laboratory, Bidston Observatory, Birkenhead, CH43 7RA, UK.
([1] now at DEOS, Delft University of Technology, Netherlands)

Confronting measurements with models provides both a test of the available models and also allows an essential test of the accuracy of the observations. In the following, 2 distinct types of gravity measurements are compared with models: (a) O1 and M2 observations from the superconducting gravimeters in the GGP network are compared with models of the Earth's body tides and models of ocean tide loading and (b) absolute gravity measurements near tide gauges are used for correcting secular trends in relative mean sea levels for vertical crustal movements and for testing models of post-glacial rebound.

(a)10 recent ocean tide models have been used to compute the O1 and M2 ocean tide loading and attraction at 15 GGP stations. The European GGP stations provide a valuable network over a relatively small area, which can be used for checking the accuracy of individual stations, testing the body tide models and testing the different ocean tide models. For example, the M2 ocean tide models of Schwiderski, FES94.1, TPXO.5 and NAO99b give a poorer fit to the European observations than the other ocean tide models. For a few of the European and global GGP stations there are discrepancies of the observations (after correction for ocean tide loading and attraction) of up to 0.3% with respect to the Dehant, Defraigne and Wahr elastic and inelastic body tide models. This is consistent with the present uncertainties in calibrations, using parallel recording with FG5 absolute gravimeters, which have quoted accuracies in the range 0.1% to 0.4% for individual stations (Meurers, 2001). The results for both the European and global GGP stations are more fully described in Baker and Bos (2002).

(b) In order to separate height variations of the land at a tide gauge from climate related changes in mean sea level, accurate measurements of land movements are required. In the UK, measurements have been made over the last few years at the tide gauges with the longest mean sea level time series using episodic GPS, continuous GPS and absolute gravity (for case studies of CGPS and absolute gravity at UK tide gauges see http://imina.soest.hawaii.edu/cgps_tg/). For absolute gravity it was decided to concentrate on the tide gauges at Newlyn in south west England and Lerwick in the Shetland Islands, which are situated on bedrock. These tide gauges are part of the Global Sea Level Observing System (GLOSS) coordinated by the Intergovernmental Oceanographic Commission. The measurements have been made with the POL absolute gravimeter FG5-103. The gravimeter has been taken regularly to fundamental gravity stations in Europe and USA (including the GGP stations at Boulder, Wettzell and Bad Homburg) in order to intercompare with other absolute gravimeters.

As well as providing corrections for the land movement component of changes in mean sea levels, the FG5 results can also be used to test models of post-glacial

rebound. In particular the absolute gravity measurements show clear evidence of subsidence in the Shetland Islands, which is consistent with the post-glacial rebound model of Lambeck and Johnston (1995). For further details of the results see Williams, Baker and Jeffries (2001).

References

Baker, T. F. and M. S. Bos (2002). Validating Earth and ocean tide models using tidal gravity measurements. Submitted to Geophysical Journal International.

Lambeck, K. and P. Johnston (1995). Land subsidence and sea level change: contributions from the melting of the last great ice sheets and the isostatic adjustments of the Earth, in *Land Subsidence*, edited by Barends, Brouwer and Schroder, pp. 3-18, Balkema, Rotterdam.

Meurers, B. (2001). Superconducting gravimetry in geophysical research today. Journal of Geodetic Society of Japan, **47**, 300-307.

Williams, S. D. P., T. F. Baker and G. Jeffries (2001). Absolute gravity measurements at UK tide gauges. Geophysical Research Letters, **28**, 2317-2320.

TIDAL FRICTION, GEODYNAMICAL PROPERTIES AND ROTATION SPEED IN THE REMOTE GEOLOGICAL PAST

Peter Varga
Geodetic and Geophysical Research Institute,
Seismological Observatory, Meredek 18, H-1112 Budapest, Hungary

1. Some remarks on the paleorotation of the Earth during Phanerozoic, Proterozoic and Archean.

The early formation of the Earth probably runs much faster as it was proposed earlier. Our planet was separating out a lighter continental crust 4.4 Ma BP (hundred million years after earth formation) (Kerr, 2000). Life begun very early in Earth's history, perhaps before 3800 million years ago (Marais, 2000). Eriksson and Simpson (2000) in the sedimentary rocks from South Africa detected tidal deformations dating 3.2 years ago. Their analysis implies that tides were not unusually strong than and that the Archean lunar orbit was similar to that seen today. Inspite of these facts it also can be concluded that our knowledge on the development of the Earth during its history is incomplete.
At present time the input of the tidal friction into Earth energetic balance is 10^{20} Nm/y (y=year). For a comparison the solar energy input is 10^{25} Nm/y, the heat flow loss, the tectonic activity and the energy released by earthquakes are 10^{22} Nm/y, 10^{20} Nm/y and 10^{18} Nm/y respectively. It can be therefore concluded that at present time the tidal despinning of Earth rotation is a significant component of the Earth's energetic household.
To estimate the role of tidal friction's input into development of the Earth and the Earth-Moon system it is necessary to determine the length of day in the early Katarchean, shortly after the Earth had been formed (4.5 Ga BP).

2. Estimate of LOD near to the time of Earth formation

With the use of fossils and tidal deposits Varga et al. (1998) infer the variations of the rotation speed during the last 3.10 Ga. It was found with the use of these data that the Earth's despinning rate was on the average about five time smaller

in the Protorezoic =Ptz) than in Phanerozoic (Pz). The corresponding linear trends are:

$LOD = 24.00 - 4.98\ t$ for the Phanerozoic (Pz)
$LOD = 21.44 - 0.97\ t$ for the Proterozoic (Ptz)

(where t is the time before present (BP) expressed in Ga=10^9 year).
With the use of the second equation at the time of Earth formation (4.5 GaBP) the result will be 17.5 hours. This value should be an extreme short value and serves as a lower bound because the despinning of the Earth's axial rotation is due to oceanic tides first of all and the solid Earth tides has only a reduced despinning effect. It can be supposed however that the first oceans were formed significantly later than 4.5 GaBP. An another estimation became possible if the database described in Varga et al., (1998) is used in an unique robust estimation process. The database can be modelled in this case by an exponential expression which gives with the use of robust estimation procedure the numerical value:

$$LOD = 4.68.e^{-0.00166t} + 19.65$$

with the use of this model the length of day 4.5 GaBP was 19.6 hours.
From the mentioned above paper of Eriksson and Simpson (2000) we can conclude that the length of day 3.2 GaBP was closer to 15 hours than to 24 hours. In other words: LOD was less than 19.5 hours. This value derived from the study of the earliest known tidal deposit serves as an upper limit both for linear and exponential extrapolations. Consequently the value 19.6 hours for LOD 4.5 GaBP serves as on upper bound also.
For the interpretation of the original LOD value the equation for the characteristic time of the lunisolar despinning τ_T can also be of use (Hubbard, 1984)):

$$K\ c = LOD^{\,6} / \tau_T$$

where

$$K = 2\ \Pi\ M_E / 3k_s\ GM^2_M\ R^3$$

Here δ is the tidal delay of the lunisolar bulge which was 6.8° for Pz and 1.5° for the Ptz (Varga, 1998). For the earlier parts of the Earth history we can suppose 1.0° - 0.5° if during the early history of our planet its surface not consists oceans. In above equation

- M_E and M_M are the masses of the Earth and the Moon
- k_S is the secular Lovenumber
- G is the gravitational constant

- c is the Earth-Moon distance
- R is the mean radius of the Earth.

For the use of the equation (1) given by Hubbard (1984) to estimate LOD 4.5 GaBP the value of c is needed in the remote past. Using the results obtained in Varga et al. (2002) for the Earth-Moon we get:

$33.844 \cdot 10^8$ m	present epoch
$3.450 \cdot 10^8$ m	$3 \cdot 10^9$ y BP
$3.200 \cdot 10^8$ m	$4.5 \cdot 10^9$ y BP

For the characteristic time of tides τ_T – to a certain extent arbitrary – we suppose three values: 10^{10} y; $7.5 \cdot 10^9$ y; $5 \cdot 10^9$ y. Of course in the reality $\tau_T > 5 \cdot 10^9$ y and with high probability $\tau_T > 7.5 \cdot 10^9$ y.
In equation (1) to calculate K the following numerical values were in use:

$k_S = 0.96$
$G = 6.671 \cdot 10^{11}$ kg^{-1} m^3 s^{-2}
$R = 6.371 \cdot 10^6$ m
$M_E = 5.973 \cdot 10^{24}$ kg
$M_M = 7.347 \cdot 10^{22}$ kg

In the following table LOD values are estimated for $4.5 \cdot 10^9$ y BP for different phase delay values, for the c values valid for present epoch, $3 \cdot 10^9$ years BP and $4.5 \cdot 10^9$ years BP and for the three characteristic time of the lunisolar damping τ_T mentioned above:

$\delta=2^{\circ}$

C (m) τ_{TID} (y)	10^{10}	$7.5\cdot 10^{9}$	$5\cdot 10^{9}$
$3.844\cdot 10^{8}$	11.39	15.19	22.78
$3.450\cdot 10^{8}$	5.95	7.94	11.91
$3.200\cdot 10^{8}$	3.79	5.05	7.58

$\delta = 1.5^{\circ}$

$3.844\cdot 10^{8}$	15.19	20.25	30.38
$3.450\cdot 10^{8}$	7.94	10.59	15.88
$3.200\cdot 10^{8}$	5.05	6.74	10.11

$\delta =1.0^{\circ}$

$3.844\cdot 10^{8}$	22.78	30.37	45.46
$3.450\cdot 10^{8}$	11.91	15.88	23.82
$3.200\cdot 10^{8}$	7.58	10.11	15.16

$\delta = 0.5^{\circ}$

$3.844\cdot 10^{8}$	45.57	60.75	91.12
$3.450\cdot 10^{8}$	23.82	31.75	47.65
$3.200\cdot 10^{8}$	15.15	20.22	30.30

In this table the values listed in lines for c = $3.844\cdot 10^{18}$ (valid for present epoch) are unrealistic for LOD $4.5\cdot 10^{9}$ y BP. Also the results in the last column can be excluded because $\tau_T > 5\cdot 10^{9}$ year. According to result of Eriksson and Simpson LOD $3.2\cdot 10^{9}$ y BP was already shorter than 19.5 hours. It is also probable that with the linear extrapolation of the paleorotational data we got the lowest bound for LOD 4.5 Ga BP (17.5 hours). So we remain with one possible conclusion: the realistic solution we got if $\delta = 0.5^{\circ}$, c = $3.200\cdot 10^{8}$

m and τ_T is between 10^{10} year and $7.5 \cdot 10^9$ year (see the values 15.15 and 20.22 in the last line of our table).

3. Conclusions

From the results of calculations demonstrated in previous section one can conclude that:

- at present we can accept that the values between 19.5 hours and 17.5 hours are giving realistic estimation for the rotation period in time of Earth formation. This means that during his lifetime our planet lost more than half of its rotational energy. What was the impact of this energy loss into the development of the Earth and of the Earth-Moon system? This question should be answered by future investigations.
- the phase shift of the tidal bulge was probably much lower at the time of very young Earth than during the Ptz and Pz when our planet had his oceans. This means: the early Earth has no oceans of continental scale distribution.
- the characteristic time of the lunisolar despinning rate τ_T is probably between 10^{10} year and $7.5 \cdot 10^9$ year.

Acknowledgement. The research work described in this paper was supported by the Hungarian Science Found OTKA (Project T029049 and T038123)

References

Eriksson, K.E., Simpson E.L., 2000: Quantifying the oldest tidal record. 3.2 Ga Moodies Group, Barberton Greenstone Belt, South Africa, Geology, 28,9,831-834

Hubbard, W.B., 1984: Planetary interiors, Van Nostrand Reinhold Company

Kerr, R.A., 2000: Geologists pursue solar system's oldest relics. Science, 290, 2239-2242

Marais, D.J.D., 2000: When did photosynthesis emerge on the Earth? Science, 289, 1703-1705

Varga, P., Denis, C., Varga, T., 1998: Tidal friction and its consequences in paleogeodesy in the gravity field variation and in tectonics. Journal of Geodynamics, 25, 61-84

Varga, P., 1998: Earth tidal phase lag and the tidal development of the Earath-Moon system. Proceedings of the XIIIth . Int. Symp. on Earth tides, Brussels.

Varga, P., Zavoti, J., Denis, C., Schreider, A. A., 2001: Complex interpretation of the Earth despinning history. Scientific contributions of IAG conference, Budapest, September 2001- Springer Verlag (in print)

Parameters of the fluid core resonance estimated from superconducting gravimeter data

Tadahiro Sato*(1), Yoshiaki Tamura (1), Koji Matsumoto (1), Yuichi Imanishi (2), and H. McQueen (3)
(1) National Astronomical Observatory, 2-12 Hoshigaoka, Mizusawa, 023-0861 Japan,
(2) Ocean Research Institute, University of Tokyo,
(3) Research School of Earth Sciences, The Australian National University
*E-mail address: tsato@miz.nao.ac.jp

Abstract

We have estimated the parameters of FCR (Free Core Resonance) based on the gravity data obtained from four SGs (Superconducting Gravimeters) at Esashi and Matsushiro in Japan, Canberra in Australia and Membach in Belgium. The corrections applied to the observed tidal factor and phase are of two for the phase delaying due to the analog filter of the SGs and for the ocean tides. We have compared the ocean tide effects computed from four global ocean tide models. They are Schwiderski model (1980) and three models of NAO99bJ (Matsumoto et al., 2000), CSR4.0 (Eans and Bettadpur, 1994) and GOT99.2b (Ray, 1999), which were derived from the TOPEX/Poseidon (T/P) altimeter data. While the three T/P models give very consistent correction values each other at each observation site, Schwiderski model clearly shows a systematic difference from them in both the amplitude and phase. We used here NAO99bJ model for the correction. The observed tidal admittances (i.e. complex tidal factors) were fitted to a dumped harmonic oscillator as a model for FCR and we have obtained the following values by stacking the four sites; 429.66+/-1.43 sidereal days, 9,350 - 10,835, -4.828E-4+/-3.4E-6, -3.0E-5+/-4.5E-6 for the eigenperiod, the Q-value and the real and imaginary parts of the resonance strength, respectively. Our results for the gravity data suggest that a systematic difference between two estimations from the gravity and the nutation, which has been shown in the previous works, is mainly caused by the inaccurate correction for the ocean tide effects.

1. Introduction

Precise observational determination of the FCR parameters is important for the study in geodynamics, because they give us useful information to constrain the physical parameters at the CMB (Core Mantle Boundary) related to the coupling between the Earth's core and mantle.

One of the motivations of this study is to clear the reason/s of a systematic difference in FCR parameters deduced from two different kinds of observations (i.e. tide and nutation), in particular the difference in Q-values, which has been shown in the previous works (for example, Neuberg et al., 1987 and Sato et al., 1994 for the gravity tide, Gwin et al., 1986 and Defaigne et al., 1994, 1995 for the nutation). Thus, in general, it is observed a tendency that the Q-values estimated from the SG data are smaller than those estimated from the VLBI nutation data. Defaigne et al. (1994) estimated the FCR parameters by stacking two data sets of the SG and VLBI. According to their results, while the results for stacking both data sets or stacking only the VLBI data sets give a large Q-value exceeding 40,000, the results for stacking only using the SG data show a small value of about 4,000, which is about 10 times smaller than the VLBI data.

2. Data and analysis

We analyzed the data obtained at four SG sites; three of GGP-Japan network, namely, Esashi and Matsushiro in Japan and Canberra in Australia, and one is Membach in Belgium.

For Membach, we used the GGP data archived at International Center for Earth Tides and distributed by the center as 'GGP-Data CD#A2'. The reason why we chose this site from the GGP sites is that 5 years data in length are available for this site. Moreover, it is well known that the ocean tide effect in the diurnal tidal band is small in the central Europe. Therefore, this may give us useful information to see an accuracy of the estimations of ocean tide effects. The geographical position of each site and the data length used here are listed in Table 1.

The tidal factors and phases were analyzed by means of an algorithm 'BAYTAP-G' (Tamura et al., 1991) using the 1-hour data corrected for the spikes and steps to the original data. To separate the atmospheric pressure effect on the gravity data, the local pressure data obtained at each site were taken in the analysis by means of a response term to be estimated.

3. Scale factors of the SGs

Figure 2 shows a comparison of the results for absolute calibration of the scale factors (μGal/Volt) to the changes in relative sensitivity those are represented using the temporal variation of the amplitude coefficients of M_2 wave. The comparison at Esashi is displayed in this figure. The amplitude coefficients of M_2 wave were obtained from successive monthly analysis of the original 1-hour data of Volt unit for the 10 years shown in Table 1. We see in Fig. 2 that the relative sensitivity of the SG is very stable, even though it is observed an annual variation for this wave or some outliers mainly caused by interruptions of the observation. The linear trends shown in Fig. 2 suggest that the change in the M2 amplitude coefficients is only -0.01 % in magnitude during the 10 years. On the other hand, the scale factors calibrated with the absolute gravimeters show a change of +0.29 % for the same observation period, which is larger than the change in relative sensitivity by about 30 times.

A similar tendency is observed in the comparison at Canberra. The Canberra SG has been calibrated with the FG5 absolute gravimeters at three times during the three years of 1998-2000 and Amalvict et al. (2001) reported the computation results for these calibrations. According to their results, the absolute scale factors show a linear change with a rate of -1.2% during the three years. On the other hand, the change in the relative sensitivity estimated from monthly variations of the M_2 amplitude coefficient is +0.054 % in magnitude.

Although the reason/s making the difference between the changes in the absolute calibrations and those in the relative sensitivities is/are not clear yet, for the SGs at Canberra and Esashi, we adopted here a weighted mean averaged over the absolute calibration values as the scale factor of each SG. We used the RMS error of each calibration as the weight. For Matsushiro and Membach, we adopted the results by Imanishi et al. (2002) and the calibration table given by Royal Observatory of Belgium (Hendrickx, personal communication, 2002), respectively. The error in the calibrations with the absolute gravimeters is estimated at a range of 0.04 % to 0.2 %.

3. Corrections

Before correcting for the effects of ocean tides, we applied a correction for the phase delaying due to the analog filter of each SG to the analysis results by BAYTAP-G. We used following values (unit: degree per cycle per day) for the correction; -0.166, -0.166, -0.168, which were estimated from a method described in Imanishi et al. (1996), and -0.1608 (Camp et al., 2000) for Esashi, Canberra, Matsushiro and Membach, respectively. Although the analog filter of the Membach SG has been changed in January 1 1998 from the TIDE filter to the GGP1 filter, we analyzed the 5 years data without dividing them into two periods, in order to avoid degradation in frequency resolution of the analysis. This has been done by being artificially shifted the time of the theoretical tide computed with BAYTAP-G by the amount corresponding to the phase difference between the TIDE and GGP1 filters, for the observation period when the GGP1 filter is used. For the other three sites, we used the data obtained by

the TIDE filter.

The ocean tide effects (attraction and loading) were estimated by using a computer code called 'GOTIC2' (Matsumoto and Sato, 2001). We have compared the four global ocean tide models; namely three of NAO99bJ (Matsumoto et al., 2000), CSR4.0 (Ray, 1999) and GOT99 (Eans and Bettadpur, 1994), which were based on the TOPEX/POSEIDON (T/P) altimeter data, and Schwiderski model (1980), which has been widely used in the study for Earth tides as a conventional standard global ocean tide model. As a result, it can be pointed out that the former three models based on the T/P data give very consistent amplitude and phase at any of the four observation sites and for any of the three major tidal waves of O_1, K_1 and M_2, even though these sites are largely separated in their locations on the earth. Compared with this, Schwiderski model shows a clear systematic difference from the T/P models in both the amplitude and phase. As an example, comparison at Canberra is shown in Figure 1.

We adopted here the NAO99bJ model for the ocean tide corrections. For the minor waves, which are not available to use a global ocean tide model, we adopt a correction value that was interpolated or extrapolated from nearby main waves (Matsumoto and Sato, 2002).

3. Estimation of FCR parameters

The FCR parameters were estimated by fitting the observed complex tidal admittances to a dumped harmonic oscillator as a model for the resonance. In order to reduce a possible effect on our analysis due to the calibration errors for the scale factor of SGs, we used the admittances normalized with the O_1 wave as previously Cummins and Wahr (1993) or Sato et al. (1994) adopted. Thus the model used here is;

$$G(\omega_i) = F(\omega_i)/F(\omega_1) - 1 = B((\omega_i-\omega_L)/(\omega_0-\omega_i))$$
$$\text{with } \omega_0 = 2\pi f_0 (1+jQ^{-1}/2).$$

Here ω_i, ω_1 and ω_0 are the angular frequencies of the i-th tidal wave, O_1 wave and FCR, respectively. $F(\omega_i)$ is the observed complex tidal admittance of the i-th wave, $F(\omega_1)$ that of the O_1 wave, B a complex coefficient representing the strength of resonance (Br for the real part and Bi for the imaginary part) , f_0 the real part of the eigenfrequency of FCR, Q^{-1} the inverse of Quality factor, and j the imaginary unit. The method used for fitting is a modification of ' Marquandt method', so that the variation range of unknown parameters to be fitted is banded by means of a dynamical biweight method (Nakagawa and Oyanagi, 1982). We searched the optimum combination of the initial values for fitting by applying this binding condition, but the final solutions were solved using the obtained optimum initial values without applying any binding conditions for all unknown parameters.

The final parameter values obtained from stacking of the four sites are 429.66+/-1.43 sidereal days (s.d.), 9,350 to 10,835, -4.828E-4+/-3.4E-6, -3.0E-5+/-4.5E-6 for the eigenperiod ($T_0 = 1/f_0$), Q-value, Br and Bi, respectively. Figure 3 shows the comparison between the observed admittances and the FCR curve computed using the parameters shown above. The waves near the resonance are displayed.

4. Discussions

4.1. Sensitivity change of SG

At Esashi, during the 10 years shown in Fig. 2, the superconducting sphere has been dropped many times by the effect of large earthquakes or to exercise the wintering members of Japanese Antarctic Research Expedition. Whenever the sphere was dropped at a frequency of once or twice a year, it has been levitated by adjusting the superconducting currents within a range of 4-5 A.

Although the adjustment of the superconducting currents of the Esashi SG has been done many times, as shown in Fig. 2, the mean relative sensitivity inferred from the M_2 amplitude coefficients is stable at a degree of about 0.01 % during the 10 years. This suggests that the sensitivity change of the SG itself is very small, insofar as we maintain the value of superconducting currents carefully. Related to this, it may be worth to note that, at both the Canberra and Esashi sites, the same analog/digital converters have been used through the observation periods shown in Table 1. On the other hand, judged from the temporal changes of the absolute calibrations and relative sensitivities shown in Fig. 2, we may also say that the long-term change in the observed amplitude of M_2 wave including the ocean tide effects is also small at the similar order shown in Fig. 2.

4.2. Reliability of the obtained FCR parameters

Based on the Esashi data, we have investigated the reliability of our FCR parameters by two methods. One is the Monte Calro method and other is a sensitivity test to the phase error in the Ψ_1 wave.

In the former test, the distribution of the solutions for each parameter was examined from 5000 data sets, which were generated by artificially adding Gaussian random numbers to the observed admittances of each wave. Variances of the random numbers are similar in magnitude to the RMS errors for the observed admittances. Although the distributions of solutions obtained from this test clearly show the correlations between f_0 and Br and between Q^{-1} and Bi as expected from the correlation matrix, we obtained the values of 428.607+/-0.137 s.d. and 14,436 to 15,076 for T_0 and Q-value as the mean values over the 5000 data sets. In this connection, by the fitting only using the observed Esashi admittances without stacking, we obtained 428.49+/-5.50 s.d. and 62,814 to 264,550 for the eigenperiod and the Q-value, respectively.

On the other hand, the sensitivity test was carried out by artificially changing the Ψ_1 phase within a range of +/-1.5 deg (about 3 times of the observation error for this wave). The amplitude of this wave is small but the estimated FCR parameters are sensitive to the Ψ_1 phase in particular the eigenperiod and the Q-value, because this wave has a period very close to the eigenperiod of FCR. The results are displayed in Fig. 4. The rectangular areas shown in this figure indicate the error range of the obtained parameter values, thus the magnitude of vertical side of each rectangular indicates the error range of the estimated parameters, which is expected from the error for the Ψ_1 phase shown by the horizontal side of each rectangular.

From the above two tests, we can say that (1) our solutions may have not a large systematic error due to the algorithm used in the fitting and (2) the estimation errors caused by the effects of the error in the observed Ψ_1 phase are at the orders of +/-1 day and -20,000 to 8333 for T_0 and Q-value, respectively. As pointed out by Zurn and Rydelek (1991), we have a case that the obtained Q-value shows a large negative value, even though the FCR cannot possess a negative Q. But it shows a possibility that the analysis for a system having a large Q-value brings a negative Q-value, when a combination of parameters in the form of f_0/Q is used for fitting and the analysis is performed in the frequency domain. Such situation appears in the results for the sensitivity test to the Ψ_1 phase. However, this and the magnitude of Q-value obtained from the stacking indicate that the gravity data also give a large Q-value exceeding about 10,000 as well as that estimated from the nutation data.

4.3. Comparisons with theory

Many of previous analyses results obtained from various observation means indicate that the observed eigenperiod shows the significant sift from the value inferred from an elastic, rotating and oceanless earth model (i.e. about 460 sidereal days, for example, Wahr, 1981).

Our result obtained here (429.66+/-1.43 s.d.) supports this too. Based on two models, namely a PREM hydrostatic model (Dziewonski and Anderson, 1981) and a nonhydrostatic inelastic model modified from the PREM model, Dehant et al. (1999a) give 456.98 s.d. and 431.37 s.d. as the eigenperiods for the former model and the later one, respectively. Our value is consistent with their non-hydrostatic inelastic value rather than the elastic-hydrostatic one and it is also consistent with the value obtained from the nutation data, for example, 433.5+/-0.3 s.d. to 433.9+/-0.5 s.d. which were obtained from the stacking the nutation data (Defraigne, et al., 1995).

Judged from the systematic difference in the ocean tide effects estimated from the Schwiderski model and from those from the T/P models (see Fig. 1), this study suggests that a systematic difference between the gravity tide and the nutation in particular in that for the Q-value is mainly due to inaccurate ocean tide correction in the previous studies, because the ocean tide effect on the nutation observation is much smaller than that on the tidal gravity observation (for example, Hass and Schuh, 1996, Dehant et al., 1999b). The Q-value obtained here indicates that, at the diurnal band, the effect of coupling at the CMB is weak as suggested from the nutation observations.

In this study, we have only used the NAO99bJ ocean model for the ocean tide correction. But it is needed to compare with the FCR parameters estimated from the admittances corrected using other ocean models, in order to constrain them much tightly. This and the comparison of the observed resonance parameters with the theory including the effect of phase shift due to the Earth's inelastic property (for example, Mathews, 2001) are remained for further study.

Acknowledgment:

A computer code 'SALS' (Statistical Analysis with Least Squares Fitting, Nakagawa and Oyanagi, 1982)' developed by the SALS group was used for the computations for fitting, The calibration results for the scale factor and phase of the Membach SG were kindly provided by Hendrickx of Royal Observatory of Belgium. The observation of GGP-Japan Network is supported by a Japanese observation project call Ocean Hemisphere Projected conducted by Y. Fukao of University of Tokyo (grant No. 09NP1101 of The Ministry of Education, Culture, Sports, Science and Technology).

References:

Amalvict, M., H. McQueen and R. Govind; 2001, Absolute Gravity Measurements and Calibration of SG-CT031 at Canberra, 1999-2000, J. Geodetic Soc. Japan, Vol.47, No.1, 410-416.

CAMP, M.V., Wenzel, H.-G., Schott, P., Vauterin, P., and Francis, O.; 2000, Accurate transfer function determination for superconducting gravimeters, Geophys. Res. Lett. 27,1,37-40.

Cummins, P.R. and Wahr, J.M.; 1993, A study of the Earth's free core nutation using International Deployment of Accelerometers gravity data, J. Geophys. Res., 98, 2091-2103.

Defraigne, P., V. Dehant and J. Hinderer; 1994, Stacking gravity tide measurements and nutation observations in order to determine the complex eigenfrequency of the nearly diurnal free wobble, J. Geophys. Res., 99, No. B5, 9203-9213.

Defraigne, P., V. Dehant and J. Hinderer; 1995, Correction to 'Stacking gravity tide measurements and nutation observations in order to determine the complex eigenfrequency of the nearly diurnal free wobble' by P. Defraigen, V. Dehant and J. Hinderer , J. Geophys. Res., 100, No. B2, 2041-2042.

Dehant, V., P. Defraigne and J. M. Wahr; 1999a, Tides for a convective Earth, J. Geophys. Res., 104, No. B1, 1035-1058.

Dehant, V., F. Arias, CH., Bizouard, P. Bretagnon, A. Brzinski, B. Buffet, N. Captaine, P. Defraigne, O. De Viron, M. Feissel, H. Fliegel, A. Forte, D. Gambis, J. Getino, R. Gross, T. Herring, H. Kinoshita, S. Klionr, M. Mathes, D. Mccarthy, X. Moisson, S. Petrov, R. M. Ponte, F. Roosbeek, D. Salatein, H. Schuh, K. Seidelmann, M. Soffel, J. Souchay, J. Vondrark, J. M. Wahr, P. Wallace, R. Weber, J. Williams, Y. Yatskiv, V. Zharov, and S. Y. Zhu; 1999b, CONSIDERATIONS CONCERNING THE NON-RIGID EARTH NUTATION THEORY, Celes. Mechan. Dynamic. Ast., 72, 245-310.

Dziwonski, A. D. and D. L. Anderson; 1981, Preliminary reference Earth model, Phys. Earth Planet. Inter., 25, 297-356.

Eanes, R. J. and S. V. Bettadpur; 1994, Ocean tides from two year of TOPEX/POSEIDON altimetry (abstract), EOS Trans., AGU, 75 (44), Fall Meet., Suppl., 61.

Gwin, C, Herring, T.A. and Shapiro, I.I.; 1986, Geodesy by Radio Interferometry; Studies of Forced Nutations of the Earth. 2. Interpretation, J. Geophys. Res., 91, 4755-4765.

Hass, R. and Schuh, H.; 1996, Determination of frequency dependent Love and Shida number from VLBI data, Geophys. Res. L., 23, No.12, 1509-1512.

Imanishi, Y., T. Sato and K. Asari; 1996, Measurement of Mechanical Responses of Superconducting Gravimeters, J. Geodetic Soc. Japan, Vol.42, No.2, 115-117.

Imanishi, Y., T. Higashi, and Y. Fukuda; 2001, Calibration of superconducting gravimeter T011 by parallel observation with absolute gravimeter FG5#210 - a Bayesian approach, submitted to J. Geophys. Int..

Mathews, P.M.; 2001, Love number and Gravimetric Fctors for Diurnal Tides, J. Geod. Soc. Japan, Vol.48, No.1, 231-236.

Matsumoto, K., T. Takanezawa and M. Ooe; 2000, Ocean Tide Models Developed by Assimilating TOPEX/POSEIDON Altimeter Data into Hydrodynamical Model: A Global Model and a Regional Model around Japan, J. Oceanography, 56, 567-581.

Matsumoto, K. and Sato, T.; 2001, GOTIC2: A Program for Computation of Ocean Tidal Loading Effect, J. Geod. Soc. Japan, Vol.48, No.1, 243-248.

Matsumoto, K. and Sato, T.; 2002, Loading contribution from minor ocean tidal constituents, in preparation.

Nakagawa, T. and Oyanagi, Y.; 1982, *Program SALS*, University of Tokyo Press, (in Japanese)

Neuburg, J., Hinderer, J. and Zurn, W.; 1987, Stacking Gravity Tide Observations in Central Europe for the Retrieval of the Complex Eigenfrequency of the Nearly Diurnal Free Wobble, Geophys. J. R. astr. Soc., 91, 853-868.

Ray, R. D.; 1999, A global ocean tide model from TOPEX/POSEIDON altimetry: GOT99.2., NASA Tech. Memo., 209478

Sato, T., Y. Tamura, T. Higashi, S. Takemoto, I. Nakagawa, N. Morimoto, Y. Fukuda, J. Segawa, and N. Seama; 1994, Resonance parameters of the free core nutations measured from three superconducting gravimeters in Japan, J. Geomag. Geoelect., 46, 571-586.

Schwiderski, E. W.; 1980, On charting global ocean tides, Rev. Geophys. Space Phys., 18, 243-268.

Tamura. Y., T. Sato, M. Ooe and M. Ishiguro; 1991, A procedure for tidal analysis with a Bayesian information criterion, Geophys. J. Int., 104, 507-516.

Wahr, J. M.: 1981, Body tides of an elliptical, rotating, elastic and oceanless Earth, Geophys. . R. Astron. Soc., 64, 677-703.

Zurn, W. and Rydelek, P.A.; 1991, Investigation of "nearly diurnal free wobble' resonance in individual tidal records, Proc. the 11 Int. Symp. on Earth Tides, Helsinki, ed. J. Kakkuri, 521-530.

Table 1. Gravimeter data used in this study

Site	Latitude	Longitude	Height (m)	SG	Period
Membach	50.609 N	6.007 E	250.00	CT#021	95/08/03 - 99/06/30
Esashi	39.148 N	141.335 E	393.00	T#007	92/01/26 - 01/12/31
Matsushiro	36.544 N	138.203 E	451.10	T#011	96/09/10 - 00/03/31
Canberra	35.321 S	149.008 E	724.00	CT#031	97/01/27 - 02/01/18

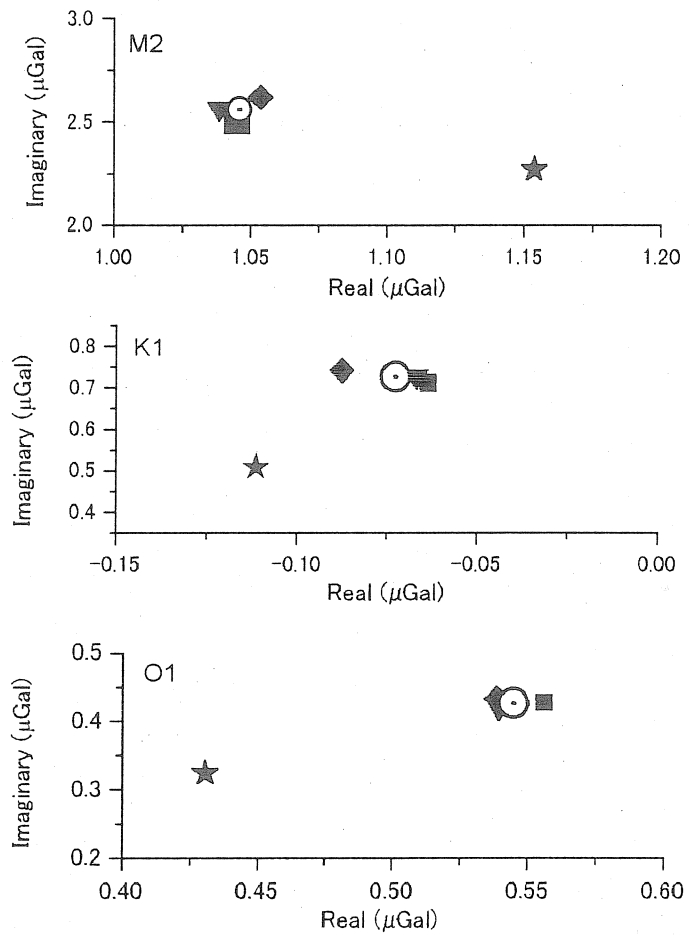

Fig. 1. Comparison of the ocean tide effects at Canberra computed from the four ocean tide models. The ocean models used are shown with the following symbols; Square: NAO99bJ, Reverse triangle: CSR4.0, Diamond: GOT99, and Star: Schwiderski. Dotted Circle shows the mean value over the three models of NAO99bJ, CSR4.0 and GOT99. A loading Green's function for the PREM earth model was used for the computation.

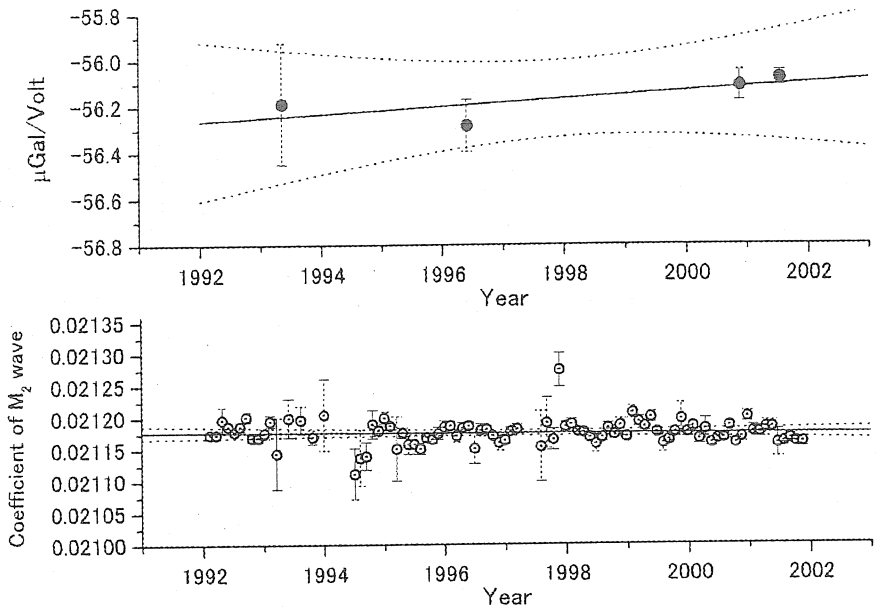

Fig. 2. Comparison between the absolute calibration and the relative sensitivity for the Esashi SG. Top: Results for the absolute calibrations and Bottom: Monthly changes in the M2 amplitude coefficient, which were computed from the data of volt unit. The solid lines and the dotted ones show the result for fitting to a linear model and the 95 % confidence intervals, respectively.

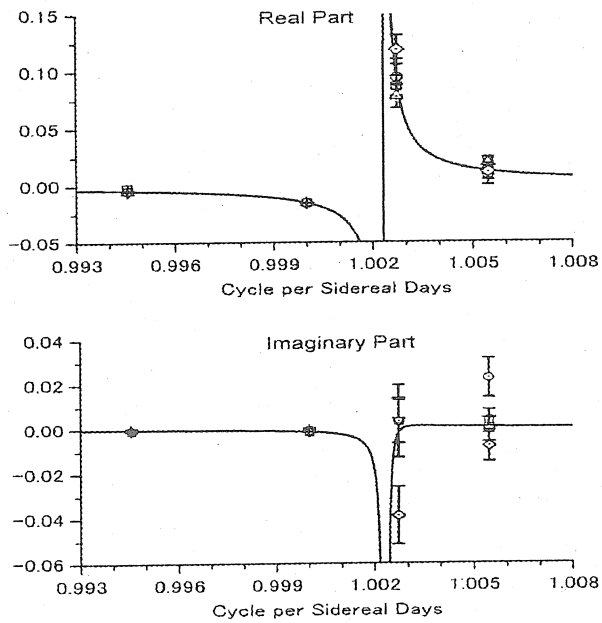

Fig. 3. Comparison between the observed admittances and the best fitted curves. Symbols stand for; Circle: Esashi, Square: Canberra, Triangle: Matsushiro, and Diamond: Membach.

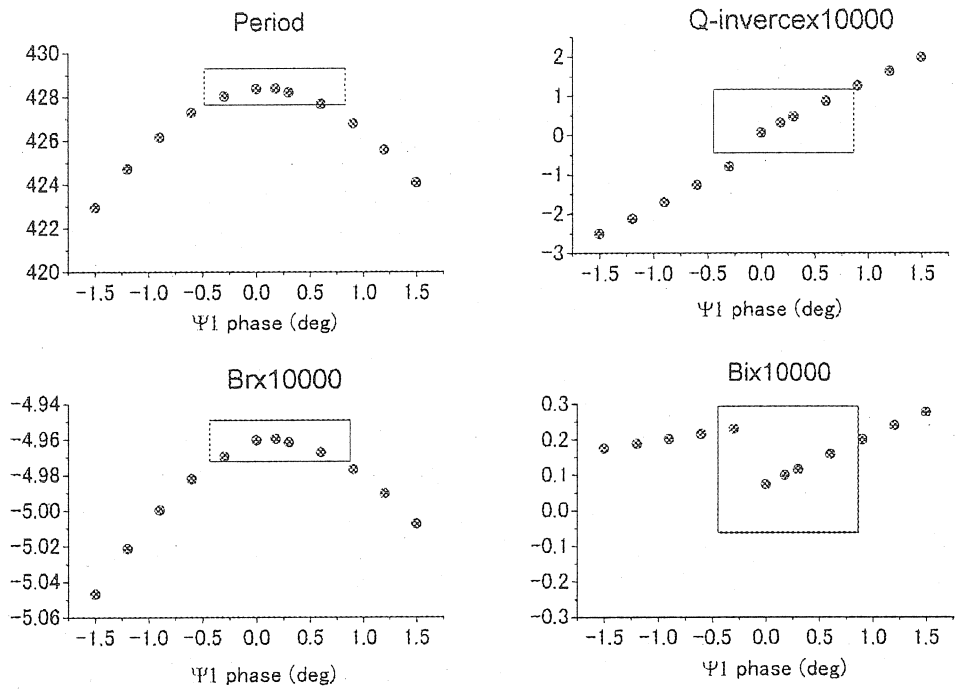

Fig. 4. Effect of the phase of Ψ_1 wave on the estimated FCR parameters. Rectangular boxes show the error range that would be expected from the observed RMS error of the Ψ_1 phase.

New Investigation of Tidal Gravity Results from the GGP Network

Bernard Ducarme*, He-Ping Sun**and Jian-Qiao Xu**
*Chercheur Qualifié au FNRS, Observatoire Royal de Belgique
Av. Circulaire 3, B-1180 Brussels, email: b.ducarme@ksb-orb.oma.be
**Institute of Geodesy and Geophysics, Chinese Academy of Sciences
54 Xu Dong road, 430077 Wuhan, China, email: heping@asch.whigg.ac.cn

Abstract

Some 20 series longer than one year are now available in the GGP data bank, including 3 dual sphere instruments. To eliminate the tidal loading effects we interpolated the contribution of the smaller oceanic waves from the 8 well determined ones i.e. Q_1, O_1, P_1, K_1, N_2, M_2, S_2 and K_2. It was done for six different oceanic models: SCW80, CSR3.0, FES95.2, TPXO2, CSR4.0 and ORI96. In the diurnal band no model is decisively better than the others and a mean tidal loading vector is giving the most stable solution for the study of the liquid core resonance. In the semi-diurnal band however the SCW80 and TPXO2 models are not convenient.

We are investigating mainly the diurnal waves around the liquid core resonance i.e. K_1, ψ_1 and φ_1. The scattering of the corrected amplitude factors for the waves O_1 and K_1 reaches 0.3%. and the tidal factors are determined with a precision slightly better than 0.1%. O1 is fitting perfectly to the DDW99 and MAT01 models but there is an offset of 0.1% for K_1. K1 exhibits a slight phase advance with respect to O1.

From our data set we computed the FCN period and found values very close to the 429.5 days deduced from the VLBI observations.

1. Introduction

Since July 1997 more than 15 superconducting gravimeters are operating in the framework of the Global Geodynamics Project (GGP) (Crossley & al.,1999), following to standardised procedures. Nineteen stations with data sets longer than one year are now available in the GGP data bank, hosted at the Royal Observatory of Belgium, including 3 dual sphere instruments. The one minute sampled original data obtained are pre-processed and analysed at the International Centre for Earth Tides (ICET) using the standard procedures (Ducarme & Vandercoilden, 2000). These data are corrected using a remove restore technique based on the T-soft software (Vauterin, 1998) and decimated to one hour sampling prior to the analysis by ETERNA software (Wenzel, 1996). Atmospheric pressure is the only auxiliary channel available for all the stations. For the dual sphere (CD) instruments the results of the U and L spheres are so close that we computed a common analysis of the two time series. For the stations Strasbourg and Wettzell we consider also the series obtained with the old T005 and T103 instruments. Finally we introduced the results of the renovated ASK228 gravimeter of Pecny (BroZ & al., 1996) which has an RMS error on the unit weight better than many of the oldest cryogenic instruments. Altogether we are thus considering 22 data sets, 10 or them outside Europe. For each of them we are able to extract 22 tidal groups: σ_1, Q_1, ρ_1, O_1, NO_1, π_1, P_1, K_1, ψ_1, φ_1, θ_1, J_1, OO_1, $2N_2$, μ_2, N_2, ν_2, M_2, L_2, T_2, S_2, K_2.

In table 1 we give the details of the different series in increasing ICET station number, which allows to see the regional distribution of stations. For recent instruments, CT or CD series, the RMS error on the unit weight is below one $nm.s^{-2}$. In Potsdam we have the only T model with an error below $1nms^{-2}$.

The barometric efficiency is always close to $-3nms^{-2}/hPa$ with three exceptions: the Askania gravimeter at Pecny, a very low coefficient at Sutherland and a very high one at Syowa. For the 19 other series we have as a mean: 3.368 ± 0.036 nms^{-2}/hPa, with a standard deviation $\sigma = 0.152$ nms^{-2}/hPa.

Table 1

Characteristics of the tidal gravity stations

T: large dewar, CT: compact, CD : dual sphere, ASK: Askania

GGP	ICET	name	Lat.	Long.	Instr.	Data set (days)	RMS error	Baro. Fact. (nms^{-2}/hPa)
BE	0200	Brussels	50.7986	4.3581	T003	6,660	1.743	-3.467±.005
MB	0243	Membach	50.6093	6.0066	CT21	1,728	1.007	-3.286±.006
ST	0306	Strasbourg	48.6223	7.680	T005	3,272	2.265	-3.128±.010
					CT26	817	0.797	-3.394±.007
BR	0515	Brasimone	44.1235	11.1183	T015	1,098	2.576	-3.053±.036
VI	0698	Vienna	48.2493	16.3579	CT25	729	0.662	-3.467±.007
WE	0731	Wetzell	49.1458	12.8794	T103	726	2.639	-3.374±.031
					CD029	2x291	0.667	-3.340±.009
PO	0765	Potsdam	52.3809	13.0682	T018	2,250	0.855	-3.313±.004
MO	0770	Moxa	50.6450	11.6160	CD34	2x580	0.590	-3.320±.005
ME	0892	Metsahovi	60.2172	24.3958	T020	1614	1.299	-3.636±.007
PC	0930	Pecny	49.9200	14.780	*ASK228*	412	0.887	*-4.894±.013*
WU	2647	Wuhan	30.5139	114.4898	CT32	985	0.750	-3.237±..010
KY	2823	Kyoto	35.0278	135.7858	T009	686	3.323	-3.183±..038
MA	2824	Matsushiro	36.5430	138.2070	T011	880	1.163	-3.523±..006
ES	2849	Esashi	39.1511	141.3318	T007	875	1.286	-3.549±..011
SU	3806	Sutherland	-32..3814	20.8109	CD37	(491+304)	0.689	*-2.657±.013*
BA	4100	Bandung	-6.8964	107.6317	T008	420	7.450	-3.524±..243
CB	4204	Canberra	-35.3206	149.0077	CT31	890	0.776	-3.392±..010
BO	6085	Boulder	40.1308	254.7672	CT024	1,401	0.997	-3.518±..007
CA	6824	Cantley	45.5850	284.1929	T012	2,386	1.443	-3.293±..006
SY	9960	Syowa	-69.0070	39.5950	T016	548	1.103	*-4.115±.009*

Table 2

Stability of the tidal analysis results

Station	Instr.	Series	$\delta(O_1)$	$\delta(K_1)$	$\delta(M_2)$	$\delta(S_2)$	Discr. %
BE0200	T003	82/86	1.15375	1.14072	1.18404	1.19826	
		86/91	1.15290	1.13982	1.18334	1.19623	
		91/96	1.15338	1.13967	1.18410	1.19643	
		96/00	1.15344	1.14019	1.18379	1.19587	
							≅0.1%
ME0243	CT21	95/97	1.14939	1.13730	1.18734	1.19285	
		98/00	1.14932	1.13734	1.18750	1.19225	
							<0.1%
ST0306	T005	87/91	1.14708	1.13520	1.18496	1.18750	
		91/96	1.14745	1.13535	1.18510	1.18794	<0.1%
	CT26	97/99	1.14871	1.13704	1.18657	1.18887	
							≅0.1%
WE0731	T103	96/98	1.14424	1.13101	1.17973	1.17684	
	CD29	98/01	1.14820	1.13531	1.18357	1.18170	
							≅0.4%
PO0765	T018	92/95	1.15003	1.13732	1.18607	1.18510	
		95/98	1.14966	1.13738	1.18592	1.18529	
							<0.1%
ME0892	T020	94/96	1.15317	1.14063	1.18178	1.17618	
		97/00	1.15304	1.14078	1.18090	1.17543	
							<0.1%
CA6824	T012	89/95	1.16655	1.14819	1.20434	1.18479	
		97/99	1.16530	1.14745	1.20270	1.18270	
							≅0.1%

To study the stability of the tidal analysis results we subdivided the longest series on one hand and compared the results of different instruments in the same station on the other hand. From the results of Table 2 it is clear that, in each station, the tidal analysis factors of the main waves are stable at the 0.1% level with the exception of Wettzell. We shall see later on that it is the T103 which is not correctly calibrated. On the contrary at Strasbourg the renovated

superconducting gravimeter agrees at the 0.15% level with the older series. As it could be expected the phase differences agree within 0°.5.
It should be pointed out that the internal analysis errors are lower by one order of magnitude.

2. Efficiency of the tidal loading correction

For tidal loading correction we are using 6 different tidal models: SCW80 (Schwiderski, 1980), CSR3.0 (Eanes, 1996), FES95.2 (Le Provost & al., 1994), TPXO2 (Egbert & al., 1994) , CSR4.0 and ORI96 (Matsumoto & al., 1995). Schwiderski is currently used as a working standard since more than 20 years but its coverage is not sufficient in many areas. CSR3 and FES95.2 have been recommended by Shum & al.(1996) and tested by Melchior & Francis (1996) on tidal gravity data.

As a first step we want to compare the efficiency of the different oceanic models for the reduction of the tidal loading influence in our data set.

For any tidal wave let us define:
- the residual vector $\mathbf{B}(B,\beta)$ expressing the difference between the observed tidal vector $\mathbf{A}(A_{obs},\alpha)$ and the body tides vector $\mathbf{R}(A_{DDW},0)$ modelled using the Dehant, Defraigne and Wahr (DDW99) non-hydrostatic model (Dehant et al., 1999), with
$A_{obs}= A_{th}.\delta_{obs}$ and $A_{DDW}= A_{th}.\delta_{DDW}$, i.e. $\mathbf{B}=\mathbf{A}-\mathbf{R}$.

- the final residual vector $\mathbf{X}(X,\chi)$ expressing the discrepancy between the $\mathbf{B}$ vector and the oceanic loading vector $\mathbf{L}(L,\lambda)$, i.e. $\mathbf{X}=\mathbf{B}-\mathbf{L}$.

We can also compute their relative importance as $\mathbf{B}/A_{th}$ and $\mathbf{X}/A_{th}$.

On the other hand, for any tidal vector $\mathbf{A}$, we can compute weighted mean vectors ($\mathbf{M}$) for the Diurnal(D) and Semi-Diurnal(SD) families by the formula:

$\mathbf{M}_D = [2*\mathbf{A}(O1) + \mathbf{A}(P1) + 3*\mathbf{A}(K1)]/6$

$\mathbf{M}_{SD} = [2*\mathbf{A}(M2) + \mathbf{A}(S2)]/3$

The weight of the waves is proportional to their amplitude. It is justified by the fact that the signal to noise ratio in the tidal gravity recording as well as in the oceanic tidal models is directly proportional to the amplitude of the tidal constituent. In table 4 we express for each station the mean vectors $\mathbf{M}_{D,SD}$ ($\mathbf{B}/A_{th}$) and $\mathbf{M}_{D,SD}$ ($\mathbf{X}/A_{th}$)

Table 3. Global comparison of the efficiency of the different oceanic models

	SCW80	CSR3.0	FES95.2	TPX02	CSR4.0	ORI96	MEAN	
	%	%	%	%	%	%	%	N
Diurnal	88.8	93.1	96.3	95.9	94.7	93.0	**95.8**	6
Semi-Diurnal	*82.5*	93.6	94.6	*77.6*	88.5	94.9	**91.7**	6
							94.2	4

For each wave we can define the efficiency of the tidal loading correction as $(\mathbf{B}-\mathbf{X})/\mathbf{B}$.
In a similar way the ratios are thus expressing the mean efficiency of the oceanic loading correction for the correspondent tidal family. As a first step we tried to determine a mean efficiency by

Table 4 . Efficiency $E_D = (M_D(\mathbb{B})-M_D(\mathbb{X}))/M_D(\mathbb{B})$ and $E_{SD} = (M_{SD}(\mathbb{B})-M_{SD}(\mathbb{X}))/M_{SD}(\mathbb{B})$ of tidal loading corrections bands averaged in Diurnal and Semidiurnal bands for different oceanic models

Station No.	Name	Diurnal waves, 6 oceanic models $M_D(\mathbb{B})$		$M_D(\mathbb{X})$		E_D	Semi-Diurnal waves, 4 oceanic models* $M_{SD}(\mathbb{B})$		$M_{SD}(\mathbb{X})$		E_{SD}
		B(%)	β(°)	X(%)	χ(°)	%	B(%)	β(°)	X(%)	χ(°)	%
BE0200	Brussels	0.36	93..94	*0.39*	-28.54	*-7.6*	5.10	60.44	*0.50*	-70.84	**90.3**
MB0243	Membach	0.42	103.19	0.03	-55.20	**91.9**	4.73	56.15	0.15	-103.95	**96.9**
ST0306	StrasbourgT	0.46	127.69	0.16	-169.13	**66.3**	4.13	55.51	0.23	-120.24	**94.4**
	StrasbourgC	0.31	111.64	0.11	-79.75	**65.2**	4.14	53.15	0.29	-84.88	**92.9**
BR0515	Brasimone	0.59	146.84	*0.36*	-157.10	*39.1*	2.25	47.26	*0.56*	-118.43	**75.1**
VI0698	Vienna	0.43	139.07	0.14	-168.50	**66.9**	2.37	40.45	0.33	-120.14	**86.1**
WE0731	WetzellT	0.67	158.51	*0.48*	-169.57	*28.5*	2.68	51.83	*0.59*	-156.66	**78.2**
	WetzellC	0.58	108.94	0.22	100.03	**62.8**	3.40	52.72	0.39	109.45	**88.5**
PO0765	Potsdam	0.37	95.33	0.08	22.72	**78.7**	3.25	43.80	0.07	-57.85	**97.7**
MO0770	Moxa	0.41	111.83	0.03	124.34	**91.9**	3.34	48.34	0.19	-156.35	**94.4**
ME0892	Metsahovi	0.43	33.50	*0.54*	7.79	*-26.0*	2.01	30.91	0.27	-31.26	**86.6**
PC0930	Pecny	0.29	98.74	011	-14.71	**65.2**	2.62	38.76	0.42	-105.12	**84.1**
WU2647	Wuhan	2.16	-23.39	0.38	6.52	**82.5**	1.38	-27.53	0.29	-11.77	**79.3**
KY2823	Kyoto	5.27	2.85	0.24	57.55	**95.5**	4.12	1.88	0.12	104.35	**97.0**
MA2834	Matsushiro	4.77	4.91	0.19	-144.22	**96.0**	3.25	12.55	0.28	-120.98	**91.3**
ES2849	Esashi	6.67	11.98	*0.52*	-12.96	**92.2**	4.63	33.69	*0.63*	-11.005	**86.3**
SU3806	Sutherland	0.75	-57.46	0.24	-74.44	**68.5**	10.02	86.57	0.15	-29.47	**98.5**
BA4100	Bandung	20.88	93.94	*0.57*	-174.12	**97.2**	2.42	-37.40	*0.61*	102.27	**74.6**
CB4204	Canberra	1.85	-61.53	0.40	-2.57	**78.5**	4.64	-71.43	0.33	-84.23	**93.0**
BO6085	Boulder	3.00	60.87	0.22	49.00	**92.6**	0.48	77.14	0.27	-112.09	*43.4*
CA6824	Cantley	1.59	40.92	*0.49*	-8.42	**69.2**	3.84	-24.01	*0.62*	-107.37	**83.7**
SY9960	Syowa	8.23	5.95	*1.22*	-18.09	**85.2**	27.08	0.97	*6.36*	5.37	**76.5**

* SCW80 and TPX02 excluded

averaging the results of all the stations for each oceanic model (Table 3). For the diurnal waves efficiencies are larger than 90% except for SCW80. In the semi-diurnal band however two models have a much lower efficiency, SCW80 and TPX02, and it was thus decided to exclude them for the detection of anomalous stations. Detailed investigations showed that it was mainly in Western Europe that these models were less efficient for tidal loading correction.

For well calibrated instruments large values of $M_{D,SD}(\mathbf{X})$ will correspond to imperfect loading correction. However large values of $M_{D,SD}(\mathbf{X})$ can also points to the stations with calibration errors, if the corresponding phase is close to 0° or 180°.
To detect calibration errors we averaged for each station the $M_{D,SD}(\mathbf{X})$ vectors of all the oceanic models, 6 in the diurnal band but only 4 in the semi-diurnal one..

In Table 4 the residues are scaled in function of the theoretical amplitude of the waves and are thus expressed in percentage. In the diurnal band the $M_D(\mathbf{B})$ residues are below 0.5% in Europe but reach 5% in Japan and up to 20% in Bandung, due to its very low latitude. In the semi-diurnal band the effect are decreasing from 5% to 2.5% from West to East in Europe. They are generally large elsewhere, except in Boulder. In Syowa and Sutherland the effects to be explained reach more than 10%.

Some series are clearly anomalous in both tidal families as Syowa and Bandung. It was expected in Syowa as the station is located at the Antarctic coast and for all the cotidal maps it is covered by water. For Bandung it is well known that Indonesian archipelago has very complex oceanic tides and it is not surprising that the oceanic loading evaluation not precise enough. The calibration is probably not in question as the final residue has a phase of 90°. In Boulder the very low efficiency of the tidal loading correction in SD is simply due to the fact that the loading amplitude is very low in this station.

In Europe the calibrations of Brasimone, Brussels and WetzellT are certainly questionable with final residues reaching 0.5%. Outside of Europe Esashi and Cantley seem also offset.

For further studies of the liquid core resonance effects we can conclude that, as previously noticed by Melchior & Francis (1996), no model is decisively better than the others in the diurnal band (Table 3) and that a mean tidal loading vector will probably give the most stable solution. The stations of Syowa and Bandung are probably to be rejected. A calibration error close to 0.5% is strongly suspected in Brussels(BE), Brasimone(BR), Cantley(CA), Esashi(ES) and WetzellT (WE,T103) and perhaps in Metsahovi(ME). Similar conclusions have been expressed by Baker & Bos (2001) using the FES99 oceanic model

3. Interpolated tidal loading effects

The tidal load vectors are directly proportional to the amplitude of the wave in the exciting tidal potential and the change of phase exhibits a regular behaviour with respect to the frequency shift. Figure 1 shows typical examples of the frequency dependant phase shift of the load vectors for different parts of the world. Therefore it is rather easy to interpolate the load vectors for the smaller components starting from the eight major components (Q1, O1, P1, K1, N2, M2, S2, K2). The load vectors have to be first normalised dividing by their theoretical amplitude in the tidal potential. However in the Diurnal band the most interesting weak components ψ_1 and φ_1 need in fact to be extrapolated as they are outside of the frequency band extending from Q1 to K1.

Another difficulty is that the core resonance does also affect the oceanic tides (Wahr and Sasao, 1981). To assume a smooth behaviour we have thus first to correct this resonance effect on the main diurnal waves, especially K1, interpolate or extrapolate the weaker

components and apply again the resonance on the results. The effect of the resonance is clearly seen on Figure 1.

This procedure has been applied on the real and imaginary parts of the oceanic load vectors computed using the 6 selected oceanic models. We computed 14 additional components: σ_1, ρ_1, NO_1, π_1, ψ_1, φ_1, θ_1, J_1, OO_1, $2N_2$, μ_2, ν_2, L_2 and T_2. The efficiency of the ocean load corrections observed for the main tidal waves is confirmed for the weaker constituents which have been interpolated or even extrapolated. In the diurnal band the mean amplitude factor is uniformly reduced of 0.6% to 0.7% for all the waves and we are thus confident in the fact that our tidal loading correction is also improving the results of the small resonant waves ψ_1 and φ_1.

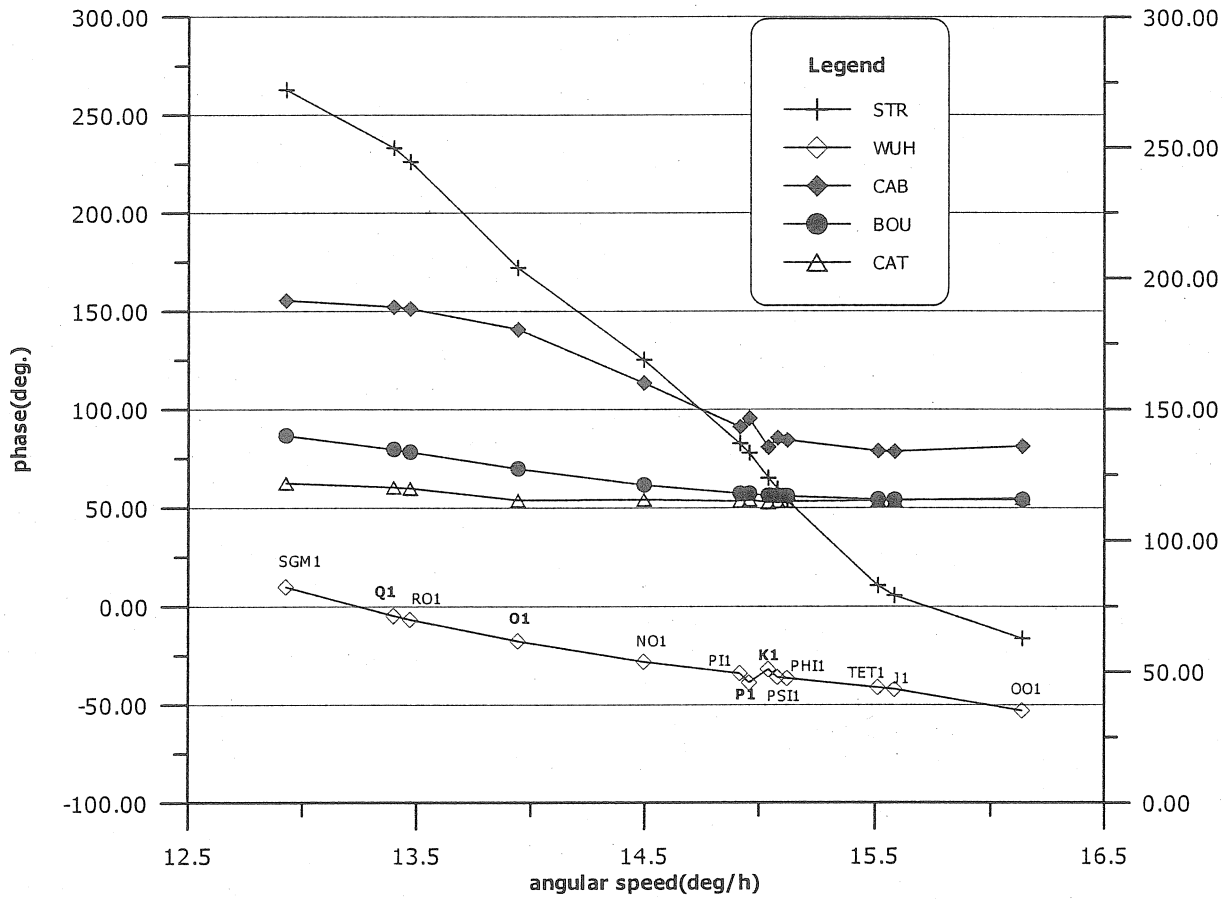

Figure 1. Phase shift of the oceanic load vectors(Diurnal band)
STR: Strasbourg, WUH: Wuhan, CAB: Canberra, BOU:Boulder, CAT: Cantley

4. Mean corrected tidal factors in the diurnal band

For each of the 13 diurnal wave groups we computed the corrected tidal gravity vectors $A_c(\delta_c A_{th}, \alpha_c)$ using the 6 tidal models, by the relation:

$$A_c(\delta_c A_{th}, \alpha_c) = A(A_{obs},\alpha) - L(L,\lambda)$$

Our main goal was to compute the best "mean" tidal factors for each wave group by averaging the six tidal models first and then the 22 series of observations. For each wave we constructed a double entry table similar to Table 5 and computed the mean value for each line or series. At this level it is important to reject the anomalous stations. In paragraph 2 we found several anomalous data sets. The problem is to know if they should be rejected beforehand. For

station with suspicious calibration at the 0.5% level it is worth to point out that their effect is practically cancelling on the mean as we find three station with too low values(Brasimone, WetzellT and Bandung) and three with too high values (Brussels, Metsahovi and Esashi). Bandung is off set by more than 1% and has certainly to be rejected. On the other hand phase anomalies are also an important criterion to reject series. Moreover for the smaller constituents the noise level becomes a larger source of variability than an 0.5% calibration error, especially for stations with a large RMS error (Table 1). We decided thus to apply simply the criterion of the 3σ level rejection on amplitude factors and phase differences for the 22 series. As expected Syowa was always rejected. Bandung was accepted for the largest constituents (K_1, O_1 and P_1). Kyoto was bad for all the small waves i.e. waves with amplitude lower than 2μgal at 45° or 5% of K1. Brasimone was rejected 6 times and a few other stations accidentally. For P_1 and K_1 we kept 21 data sets and as a minimum 17 for ψ_1. The lowest standard deviations are 0.3% on the amplitude factors and 0.08° on the phase differences for P_1 and K_1. It explains why only stations with a large calibration error will be rejected as for example Syowa in Table 7. For elimination due to the phase we see two examples in Table 5: Syowa and Wetzell C.

We can draw some interesting conclusions from Table 5. As already stated the mean observed tidal factor 1.1614 is reduced to 1.1544 and the discrepancy with the DDW99 model is thus reduced from 0.62% to 0.1%. We see also that the standard deviations on the lines are systematically different from the standard deviations on the columns . We computed the standard deviation of the mean corrected amplitude factor and phase difference ($\delta_c = 1.1544$, $\alpha_c = 0.01°$) starting either from each series averaged over the 6 maps (column MEAN1) σ_1 or from the average of the 20 series for each map (line MEAN2) σ_2 and found very different results:

on δ_c $\sigma_1 = 0.32\%$ and $\sigma_2 = 0.07\%$

on α_c $\sigma_1 = 0.045°$ and $\sigma_2 = 0.025°$.

If we consider that the variance on each element of the table is the same, the variance on the mean is divided by the number of elements i.e. 6 for a line or 20 for a column. The two standard deviations should then be in the ratio of the square roots i.e. 1.8. It is true for the phase differences with a ratio $\sigma_1 / \sigma_2 = 1.8$, but it is not true for the amplitude factor with a ratio 4.6 i.e. 2.5 times larger. On one hand it means that the dispersion due to the calibration errors in the stations is larger than the dispersion due the difference between the oceanic tidal models. On the other hand it confirms that the phase lag corrections are correct at the level of a few seconds.

In Table 6 we compare σ_1 and $\sigma_2.(\sqrt{N}/6)$ and we see that this noise amplification for the δ factors is true for all the waves except at the very edge of the spectrum for the waves σ_1 and OO_1, where the extrapolation of the oceanic tides models increases the noise.

Table 5

Complete data set for wave O_1

Stations are ordered according to absolute value of latitude

Data sets	Observed		SCW80		CSR3.0		FES96.2		TPXO2		CSR4.0		ORI96		MEAN 1		STD. DEV.		MODEL	Discr.
	δ	α	δ	α	δ	α	δ	α	δ	α	δ	α	δ	α	δ	α	δ	α	δ	
*SY9960	1.2690	.84	1.1814	-.11	1.1698	-.83	1.1625	.11	1.1685	.45	1.1596	-.87	1.1698	-.07	**1.1686**	**-.219**	.0076	.53	1.15439	1.23%
ME0892	1.1531	.25	1.1567	.03	1.1570	.10	1.1566	.05	1.1577	.07	1.1591	.03	1.1653	.06	1.1587	.057	.0033	.03	1.15435	.38%
PO0765	1.1499	.19	1.1537	.09	1.1543	.10	1.1536	.07	1.1547	.13	1.1544	.08	1.1547	.03	1.1542	.083	.0005	.03	1.15431	-.01%
BE0200	1.1533	.07	1.1566	.01	1.1577	.04	1.1569	-.02	1.1582	-.03	1.1574	-.04	1.1577	-.16	1.1574	-.033	.0006	.07	1.15430	.27%
MO0770	1.1487	.14	1.1527	.06	1.1534	.09	1.1525	.04	1.1534	.10	1.1534	.05	1.1535	-.01	1.1531	.055	.0004	.04	1.15430	-.10%
MB0243	1.1494	.11	1.1530	.05	1.1541	.08	1.1533	.02	1.1541	.06	1.1539	.02	1.1539	-.06	1.1537	.028	.0005	.05	1.15430	-.05%
PC0930	1.1489	.08	1.1526	.01	1.1535	.04	1.1524	-.01	1.1535	.03	1.1534	-.02	1.1537	-.05	1.1532	.000	.0005	.03	1.15429	-.10%
WE0731T	1.1442	.12	1.1480	.05	1.1489	.08	1.1479	.03	1.1488	.07	1.1488	.03	1.1490	-.01	1.1486	.042	.0005	.03	1.15429	-.50%
*WE0731C	1.1482	.23	1.1520	.17	1.1528	.19	1.1518	.14	1.1528	.19	1.1528	.15	1.1530	.11	1.1525	**.158**	.0005	.03	1.15429	-.15%
ST0306T	1.1472	.07	1.1515	.04	1.1524	.06	1.1513	.01	1.1522	.05	1.1521	.01	1.1523	-.04	1.1520	.022	.0005	.04	1.15428	-.20%
ST0306C	1.1487	.06	1.1530	.02	1.1539	.04	1.1528	-.01	1.1537	.03	1.1536	-.01	1.1538	-.06	1.1535	.002	.0005	.04	1.15428	-.07%
VI0698	1.1479	.10	1.1514	.03	1.1525	.05	1.1513	.00	1.1524	.05	1.1524	.00	1.1524	-.02	1.1521	.018	.0006	.03	1.15428	-.19%
CA6824	1.1663	.54	1.1590	-.01	1.1579	.05	1.1587	-.03	1.1590	-.05	1.1579	.01	1.1586	-.02	1.1585	-.008	.0005	.03	1.15427	.37%
BR0515	1.1462	.07	1.1500	.06	1.1508	-.01	1.1498	-.07	1.1496	.02	1.1504	-.05	1.1506	-.07	1.1502	-.020	.0005	.05	1.15426	-.35%
BO6085	1.1642	1.31	1.1552	.15	1.1537	.08	1.1563	.02	1.1551	.02	1.1542	.04	1.1547	.08	1.1549	.065	.0009	.05	1.15423	.06%
ES2849	1.2215	1.33	1.1540	-.09	1.1605	-.12	1.1623	.12	1.1619	.17	1.1580	-.06	1.1612	-.09	1.1596	-.012	.0032	.12	1.15423	.47%
MA2834	1.2043	.70	1.1486	-.13	1.1535	-.18	1.1535	.03	1.1542	.11	1.1529	.00	1.1541	-.14	1.1528	-.052	.0021	.11	1.15421	-.12%
CB4204	1.1748	-.76	1.1593	-.14	1.1566	-.02	1.1541	-.16	1.157	.07	1.1567	.00	1.1575	.10	1.1570	-.025	.0017	.11	1.15421	.24%
KY2823	1.2097	.59	1.1523	-.01	1.1563	-.06	1.1558	.15	1.1543	.20	1.1547	.06	1.1567	-.01	1.1550	.055	.0016	.10	1.15420	.07%
SU3806	1.1636	.12	1.1555	-.11	1.1535	-.16	1.1533	-.11	1.1554	.01	1.1533	-.10	1.1543	-.11	1.1542	-.097	.0007	.10	1.15419	.00%
WU2647	1.1793	-.38	1.1571	-.03	1.1590	-.15	1.1583	.08	1.1584	.14	1.1586	-.05	1.1588	-.06	1.1584	-.012	.0007	.10	1.15418	.36%
BA4100	1.1254	10.93	1.1587	*1.07	1.1586	.67	1.1460	.02	1.1528	-.66	1.1394	.16	1.1413	*1.54	1.1492	.048	.0083	.55	1.15410	-.43%
MEAN 2	1.1614	.010	1.1537	.004	1.1549	.039	1.1538	.012	1.1549	.030	1.1537	.008	1.1554	-.034	**1.1544**	**.010**	**.0007**	**.025**	1.15425	.01%
STD.DEV.			0.0032	.076	0.0029	.175	0.0038	.071	0.0032	.174	0.0043	.057	0.0038	.069	**0.0032**	**.045**				

stations to be eliminated

	ampl.	phase
1	SY09960*	SY09960*
2		WE07313*

5. Comparison of the experimental results with different models

In table 6 we give the mean corrected tidal factors and phase differences for the 13 diurnal components and we compare them with several models DDW99 (non hydrostatic), MAT01 (Mathews, 2001) and several models obtained by fitting the data on a resonance model, using the waves O_1, P_1, K_1, ψ_1 and ϕ_1 i.e.: SDX1, SDX2 and SDX3 (cfr §6 and Table 7). The models are normalised on O1 with $\delta = 1.1544$ and $\alpha = 0.0°$.

In Table 6 we see that in fact these three models are very close when expressed in terms of amplitude factors and phase differences. On K1 the difference is only at the level of the fourth decimal, smaller than the associated RMS error on the tidal factor. Even on ψ_1 the difference is at the level of the experimental errors. As expected the SXD2 and SXD3 models, which are using directly the experimental values of Table 8, fit very well ψ_1, with a slight positive phase

For what concerns the comparison of the mean observed tidal factors with the DDW99 (non hydrostatic) and MAT01 models there are some contradictory remarks. These models are perfectly fitting O_1 at the level of the RMS errors, but are 0.1% too low with respect to K_1. In a previous reduction with 15 series(Ducarme & Sun, 2001) we already found a similar offset with $\delta(K_1) = 1.1356$. Concerning the slight phase advance of K_1 with respect to O1, forecasted by Mathews, no firm conclusion is possible as its magnitude is of the order of the associated RMS error on the phase differences. The positive result obtained in Ducarme & Sun (2001) is probably an artefact of the Schwiderski model in Western Europe. Concerning the small resonant waves ψ_1,and φ_1 the RMS errors have been largely improved as, in the previous paper, we had only 9 selected stations, most of them in Europe. The model of Mathews fits better the observations and the experimental models, especially for φ_1.

6. The Free Core Nutation

As already explained, we computed different solutions for the Free Core Nutation (FCN) deduced from our experimental data.

SDX1: stacking of the results of 19 stations (Sun & al., 2002)

SDX2: direct computation from the experimental results of table 8 with a weight inversely proportional to the RMS error on the amplitude factors $\sigma_1/\sqrt{N}$

SDX3: direct computation from the experimental results of table 8 with a weight proportional to $A_{th}.\sqrt{N}/\sigma_1$

The best solutions are obtained with the mean of the oceanic models (6 maps). The three solutions converge to the value deduced from the VLBI observations: 429.5 days.

It should be pointed out that the Mathews model is associated with a FCN period of 430,04 (429.93-430.48) days (Mathews & al.,2002). In the DDW99 model (Dehant & al., 1999) the FCN period was forced on 431 days, which was the value given by the VLBI observations at that time.

For SDX2 and SDX3 we also performed individual computations with the results obtained using each of the 6 oceanic models for loading corrections. These solutions are scattered between 425.3 and 435.6. CSR4.0 gives the minimum value and TPXO2 the maximum one. ORI96 provides also a too large value. The two approaches SXD2 and SXD3 are always very close.

Table 6

Mean tidal factors for the diurnal waves

	Mean factors		σ_1	σ_2*	DDW	MAT01	SXD1	SXD2	SXD3
Wave	δ_c	α_c	%	%		δ	δ	δ	δ
N	*(ε_δ)*	*(ε_α)*				*(α)*	*(α)*	*(α)*	*(α)*
σ_1	1.1550	0.164	0.47	0.52	1.1542	1.1541	1.15467	1.15467	1.15467
19	*±.0011*	*±.043*				*-0.028*	*0.000*	*0.000*	*0.000*
Q_1	1.1538	0.044	0.37	0.25	1.1543	1.1541	1.15458	1.15459	1.15459
20	*±.0008*	*±.026*				*-0.026*	*0.000*	*0.000*	*0.000*
ρ_1	1.1545	0.017	0.35	0.20	1.1543	1.1541	1.15457	1.15457	1.15457
17	*±.0009*	*±.048*				*-0.026*	*0.000*	*0.000*	*0.000*
•O_1	1.1544	0.010	0.32	0.13	1.1543	1.1540	1.15440	1.15440	1.15440
20	*±.0007*	*±.010*				*-0.024*	*0.000*	*0.000*	*0.000*
NO_1	1.1553	-0.023	0.58	0.20	1.1539	1.1535	1.15386	1.15385	1.15385
19	*±.0012*	*±.041*				*-0.021*	*0.000*	*0.000*	*0.000*
π_1	1.1510	-0.054	0.67	0.12	1.1507	1.1504	1.15091	1.15087	1.15087
17	*±.0016*	*±.091*				*-0.008*	*-0.002*	*-0.002*	*0.000*
P_1	1.1501	-0.039	0.29	0.13	1.1491	1.1489	1.14949	1.14953	1.14942
21	*±.0006*	*±.016*				*-0.002*	*-0.003*	*-0.003*	*0.000*
K_1	1.1362	0.025	0.31	0.11	1.1348	1.1349	1.13664	1.13643	1.13641
21	*±.0007*	*±.015*				*0.062*	*-0.004*	*-0.012*	*0.004*
ψ_1	1.2630	0.073	1.36	0.10	1.2717	1.2655	1.25993	1.26302	1.26217
16	*±.0034*	*±.230*				*0.022*	*0.360*	*0.071*	*0.110*
φ_1	1.1691	0.061	0.79	0.25	1.1706	1.1693	1.16856	1.16878	1.16876
19	*±.0018*	*±.096*				*-0.068*	*0.016*	*0.010*	*0.002*
θ_1	1.1569	0.097	0.79	0.24	1.1571	1.1564	1.15643	1.15646	1.15646
18	*±.0019*	*±.132*				*-0.028*	*0.002*	*0.001*	*0.000*
J_1	1.1557	0.014	0.52	0.27	1.1569	1.1562	1.15622	1.15625	1.15625
19	*±.0012*	*±.055*				*-0.027*	*0.001*	*0.001*	*0.000*
OO_1	1.1513	0.300	0.75	0.58	1.1563	1.1556	1.15557	1.15559	1.15559
18	*±.0017*	*±.071*				*-0.024*	*0.001*	*0.001*	*0.00*

N: number of series, σ_1: standard deviation on series, $\sigma_2^* = \sigma_2.(\sqrt{N}/6)$: normalised standard deviation on oceanic models, ε : RMS errors on tidal factors, • reference for SXD models.

Table 7

Experimental models of the core resonance

Oceanic model	SXD1		SXD2		SXD3	
	T(days)	Q	T(days)	Q	T(days)	Q
6 maps	429.9	20769	429.1	-1725650	429.7	54871
SCW80	432.1	12760	428.3	280847	429.5	78378
CSR3.0	428.6	28503	429.1	-34855	429.3	-75594
FES95.2	432.9	17492	427.9	1467138	427.2	41093
TPXO2	425.9	16250	432.4	-31252	435.6	-117705
CSR4.0	434.7	-60940	425.9	1732741	425.3	43722
ORI96	434.6	9387	431.8	24732	433.3	15152

SXD: Sun-Xu-Ducarme (Sun & al., 2002b)

7. The semi-diurnal waves

We applied a similar procedure to compute mean tidal factors and phase differences for the 9 semi-diurnal components (Table 8).It seems that the extrapolation of the oceanic loading is less stable than in the diurnal band. Very large error bars are associated with $2N_2$ and μ_2, T_2 and ν_2 give satisfactory results but not L_2.
In table 8 we give the solutions using 6 and 4 tidal models respectively. The systematic difference of the results obtained using SCW80 and TPX02, already detected in §2, is fully confirmed. The standard deviation σ_2 is greatly reduced using only 4 models. For all the waves except K_2 there is a systematic increase of at least 0.1% after the suppression of the 2 models. For M2 the mean corrected tidal factors computed using SCW80 and TPX02 are 0.5% lower than the values obtained with the 4 other ones, which agree between themselves to within 0.05% The solution with 4 oceanic models agree with the reference value 1.1619 for the two major constituents M_2 and S_2.

For what concerns the phase differences they are close to zero for the frequency band ranging from N_2 to M_2, but there is a large systematic offset of -0.25° from L_2 to S_2.

It seems that the more turbulent characteristics of the semi-diurnal oceanic tides are responsible of the less stable solutions and increase the difference between the oceanic models. We should investigate more recent models such as FES99.

Table 8

Averaged tidal factors for the semi-diurnal waves

	Mean factors 6 maps		σ_1	σ_2*	DDW	Mean factors 4maps		σ_1	σ_2**
Wave *N*	δ_c *(ε_δ)*	α_c *(ε_α)*	%	%		δ_c *(ε_c)*	α_c *(ε_c)*	%	%
$2N_2$	1.1623	-0.169	0.68	0.84	1.1619	1.1658	-0.247	0.83	0.20
13	*±.0019*	*±.132*				*±-.0023*	*±.166*		
μ_2	1.1609	-0.247	0.80	1.11	1.1619	1.1646	-0.306	1.06	0.26
19	*±.0018*	*±.0245*				*±.0024*	*±.155*		
N_2	1.1613	-0.086	0.35	0.81	1.1619	1.1631	-0.110	0.41	0.11
18	*±.0009*	*±.048*				*±.0009*	*±.033*		
ν_2	1.1598	-0.045	0.50	0.80	1.1619	1.1618	-0.036	0.40	0.16
21	*±.0011*	*±.035*				*±0.009*	*±.0034*		
M_2	1.1602	0.008	0.31	0.55	1.1619	1.1621	-0.009	0.28	0.11
19	*±.0007*	*±.021*				*±.0006*	*±.024*		
L_2	1.1604	-0.313	1.14	0.31	1.1619	1.1615	-0.297	1.18	0.16
16	*±.0029*	*±.099*				*±.0030*	*±.0092*		
T_2	1.1616	-0.360	0.51	0.35	1.1619	1.1625	-0.432	0.48	0.39
15	*±.0013*	*±.061*				*±.0012*	*±.066*		
S_2	1.1603	-0.229	0.16	0.34	1.1619	1.1614	-0.280	0.20	0.17
19	*±.0004*	*±.032*				*±0.004*	*±0.037*		
K_2	1.1634	-0.034	0.31	0.40	1.1619	1.1638	-0.114	0.35	0.38
20	*±.0007*	*±.047*				*±.0008*	*±.060*		

N: number of series, σ_1: standard deviation on series, σ_2*= $\sigma_2.(\sqrt{N/6})$: normalised standard deviation (6 oceanic models), σ_2**= $\sigma_2.(\sqrt{N/4})$: normalised standard deviation (4 oceanic models), ε : RMS errors on tidal factors.

8. Conclusions

We performed a careful study of the results obtained with superconducting gravimeters installed in 20 different stations, most of them belonging to the GGP network (Crossley et al., 1999). To take full advantage from the unprecedented precision of these data, it was necessary to compute tidal loading corrections not only for eight main waves (Q1, O1, P1, K1, N2, M2, S2, K2) but also for other weaker components, especially in the diurnal band near the liquid core resonance frequency. We had thus to interpolate or extrapolate the existing load vectors

at neighbouring frequencies, taking into account the effect of the resonance itself on the oceanic tides, in order to keep only smooth functions of the frequency. We used 6 different tidal models SCW80, CSR3.0, FES96.2, TPXO2, CSR4.0 and ORI96.

To have an idea of the efficiency of these load corrections, we used weighted average of the main diurnal or semi-diurnal components to compute the discrepancy between the observed tidal vectors and the DDW99 non-hydrostatic model, before and after tidal loading correction. We found efficiencies close to 95% in the diurnal as well as the semi-diurnal band for the mean of the 6 tidal models. However SCW80 is less efficient in the two tidal bands and TPXO2 not convenient in the semi-diurnal one.

We found that there are still calibration errors at the 0.5% level in the GGP network. This fact is emphasised by the fact that, for most of the tidal waves, the standard deviation on the stations is 2.5 times larger than the standard deviation on the oceanic models.

We computed for 13 diurnal components mean values of the corrected amplitude factors and phase differences and compared them with several models of the FCN resonance.

The mean amplitude factor for O1 agrees perfectly with the DDW99 non-hydrostatic model as well as with the MAT01 model, but there is an offset of 0.1% on K1. The model of Mathews fits better the observed resonance. However we cannot confirm the predictions of the MAT01 model i.e. a slight phase advance for K1 and ψ_1,contrasting with a phase lag for φ_1 as the RMS error on the phases is still too large. A phase very slight phase advance of K_1 is also found in the SXD3 model.

Different computations of the FCN period from our data set gave quite satisfactory results as we obtain periods comprised between 429.1 and 429.9 days, converging towards the value 429.5 days deduced from VLBI observations.

For the 9 semi-diurnal constituents the modelling is not good. SCW80 and TPX02 give too low corrected amplitudes factors (0.5% for M_2) and the interpolation procedure is not stable. It seems that the more turbulent characteristics of the semi-diurnal oceanic tides are responsible of less stable solutions and increase the differences between oceanic models.

Acknowledgements

The authors are grateful to D.Crossley , GGP Chairman, and all the GGP station managers: G.Casula (Brasimone, I), H.J.Dittfeld (Potsdam, D), M.&G.Harnisch (Wettzell, D), J.Hinderer (Strasbourg, F), Y.Imanishi(Matsushiro,JP), C.Kroner(Moxa,D), J.Merriam (Cantley, CDN), B.Meurers (Vienna,A), J.Neumeyer (Sutherland, SA), T.Sato(Esashi, JP and Canberra, AUS), K.Shibuya (Syowa, Antarctica), S.Takemoto (Bandung, Indonesia and Kyoto, JP), M.Van Camp (Membach, B), T.Van Dam and D.Crossley (Boulder, USA) and H.Virtanen (Metsahovi, SF). Z.Simon provided the excellent data set of Pecny, Czech Republic.

The authors wishes to express their thanks to M.Hendrickx and L.Vandercoilden, from the Royal Observatory of Belgium, who are maintaining the GGP data base at ICET and preprocessing all the incoming data before decimation to hourly intervals. This study was realised in the framework of the Bilateral Scientific and Technical Agreements between Belgium and China (project "SG observations and Geodynamics", BL/33/C17). H.P.Sun and J.Q. Xu are partly supported by the Natural Sciences Foundation of China, grants n° 49925411 and 40174022.

References

Baker, T.F., Bos, M.S. (2001): Tidal gravity observations and ocean tide models. Proc. 14th Int. Symp. on Earth Tides, Journal of the Geodetic Society of Japan, 47, 1, 76-81.

Broz, J., Simon Z., Zeman, A.(1997): Tidal station Pecny: Results of 20 years of observation with the gravimeters GS15 No 228. VUGTK, Proceedings of Research Work 1996, 75-88

Crossley, D., Hinderer, J., Casula G., Francis O., Hsu, H.T., Imanishi, Y., Jentzsch G., Kääriäinen J., Merriam, J., Meurers B., Neumeyer J., Richter B., Shibuya K., Sato T., Van Dam T. (1999): Network of superconducting gravimeters benefits a number of disciplines. EOS, **80**, 11, 121/125-126

Dehant, V., Defraigne, P. and Wahr, J. (1999): Tides for a convective Earth J. Geophys. Res., **104**, B1, 1035-1058.

Ducarme, B., Sun, H.P. (2001): Tidal gravity results from GGP network in connection with tidal loading and Earth response. Proc. 14th Int. Symp. on Earth Tides, Journal of the Geodetic Society of Japan, **47**, 1, 308-315.

Ducarme, B., Vandercoilden, L. (2000): First results of the GGP data bank at ICET. Proc. Workshop "High Precision Gravity Measurements with application to Geodynamics, March 24-26,1999. Cahiers du Centre Européen de Géodynamique et de Séismologie, **17**, 117-124.

Eanes, R., Bettadpur (1996): The CSR3.0 global ocean tide model: Diurnal and Semi-diurnal ocean tides from TOPEX/POSEIDON altimetry, CRS-TM-96-05, Univ. of Texas, Centre for Space Research, Austin, Texas

Egbert, G., Bennett, A., Foreman, M. (1994): TOPEX/Poseidon tides estimated using a global inverse model. Journal of Geophysical Research, **99**(C12), 24821-24852.

Le Provost, C., Genco, M.L., Lyard, F., Vincent, P., Canceil, P.(1994): Spectroscopy of the ocean tides from a finite element hydrodynamic model. Journal of Geophysical Research, **99**(C12), 24777-24797.

Mathews, P.M. (2001): Love numbers and gravimetric factor for diurnal tides. Proc. 14th Int. Symp. on Earth Tides, Journal of the Geodetic Society of Japan, **47**, 1, 231-236.

.Mathews, P.M., Herring, T.A., Buffett, B.A. (2002): Modeling of nutation-precession: New nutation series for nonrigid Earth and insights into the Earth's interior. Journal of Geophysical Research (under press).

Matsumoto, K., Ooe, M., Sato, T., Segawa, J. (1995): Ocean tides model obtained from TOPEX/POSEIDON altimeter data. J. Geophys Res., **100**, 25319-25330.

Melchior, P., Francis, O. (1996): Comparison of recent ocean tide models using ground-based tidal gravity measurements. Marine Geodesy, **19**, 291-330

Schwiderski, E.W. (1980): Ocean Tides I, Global ocean tidal equations. Marine Geodesy, **3**, 161-217.

Shum, C.K., Andersen, O.B., Egbert, G., Francis, O., King, C., Klosko, S., Le Provost, C., Li X., Molines, J.M., Parke, M., Ray, R., Schlax, M., Stammer D., Temey, C., Vincent P., Woodworth P.L., Wunsch C.(1996): Comparison of newly available deep ocean tide models by the TOPEX/POSEIDON Science Working Team. Journal of Geophysical Research

Sun, H.P., Ducarme, B., Xu, J.Q.(2002): Determination of the Free Core Nutation Parameters by Stacking Tidal Gravity Measurements from GGP network. Proc. GGP Workshop, Jena, March 11-15,2002.

Vauterin, P. (1998): Tsoft: graphical & interactive software for the analysis of Earth Tide data, Proc. Thirteenth Int. Symp. Earth Tides, Brussels, July 22-25 1997, Observatoire Royal de Belgique, Série Géophysique, 481- 486.

Wahr, J.M., Sasao, T. (1981): A diurnal resonance in the ocean tide and in the Earth's load response due to the resonant free core nutation. Geoph. J. R. Astr. Soc., **64**, 747-765.

Wenzel, H.G.(1996): The nanogal software: data processing package ETERNA 3.3, Bull. Inf. Marées Terrestres, **124**, 9425-9439.

THEORETICAL DESCRIPTION OF THE EXTENSIONAL AND ROTATIONAL STRAIN TENSOR COMPONENTS

Varga P., Mentes Gy., Eperne Papai I.
GEODETIC AND GEOPHYSICAL RESEARH INSTITUTE OF THE HUNGARIAN ACADEMY OF SCIENCES
Sopron, Csatkai Endre u. 6-8,H-9400, Hungary.
E-mail:varga@seismology.hu

Abstract:

Equations are provided for scientists dealing with deformations of the Earth. The equations are based on spheroidal Love-Shida numbers for the case of a symmetric, non-rotating, elastic, isotropic (SNREI) Earth with a liquid core. By these means, the strain tensor components were calculated for the case of zonal, tesseral and sectorial tides both for extensional and rotation strain tensor components.

1. INTRODUCTION

The study of strains due to different geophysical phenomena has been discussed in research contributions since long. Neverthaless the equations which describe the tensor components are often consist misprints and the complete description according to authors knowledge never was publisted earlier.
The paper is using the similar way of the derivation of theoretical equations as it was done by Varga & Grafarend (1996) for the stress tensor components. A special attention is given to the rotational strain components because they can be used succesfully in study of tectonical processes, in observation of seismic waves and in earth tidal studies (Watanabe, 1962; Ozawa 1975; Voosoghi 2000).

2. THE TIDAL POTENTIAL AND TIDE GENERATED DISPLACEMENTS

The tidal potential can be written as (Varga, Grafarend, 1996)

$$W_{2i} = \frac{3}{4} GM \frac{r^2}{d^3} Y_{2i}(\Phi, \lambda) = V_2(r, d) Y_{2m}(\Phi, \lambda) \qquad (1)$$

G - gravitational constant
M - the mass of the tide generating body
r - the distance from the Earth centre
d - Earth-Moon distance
Φ - northern latitude
λ - eastern longitude
i - can take the value $m = 0$ (long-periodic zonal tide)
$m = 1$ (diurnal tesseral tide)
$m = 2$ (semi-diurnal sectorial tide)

The reference system:
- the vertical axis points to the centre of the Earth
- the horizontal axes are oriented to south along the meridian and to west in the first vertical

In this system in (1) the spherical components are:

$$
\begin{aligned}
Y_{20} &= 3\left(\sin^2\Phi - \frac{1}{3}\right)\left(\sin^2\delta - \frac{1}{3}\right) && \text{- zonal tides}\\
Y_{21} &= \sin 2\Phi \sin 2\delta \cos H^* && \text{- tesseral tides}\\
Y_{22} &= \cos^2\Phi \cos^2\delta \cos 2H^* && \text{- sectorial tides}
\end{aligned}
\qquad (2)
$$

δ declination
H^* hour angle

For the calculation of the tidal strain components the derivati ves of Y_{2m} are needed:

a. Latitudional first and second order derivatives
b. Longitudional first and second order derivatives
c. Mixed second order derivatives

a. Latitudional derivates	b. Longitudional derivates	c. Mixed derivates
$\frac{\partial Y_{20}}{\partial\Phi} = 3\sin 2\Phi\cdot\left(\sin^2\delta - \frac{1}{3}\right)$	$\frac{\partial Y_{20}}{\partial\lambda} = 0$	
$\frac{\partial Y_{21}}{\partial\Phi} = 2\cos\Phi\cdot\sin 2\delta\cdot\cos H^*$	$\frac{\partial Y_{21}}{\partial\lambda} = \sin 2\Phi\sin 2\delta\cdot\sin H^*$	
$\frac{\partial Y_{22}}{\partial\Phi} = -\sin 2\Phi\cos^2\delta\cdot\cos 2H^*$	$\frac{\partial Y_{22}}{\partial\lambda} = 2\cos^2\Phi\cos^2\delta\cdot\sin 2H^*$	
$\frac{\partial^2 Y_{20}}{\partial\Phi^2} = 6\cos 2\Phi\cdot\left(\sin^2\delta - \frac{1}{3}\right)$	$\frac{\partial^2 Y_{20}}{\partial\lambda^2} = 0$	$\frac{\partial^2 Y_{20}}{\partial\Phi\partial\lambda} = 0$
$\frac{\partial^2 Y_{21}}{\partial\Phi^2} = -4\sin 2\Phi\cdot\sin 2\delta\cos H^*$	$\frac{\partial^2 Y_{21}}{\partial\lambda^2} = -\sin 2\Phi\sin 2\delta\cdot\cos H^*$	$\frac{\partial^2 Y_{21}}{\partial\Phi\partial\lambda} = 2\cos 2\Phi\sin 2\delta\cdot\sin H^*$
$\frac{\partial^2 Y_{22}}{\partial\Phi^2} = -2\cos 2\Phi\cos^2\delta\cos 2H^*$	$\frac{\partial^2 Y_{22}}{\partial\lambda^2} = -4\cos^2\Phi\sin^2\delta\cdot\cos 2H$	$\frac{\partial^2 Y_{22}}{\delta\Phi\partial\lambda} = -2\sin 2\Phi\cdot\cos^2\delta\sin 2H^*$
Eqs (3a)	Eqs (3b)	Eqs (3c)

The strain field defined on a spherical surface (i.e. on the surface of the Earth $r = a$ (or on any spherical surface within it) can be decomposed into a spheroidal and a toroidal component. Because in this paper we concentrating on phenomena related to the tidal potential (Eq.(1)) only spheroidal strain is considered and the SNREI (symmetric non – rotating, elastic, isotropic) Earth with a liquid outer cove are taken into consideration.
In this case the tide generated displacement (Grafarend, 1986):

$$
\begin{aligned}
&d(r,\lambda,\Phi) = (d_r, d_\lambda, d_\Phi)\\
&d_{r_m}(r,\lambda,\Phi) = H(r)\cdot g(a)^{-1} Y_{nm}(\Phi,\lambda) V_n(r,d)\\
&d_{\Phi_m}(r,\lambda,\Phi) = T(r)(rg(a))^{-1}\frac{\partial Y_{nm}(\Phi,\lambda)}{\partial\Phi} V_n(r,d)\\
&d_{\lambda_m}(r,\lambda,\Phi) = T(r)(r\cos\Phi\cdot g(a))^{-1}\frac{\partial Y_{nm}(\Phi,\lambda)}{\partial\lambda} V_n(r,d)
\end{aligned}
\qquad (4a)
$$

The corresponding derivatives of the displacement vector are:

$$\frac{\partial d_{r_m}(r,\lambda,\Phi)}{\partial r} = \frac{\partial(H(r)V_2(r,d))}{\partial r} g(a)^{-1} Y_{nm}(\Phi,\lambda)$$
$$\frac{\partial d_{\Phi_m}(r,\lambda,\Phi)}{\partial \Phi} = T(r)(g(a)\cdot r)^{-1} \frac{\partial^2 Y_{nm}(\Phi,\lambda)}{\partial \Phi^2} V_n(r,d) \qquad (4b)$$
$$\frac{\partial d_{\lambda_m}(r,\lambda,\Phi)}{\partial \lambda} = T(r)(g(a)\cdot r\cdot\cos\Phi)^{-1} \frac{\partial^2 Y_{nm}(\Phi,\lambda)}{\partial \lambda^2} V_n(r,d)$$

3. EQUATION OF MOTION

In Eqs. (4) the auxiliary functions $H(r)$ and $T(r)$ are for characterisation of the radial and lateral displacement along the radius and at the surface $(r=a)$ they are the Love $h = H_{(a)}$ and Shida $\ell = T_{(a)}$ numbers respectively.

The Love number k is not needed in this study of the lunisolar strain tensor components It is:

$$k = R(a) - 1$$

The functions $H(r)$, $T(r)$ and $R(r)$ for different orders n can be obtained from the solution of the equation system of motion.

Let us introduce the following auxiliary functions (Molodensky, 1953):

$$M_n(r) = r^2\mu(r)\left(\frac{\partial T_n(r)}{\partial r} + H_n(r) - \frac{2}{r}T_n(r)\right) \qquad (5)$$
$$N_n(r) = \left(\lambda^*(r) + 2\mu(r)\right)\frac{\partial H_n(r)}{\partial r} + \lambda(r)\left[\frac{2}{r}H_n(r) - \frac{n(n+1)}{r^2}T_n(r)\right] \qquad (6)$$
$$L_n(r) = r^2\left(\frac{\partial R_n(r)}{\partial r} - 4\pi G\rho(r)H_n(r)\right) \qquad (7)$$

With the use of Eqs.(5) – (7) the equations of motion can be written as

$$-\frac{\partial M_n(r)}{\partial r} = \rho(r)\cdot r^2\left(R_n(r) + \frac{\partial W(r)}{\partial r}H_n(r)\right) + N_n(r)r^2 + 2\mu(r)\left[H_n(r) - (n^2+n-1)T_n(r) - \frac{\partial H_n(r)}{\partial r}r^2\right] \qquad (8)$$

$$-\frac{\partial N_n(r)}{\partial r} = \rho(r)\left[\frac{L_n(r)}{r^2} - 4\frac{\partial W(r)}{\partial r}\frac{H_n(r)}{r} + \frac{n(n+1)}{r^2}T_n(r)\frac{\partial W(r)}{\partial r}\right] + \frac{2\mu(r)}{r}\left[2\frac{\partial H_n(r)}{\partial r} - \frac{2H_n(r)}{r} + \frac{n(n+1)}{r^2}T_n(r)\right] - \frac{n(n+1)}{r^n}M_n(r) \qquad (9)$$

$$\frac{\partial L_n(r)}{\partial r} = n(n+1)\left(R_n(r) - 4\pi G\rho(r)T_n(r)\right) \qquad (10)$$

where $\mu = \mu(r)$ and $\lambda^* = \lambda^*(r)$ are the Lamé constans, $\rho(r)$ is the density function and $W = W(r)$ denotes the geopotential.

To describe the normal (radial) and horizontal (lateral) strain components the Eqs 5, 6 are needed which provide the tangential (M_m) and normal (N_n) stresses. The auxiliary functions H_n and T_n are also needed for the radial and the tangential displacements.

If a system of dimensionless units is introduced (the radius of the Earth is $a = 1$, $g(a) = 1$ is the mean acceleration of the gravity at the surface, the unit of the density is the mean density of the Earth and the gravitional constant is $G = \frac{3}{4}\pi$) the boundary conditions at the Earth's surface $(r = a = 1)$ can be given as (Varga, 1983):

$$
\begin{aligned}
N_n(a) &= -\frac{2n+1}{3} \cdot \alpha_N \\
M_n(a) &= \frac{2n+1}{3n(n+1)} \cdot \alpha_M \\
L_n(a) &= (2n+1) \cdot \alpha_L
\end{aligned}
\tag{11}
$$

α_N, α_M and α_L may take only the values 0 or 1.

1. In the case of earth tides
   $\alpha_N = 0 \quad \alpha_M = 0 \quad \alpha_L = 1$
   and we get with Eqs. (5) –(11) the Love-Shida numbers h_n, k_n and ℓ_n.
2. .If the normal load acting at the Earth's surface
   $\alpha_N = 1 \quad \alpha_M = 0 \quad \alpha_L = 1$
   and we get the load numbers h_n', k_n' and ℓ_n'.
3. If the stress which acts on the Earth is not connected with masses, consequently the load is potential free, the so called potential free Love numbers can be obtained
   $\alpha_N = 1 \quad \alpha_M = 0 \quad \alpha_L = 0$ for the normal stress
   $\alpha_N = 0 \quad \alpha_M = 1 \quad \alpha_L = 0$ for the tangential stress
   The two triplets of potential free Love numbers can be denoted as h_n'', k_n'', ℓ_n'' and h_n''', k_n''', ℓ_n'''.

4. THE STRAIN TENSOR, SURFACE AND VOLUME DILATATION

The linear strain tensor has the following components:

$$e_{rr_m} = \frac{\partial d_{r_m}}{\partial r} \tag{12}$$

$$e_{\Phi\Phi_m} = \frac{1}{r}\frac{\partial d_{\Phi_m}}{\partial \Phi} + \frac{d_{r_m}}{r} \tag{13}$$

$$e_{\lambda\lambda_m} = \frac{1}{r \cdot \cos\Phi}\frac{\partial d_{\lambda m}}{\partial \lambda} + \frac{dr_m}{r} + \operatorname{tg}\Phi \frac{d_{\Phi_m}}{dr} \tag{14}$$

$$e_{r\Phi_m} = \frac{1}{2}\left(\frac{1}{r}\frac{\partial d_{r_m}}{\partial \Phi} + \frac{\partial d_{\Phi m}}{\partial r} - \frac{d_{\Phi m}}{r}\right) \tag{15}$$

$$e_{r\lambda_m} = \frac{1}{2}\left(\frac{\partial d_{\lambda m}}{\partial r} + \frac{1}{r\cdot\cos\Phi}\frac{\partial d_{r m}}{\partial \lambda} - \frac{d_{\lambda m}}{r}\right) \tag{16}$$

$$e_{\Phi\lambda_m} = \frac{1}{2}\left(\frac{1}{r}\frac{\partial d_{\lambda m}}{\partial \Phi} + \frac{1}{r\cos\Phi}\frac{\partial d_{\Phi m}}{\partial \lambda} - \mathrm{tg}\,\Phi\frac{d_{\lambda_m}}{r}\right) \tag{17}$$

To describe the surface deformation and the dilatation

$$e_{\Phi\Phi} + e_{\lambda\lambda} \qquad \text{and} \qquad e_{\Phi\Phi} + e_{\lambda\lambda} + e_{rr}$$

the following auxiliary functions can be introduced:

$$S_n(r) = \frac{1}{r}\left[2H_n(r) - n(n+1)T_n(r)\right] \tag{18}$$

$$F_n(r) = \frac{\partial H_n(r)}{\partial r} + \frac{2}{r}H_n(r) - \frac{n(n+1)}{r^2}T_n(r) \tag{19}$$

Eqs.(12) – (17) render possible, together with Eqs. (4) – (10) the determination of the strain-tensor components for the elastic Earth mantle:

$$e_{rr}(r) = \frac{1}{\lambda(r)+2\mu(r)}\left\{\lambda(r)\left[n(n+1)T_n(r) - 2H_n(r)\right] + N_n(r)\right\}V_n(r,d)Y_{n,m}(\Phi,\lambda) \tag{20}$$

$$e_{\Phi\Phi}(r) = \left[\frac{T_n(r)}{r}\frac{\partial^2 Y_{n,m}(\Phi,\lambda)}{\partial\Phi^2} + \frac{H_n(r)}{r}Y_{n,m}(\Phi,\lambda)\right]V_n(r,d) \tag{21}$$

$$e_{\lambda\lambda}(r) = \left[\frac{T_n(r)}{r}\left(\mathrm{tg}\,\Phi\frac{\partial Y_{n,m}(\Phi,\lambda)}{\partial\Phi} + \frac{1}{\cos^2\Phi}\frac{\partial^2 Y_{n,m}(\Phi,\lambda)}{\partial\lambda^2}\right) + \frac{H_n(r)}{r}Y_{n,m}(\Phi,\lambda)\right]V_n(r,d) \tag{22}$$

$$e_{\Phi\lambda}(r) = \frac{T_n(r)}{r\cos\Phi}\left(2\frac{\partial^2 Y_{n,m}(\Phi,\lambda)}{\partial\Phi\partial\lambda} - \mathrm{tg}\,\Phi\frac{\partial Y_{n,m}(\Phi,\lambda)}{\partial\Phi}\right)V_n(r,d) \tag{23}$$

$$e_{r\Phi}(r) = \frac{M_n(r)}{\mu(r)}\frac{\partial Y_{n,m}(\Phi,\lambda)}{\partial\Phi}V_n(r,d) \tag{24}$$

$$e_{r\lambda}(r) = \frac{M_n(r)}{\mu(r)}\frac{1}{\cos\Phi}\frac{\partial Y_{n,m}(\Phi,\lambda)}{\partial\lambda}V_n(r,d) \tag{25}$$

Surface deformation and dilation:

$$e_{\Phi\Phi}(r) + e_{\lambda\lambda}(r) = \frac{1}{r}\left[2H_n(r) - n(n+1)T_n(r)\right]Y_{n,m}(\Phi,\lambda)V_n(r,d) \tag{26}$$

$$e_{\Phi\Phi}(r) + e_{\lambda\lambda}(r) + e_{rr}(r) = \left\{\frac{1}{r}\left(2H_n(r) - n(n+1)T_n(r)\right)\left(\frac{2\mu(r)}{\lambda(r)+2\mu(r)}\right) + \frac{N_n(r)}{\lambda(r)+2\mu(r)}\right\}Y_{n,m}(\Phi,\lambda)V_n(r,d) \tag{27}$$

- In case of lunisolar effect there is no normal and lateral stress on the Earth's surface $(N(a)=M(a)=0)$. Therefore if $r=a$ the r.h.s. of Eqs. (24) – (25) are equal to zero, in case of Eq. (20) the 2^{nd} term of r.h.s. *is* $=0$.
- If $r=a$ than $H_n(a)=h_n$ and $T_n(a)=\ell_n$.

Evidently different equations are valid for zonal $(m=0)$, tesseral $(m=1)$and sectorial $(m=2)$ tides. With the use of (20) – (27) together with Eqs. (2) – (4) for the strain tensor components the following expressions can be obtained.

a. Zonal strain-tensor

$$e_{rr}=\frac{3\lambda(a)}{\lambda(a)+2\mu(a)}(6\ell_2-2h_2)\left(\sin^2\Phi-\frac{1}{3}\right)\left(\sin^2\delta-\frac{1}{3}\right)V_2(a,d)$$

$$e_{\Phi\Phi}=\left[6\ell_2\cos 2\Phi+3h_2\left(\sin^2\Phi-\frac{1}{3}\right)\right]\left(\sin^2\delta-\frac{1}{3}\right)V_2(a,d)$$

$$e_{\lambda\lambda}=3\left[(2\ell_2+h_2)\sin^2\Phi-\frac{h_2}{3}\right]\left(\sin^2\delta-\frac{1}{3}\right)V_2(a,d)$$

$$e_{\Phi\lambda}=6\ell_2\frac{\sin\Phi}{\cos^2\Phi}\left(\sin^2\delta-\frac{1}{3}\right)V_2(a,d)$$

$$e_{r\Phi}=0$$

$$e_{r\lambda}=0$$

b. Tesseral strain-tensor

$$e_{rr}=\frac{\lambda(a)}{\lambda(a)+2\mu(a)}(6\ell_2-2h_2)\sin 2\Phi\sin 2\delta\cos H^*V_2(a,d)$$

$$e_{\Phi\Phi}=(h_2-4\ell_2)\sin 2\Phi\sin 2\delta\cos H^*V_2(a,d)$$

$$e_{\lambda\lambda}=[2\ell_2\,\mathrm{tg}\,\Phi(2\cos 2\Phi-1)+h_2\sin 2\Phi]\sin 2\delta\cos H^*V_2(a,d)$$

$$e_{\Phi\lambda}=\frac{2\ell_2}{\cos\Phi}\cos 2\Phi(2\sin H^*-\mathrm{tg}\,\Phi\cos H^*)\sin 2\delta V_2(a,d)$$

$$e_{r\Phi}=0$$

$$e_{r\lambda}=0$$

d. Sectorial strain-tensor

$$e_{rr}=\frac{\lambda(a)}{\lambda(a)+2\mu(a)}(6\ell_2-2h_2)\cos^2\Phi\cos^2\delta\cos 2H^*V_2(a,d)$$

$$e_{\Phi\Phi}=(h_2\cos^2\Phi-2\ell_2\cos 2\Phi)\cos^2\delta\cos 2H^*V_2(a,d)$$

$$e_{\lambda\lambda}=[h_2\cos^2\Phi\cos^2\delta-2\ell_2(\sin^2\Phi-2)\sin^2\delta]\cos 2H^*V_2(a,d)$$

$$e_{\Phi,\lambda}=\frac{\ell_2}{\cos\Phi}\sin 2\Phi(\mathrm{tg}\,\Phi-4)\cos^2\delta\sin 2H^*V_2(a,d)$$

$$e_{r\Phi}=0$$

$$e_{r\lambda}=0$$

For the surface deformation and dilation we obtained:

a. Zonal tides

$$e_{\Phi\Phi} + e_{\lambda\lambda} = (2h_2 - 6\ell_2)\left(3\sin^2\Phi - \frac{1}{3}\right)\left(\sin^2\delta - \frac{1}{3}\right)V_2(a,d)$$

$$e_{rr} + e_{\Phi\Phi} + e_{\lambda\lambda} = \frac{2\mu(a)}{\lambda(a)+2\mu(a)}(2h_2 - 6\ell_2)\left(3\sin^2\Phi - \frac{1}{3}\right)\left(\sin^2\delta - \frac{1}{3}\right)V_2(a,d)$$

b. Tesseral tides

$$e_{\Phi\Phi} + e_{\lambda\lambda} = (2h_2 - 6\ell_2)\sin 2\Phi \sin 2\delta \cos H^* V_2(a,d)$$

$$e_{rr} + e_{\Phi\Phi} + e_{\lambda\lambda} = \frac{2\mu(a)}{\lambda(a)+2\mu(a)}(2h_2 - 6\ell_2)\sin 2\Phi \sin 2\delta \cos H^* V_2(a,d)$$

c. Sectorial tides

$$e_{\Phi\Phi} + e_{\lambda\lambda} = (2h_2 - 6\ell_2)\cos^2\Phi \cos^2\delta \cos 2H^* V_2(a,d)$$

$$e_{rr} + e_{\Phi\Phi} + e_{\lambda\lambda} = \frac{2\mu(a)}{\lambda(a)+2\mu(a)}(2h_2 - 6\ell_2)\cos^2\Phi \cos^2\delta \cos 2H^* V_2(a,d)$$

5. THE ROTATIONAL STRAIN TENSOR COMPONENTS

To describe the deformations beside the strains the rotation vector also has to be used. They three components can be related to the three shear components of the strain tensor.
Eqs. (15) – (17) can be written in the following form:

$$2e_{\Phi\lambda_m}(r) = \frac{1}{r\cos\Phi}\left[\frac{\partial}{\partial\Phi}\left(d_{\lambda_m}\cdot\cos\Phi\right) + \frac{\partial d_{\Phi_m}}{\partial\lambda}\right] \tag{28}$$

$$2e_{\lambda r_m}(r) = \frac{1}{r\cdot\cos\Phi}\frac{\partial d_{rm}}{d\lambda} + \frac{1}{r}\frac{\partial}{\partial r}\left(rd_{\lambda_m}\right) = 0 \tag{29}$$

$$2e_{\Phi r_m}(r) = \frac{1}{r}\frac{\partial}{\partial r}\left(rd_{\Phi_m}\right) + \frac{1}{r}\frac{\partial d_{rm}}{\partial\lambda} = 0 \tag{30}$$

The rotational components around axes normal to the plane of corresponding shear strains are

$$2\rho_{r_m}(r) = \frac{1}{r\cos\Phi}\left[\frac{\partial}{\partial\Phi}\left(d_{\lambda_m}\cos\Phi\right) - \frac{\partial d_{\Phi_m}}{\partial\lambda}\right] = 0 \tag{31}$$

$$2\rho_{\Phi_m}(r) = \frac{1}{\cos\Phi}\frac{\partial d_{\lambda_m}}{\partial\lambda} - \frac{1}{r}\frac{\partial}{\partial r}\left(rd_{\lambda_m}\right) \tag{32}$$

$$2\rho_{\lambda_m}(r) = \frac{1}{r}\frac{\partial}{\partial r}\left(rd_{\Phi_m}\right) - \frac{1}{r}\frac{\partial d_{r_m}}{\partial\lambda} \tag{33}$$

These three equations with Eqs. (4) – (10) give the rotational components in the form:

$$\rho_{r_m}(r) = \frac{M(r)}{\mu(r)\cos\Phi}\frac{\partial Y_{n,m}(\Phi,\lambda)}{\partial\lambda}V_n(r,d) = 0$$

$$\rho_{\Phi_m}(r) = \left[\frac{2}{r}\left(H_n(r) - T_n(r) - \frac{M_n(r)}{\mu(r)}\right)\right]\frac{1}{\cos\Phi}\frac{\partial Y_{n,m}(\Phi,\lambda)}{\partial\lambda}V_n(r,d)$$

$$\rho_{\lambda_m}(r) = \left[\frac{2}{r}\left(H_n(r) - T_n(r) - \frac{M_n(r)}{\mu(r)}\right)\right]\frac{\partial Y_{n,m}(\Phi,\lambda)}{\partial\Phi}V_n(r,d)$$

Similarly to the strain-tensor for the surface of the Earth we have:

a. Zonal rotational components

$$\rho_\Phi = 0$$

$$\rho_\lambda = 6(h_2 - \ell_2)\sin 2\Phi\left(\sin^2\delta - \frac{1}{3}\right)V_2(a,d)$$

b. Tesseral rotational components

$$\rho_\Phi = 4(h_2 - \ell_2)\sin\Phi\sin 2\delta\sin H^* V_2(a,d)$$

$$\rho_\lambda = 4(h_2 - \ell_2)\cos 2\Phi\sin 2\delta\sin H^* V_2(a,d)$$

c. Sectorial rotational components

$$\rho_\Phi = 4(h_2 - \ell_2)\cos\Phi\cos^2\delta\sin 2H^* V_2(a,d)$$

$$\rho_\lambda = -4(h_2 - \ell_2)\cos\Phi\sin\Phi\cos^2\delta\sin 2H^* V_2(a,d)$$

Why is it interesting to observe the rotational strain?

a. Tidal observations (magnitude $\sim 10^{-8}$).
b. The rotational strain about the vertical axis responds merely to SH waves. Seismic waves S and Love waves can be recorded without any disturbance caused by P waves.
c. Tectonical rotational strain can be observed ($n \cdot 10^{-8} rad \cdot y^{-1}$, where $n \le 5$) (Voosoghi, 2000).
d. Rotational motions in the earthquake source area.

Realization of the rotational strainmeter:

1. WATANABE H. 1962
2. OZAWA I. 1966

- The sensitivity of the instruments was at that time ~ 10^{-9}. Today this value is by one or two order lower
- The drift and the relatively low resolution was due to galvanometric recording of the signals generated by electrodynamic transducers or due to the use a horizontal pendulum to transform differential variations into tilt.

6. CONCLUSIONS

The rotation strain components can be observed both by means of rotational strainmeters similar to proposed by Watanabe (1962) and Ozawa (1975) long time ago or by the possibilities offored by present day methods of space geodesy.

The rotational strain about the vertical axis responds merely to SH waves. Seismic S and Love waves with rotational strainmeters can be recorded without any disturbance caused by P waves.

Tectonicalrotational strain can be observed by VLBI and GPS observations. Their magnitude is $10^{-7} - 10^{-8} rad \cdot year^{-1}$ (Voosoghi, 2000).

Acknowledgements. This work was supported in the frame of German-Hungarian Scientific and Technological Cooperation (Hungarian project number: D-8/99). The German co-operant was the Friedrich Schiller Universitaet, Institut für Geowissenschaften,Jena. Authors also enjoyed the financial support of the Hungarian science fundation OTKA (Grant T038123).

References

Grafarend E., 1986: Three-dimensional deformation analysis: global vector spherical harmonic and local finite element representation, Tectonophysics, 130, 337-359.

Melchior P., 1983: The tides of the planet Earth. Second Edition. Pergamon Press.

Molodensky S. M., 1953: Elastic tides, free nutations and some questions concerning the inner structure of the Earth. Trudi Geofis. Inst-Akad. Nauk SSSR, 19(146), 3-42 (in Russian).

Ozava I., 1975: Rotational strainmeter and the observation of the shear strain of the Earth tide with this intrumnt, Bulletin d'Information Marees Terrestres No. 52, 2398-2409.

Varga P., 1983: Potential free Love numbers. Manuscripta Geodetica, 8, 85-92.

Varga P., Grafarend E., 1996: Distribution of the lunisolar tidal elastic stress tensor components within the Earth's mantle. Physics of the Earth and Planetary Interiors, 93, 285-297.

Watabene H., 1962: A rotational strain seismometer. Disaster Prevention Research Institute Kyoto University, Bulletin No. 58, 1-15.

Voosoghi B., 2000: Intrinsic deformation analysis of the Earth surface based on 3 dimensional displacement fields derived from space geodetic measurenments. Technical Reports Department of Geodesy and Geoinformatics (Universitaet Stuttgart) Report Nr. 2000.3.

Meeting of the ETC-Working Group 7 on Analysis of Environmental Data for the Interpretation of Gravity Measurements

Jena, March 13 - 15, 2002

Program

Wednesday, 13 March, Session 10 - Environmental Effects

C. Kroner and Jentzsch, G.: Introduction

Observ.: Monitoring of environmental parameters

Wednesday, 13 March, Session 11 - Barometric pressure and gravity

V. Buhl and **C. Gerstenecker**: Correction of earth tidal gravity observations using GPS-measurements

J. Arnoso, B. Ducarme, **A.P. Venedikov**, and R. Vieira: Time variations and anomalies in the air pressure admittance of superconducting tidal gravity data

D. Crossley, Hinderer, J. and Rosat, S.: Using atmosphere-gravity correlation to derive a time-dependent admittance

visit to Moxa Observatory

departure: car park Lutherplatz, 13:30
return: car park Lutherplatz, around 18:30

Thursday, 14 March, Session 12 - Hydrology and gravity

D. Simon: Modelling of the field of gravity variations induced by the seasonal air mass warming during 1998-2000

R. IJpelaar, Troch, P., Warmerdam, P. ,Stricker, H., and Ducarme, B.: Detecting hydrological signals in time series of in-situ gravity measurements: a first approach

S. Takemoto, Fukuda, Y., Higashi T., Abe, M., Ogasawara, S., Dwipa, S., Kusuma, D. S., and Andan, A.: Effect of groundwater changes on SG observations in Kyoto and Bandung

Harnisch, M., Harnisch, G.: Seasonal variations of hydrological influences on gravity measurements at Wettzell

Zerbini, S., Richter, B., Romagnoli, C., Lago, L., Domenichini, F., and Simon, D.: Effects of environmental parameters on height and gravity variations

K. Nawa, Suda, N., Aoki, S., Shibuya, K., **Sato, T.**, and Fukao, Y.: Influence of sea level variations in seismic normal mode band on superconducting gravimeter observation at Syowa Station

Thursday, 14 March, Session 13 - Barometric pressure and seismological data

W. Zürn: Simplistic models of vertical seismic noise above 0.1 mHz derived from local barometric pressure

W. Zürn and Neumann, U.: Simplistic models of atmospheric signals in horizontal seismograms

K. Fischer: Sources and transfer mechanism of seismic noise: Preliminary results from FEM models

J. Exß and Zürn, W.: Reduction of noise in horizontal long period seismograms using local atmospheric pressure

Gy. Mentes: Microbarograph for investigation of geodynamical phenomena caused by atmospheric pressure variations influenced by lunisolar effects

Thursday/Friday, 14/15 March, Session 14 - Environmental effects and strain

Mentes, Gy., and Eperne Papai I.: The effect of atmopsheric pressure on strain measurements at the Sopron Observatory, Hungary

H. Ishii: Environmental effects on strain observation, their applications for geophysical study and necessity of deep borehole observation for noiselessly high quality

Friday, 15 March, Session 15 - Environmental effects and tilt

A. Kopaev, V. Milyukov, and V. Yushkin: Pressure and temperature effects in tilt, strain, and gravity observations near Mt. Elbrus, Central Caucasus

M. Westerhaus: Environmental effects on tilt measurements at Merapi Volcano

Th. Klügel: Tilt variations at shallow depth: implications for the installation of a laser gyroscope at the Geodetic Observatory Wettzell

G. Jentzsch, Graupner, St., Weise, A., Ishii, H., and Nakao, Sh.: Environmental effects in tilt data of Nokogiriyama Observatory

Friday, 15 March, Session 16 - Closing

General discussion, recommendations, etc.

Correction of earth tidal gravity observations using GPS-measurements

Volker Buhl, Carl Gerstenecker
Institute of Physical Geodesy, Darmstadt University of Technology, Petersenstr. 13, 64287 Darmstadt, Germany, e-mail: gerstenecker@geod.tu-darmstadt.de

Abstract: Residuals of earth tidal gravity observations are mainly generated by air pressure changes. The largest part of this effect can be corrected by using the linear air pressure regression coefficient $\Delta p/\Delta g$ [ngal/HPa]. This regression coefficient considers mainly the radial symmetric air pressure distribution over the earth tidal station. Asymmetric effects are not taken into consideration.
GPS-measurements are strongly disturbed by tropospheric effects. Radial symmetric changes of the troposphere are estimated by continous stationary GPS-observations. However the usual zenith path delay of GPS-signals reflects similar effects as the air pressure regression coefficient.
In a pilot study we have investigated the possibilities to determine residual gravity changes due to asymmetric air pressure distributions over the stations. As awaited zenith pathe delay shows no correlation with the residual gravity changes. Strong correlations are found however, if we determine azimuth dependend tropospheric effects on GPS-measurements.

Time variations and anomalies in the air pressure admittance of superconducting tidal gravity data

J. Arnoso[1], B. Ducarme[2], A.P. Venedikov[3] and R. Vieira[1]

[1] Instituto de Astronomía y Geodesia (CSIC-UCM). Universidad Complutense de Madrid. Facultad de Matemáticas. 28040 Madrid, Spain. arnoso@iagmat1.mat.ucm.es, vieira@iagmat1.mat.ucm.es

[2] Royal Observatory of Belgium (Belgian National Fund for Scientific Research), Av.Circulaire 3, B-1180 Brussels. ducarme@oma.be

[3] Geophysical Institute, Bulgarian Academy of Sciences, Acad. Bonchev street block 3, Sofia 1113, vened@geophys.bas.bg

Abstract

The new VAV tidal analysis program is designed to deal simultaneously with non-tidal as well as tidal signals. The main goal of this paper is to study a well-known non-tidal signal: the air pressure influence, through the time variations of its admittance in some data sets of superconducting gravimeters from the Global Geodynamics Program (GGP). Unhappily, except in Boulder, where seasonal variations of the air pressure influence are obvious, the detected anomalies are due to gross errors in the data which are reducing strongly the signal to noise ratio. Thus the first conclusion is a trivial one: it is impossible or too difficult to find useful non-tidal signals, when the data still contain gross errors, i.e. non-useful non-tidal signals. Another conclusion of our investigation is that non-careful interpolations can generate very bad, non-stationary noise in data series of very good quality. It is thus important to reduce to a minimum any "repair" of the data prior to the analysis. The amount of "repair" depends strongly from the analysis method. With its ability to analyze non-equidistant data with any sampling rate, VAV can simply suppress perturbed data and ignore gaps.

1. Introduction

The Earth tide data processing has to deal with the general model:

Tidal data = Tidal signal + Non-tidal signals + noise

The tidal signal is the useful signal for the tidal domain, e.g. in connection with the Earth's structure and properties. Nevertheless, the model above clearly shows that the lack of attention paid to the non-tidal signals may badly affect just the useful signal.

For other domains, in particular the so-called "Earth deformations", the non-tidal signals are useful signals, e.g. for the search of earthquake and volcano precursors. In this case the tidal signal is only a noise. However, just in the same way as above, a careless treatment of the tidal signal will spoil the detection of the useful non-tidal signals. Examples of such inadequate treatments are the eliminations of the tidal signal through an elementary filtration.

A conclusion from these simple considerations is that the tidal data processing should deal, for whatever purpose, most carefully with both tidal and non-tidal signals.

A general problem of the model is how to distinguish between noise and non-tidal signals.

All methods for Earth tide data analysis accept implicitly or explicitly that the noise of the data is a random stationary phenomenon. Hence, all components of the data, which are not tidal waves and, in the same time, which are non-stationary phenomena, should be considered as non-tidal signals. Typical examples are instrumental drift, jumps, too big residuals, time variations of the tidal parameters, etc.

A problem for the use of the non-tidal signals is that

non - tidal signals may be { useful signals of geophysical origin or
anomalies or perturbations of instrumental and human origin

The problem is to distinguish between these two phenomena. One thing is clear. If we are sure that the anomalies are rare, it is easy to find the useful signals and, vice versa, if there are too many anomalies, it may be too difficult or impossible to distinguish the useful signals. A bad news is that some of the anomalies may be generated by improper manipulation and processing of the data. The good news is that we have the possibility to avoid all improper manipulations and apply a correct data processing.

This present paper is an attempt to study a well known non-tidal signal, the time variations of the air-pressure admittance, i.e. the variations of the cross-regression coefficient, say b, of the observed tidal gravity with the air-pressure. We usually suppose that b is a constant. The deviations from this hypothesis may indicate that either we need an improvement of the model of the admittance or we have a kind of anomalous signal.

The results presented in this paper have been obtained through special options of the new computer program VAV (Venedikov et al., 2001). In the next section 2 we shall describe the algorithm of the option.

In the following sections we shall give some examples of application. They have been obtained through the application of VAV on 3 series of superconducting gravity data (Table 1) of the Global Geodynamic Project (GGP) (Crossley, 2000), collected in the International Centre for Earth Tides (Ducarme et al., 2000).

Table 1. List of series of superconducting gravitmeter data.

Station, Country	Instrument or sensor	Latitude, Longitude	Time interval
Boulder, USA	GWR C024	40.13°, 254.77°	12.04.1995-01.08.1998
Cantley, Canada	GWR T012	45.58°, 284.19°	07.11.1989-31.12.1998
Strasbourg, France	GWR T005, GWR C026	48.62°, 7.68°	11.07.1987-25.06.1996 01.03.1997-30.04.1998

In the examples we have used, in parallel to the time variations of the b coefficients, residuals of the filtered numbers (e.g. Figures 2 and 3 in section 3), provided by VAV. These residuals are a convenient tool to find non-tidal signals because we get them at once for a whole time window, e.g. every 48 hours. The filtered numbers, as well as the residuals are complex numbers, but we use only the real modulus. A threshold level (the horizontal straight line in the graphics) is computed with very high confidential probability. In such a way every value, which exceeds this level, can be considered as a non-tidal signal with a high confidence.

2. The main algorithm

The trivial way to study the time variations of some parameters is to partition the data into segments and process the data, separately in every segment. Here we propose to apply a global analysis on the whole series of the data, but to accept that in every segment we have a different or individual regression coefficient. In such a way we get global estimates of the tidal parameters, by using a highest possible separation in tidal groups, accompanied by a set of regression coefficients, related with every segment.

Generally, the multi channel analysis is based on model equations like

$$\mathbb{U} = \mathbb{A}\mathbb{x} + \mathbb{V}\mathbb{b} + \mathbb{e}, \tag{1}$$

where $\mathbb{U}$ is a vector (column vector) of filtered tidal data, after the elimination of the drift, $\mathbb{x}$ is a vector of the tidal unknowns $\xi = \delta\cos\kappa$ and $\eta = -\delta\sin\kappa$ for a set of tidal groups, $\mathbb{A}$ is a known matrix, appropriately created by using the theoretical amplitudes and phases, $\mathbb{b}$ is a vector of unknown cross-regression coefficients, representing one or several admittance functions, $\mathbb{V}$ is a known matrix created by using, in one or another way, the observed values of the 2nd, 3rd,... channels, e.g. air-pressure, temperature etc. and $\mathbb{e}$ is the noise.

The estimation of the time variations of $\mathbb{b}$ is always related with a partition of the data into N time segments: $S(t_1), S(t_2), \ldots S(t_N)$ related with the epochs $t_1, t_2, \ldots t_N$, as shown in Figure 1

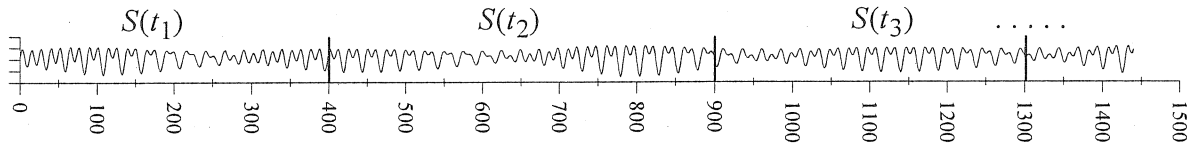

Figure 1. Partition of the data into segments.

Corresponding to the partitioning we have

$$\mathbb{U} = \begin{pmatrix} \mathbb{U}_1 \\ \mathbb{U}_2 \\ \vdots \\ \mathbb{U}_k \end{pmatrix}, \ \mathbb{A} = \begin{pmatrix} \mathbb{A}_1 \\ \mathbb{A}_2 \\ \vdots \\ \mathbb{A}_N \end{pmatrix}, \ \mathbb{V} = \begin{pmatrix} \mathbb{V}_1 \\ \mathbb{V}_2 \\ \vdots \\ \mathbb{V}_N \end{pmatrix} \text{ and } \ \mathbb{e} = \begin{pmatrix} \mathbb{e}_1 \\ \mathbb{e}_2 \\ \vdots \\ \mathbb{e}_N \end{pmatrix} \tag{2}$$

where $\mathbb{U}_j, \mathbb{A}_j, \mathbb{V}_j$ and $\mathbb{e}_j$ are matrix components of $\mathbb{U}, \mathbb{A}, \mathbb{V}$ and $\mathbb{e}$ respectively, related with the segment $S(t_j), j = 1, \ldots N$.

One possibility to obtain the time variations is to apply the general equation (1) separately for every $S(t_j)$, i.e. to deal with the equations

$$\mathbb{U}_j = \mathbb{A}_j\mathbb{x}_j + \mathbb{V}_j\mathbb{b}_j + \mathbb{e}_j \ \text{ separately for every } \ S(t_j), j = 1, \ldots N \tag{3}$$

From the separate solution of these N systems we shall get the estimates

$$\tilde{\mathbb{x}}_j = \tilde{\mathbb{x}}(t_j) \text{ and } \tilde{\mathbb{b}}_j = \tilde{\mathbb{b}}(t_j), j = 1, \ldots N \tag{4}$$

i.e. the tidal unknowns and the regression coefficients as discrete functions of the time.

A week point is that $\tilde{\mathbb{x}}_j$ so obtained are not estimates of the global tidal unknowns $\mathbb{x}$ in (1). E.g., for data larger than 1 year, $\mathbb{x}$ in (1) may involve unknowns for each of the tidal groups: CHI1, PI1, P1, S1, K1, PSI1, PHI1 and TET1, all of them having different amplitude factors. If the segments are as short as a few months, all these groups should be included in one and the same group K1. Hence the elements of $\tilde{\mathbb{x}}_j$ are not the same as those of $\mathbb{x}$ and they are estimated

with a lower precision. Something more, the association of groups with different amplitude factors in one group will produce time variations that may affect the estimated regression coefficients.

In this relation VAV works with a single system of equations.

$$\mathbf{U} = \begin{pmatrix} \mathbf{U}_1 \\ \mathbf{U}_2 \\ \vdots \\ \mathbf{U}_N \end{pmatrix} = \begin{pmatrix} \mathbf{A}_1 \\ \mathbf{A}_2 \\ \vdots \\ \mathbf{A}_N \end{pmatrix} .\mathbf{x} + \begin{pmatrix} \mathbf{V}_1 & & \mathbf{O} \\ & \mathbf{V}_2 & \\ & & \ddots \\ \mathbf{O} & & \mathbf{V}_N \end{pmatrix} . \begin{pmatrix} \mathbf{b}_1 \\ \mathbf{b}_2 \\ \vdots \\ \mathbf{b}_N \end{pmatrix} \tag{5}$$

Thus the terms $\mathbf{U}$ and $\mathbf{A}$ from (1) remain the same, but the matrix $\mathbf{V}$ and the vector $\mathbf{b}$ are considerably transformed.

From the solution of (5) by the method of the least squares we get global estimates $\tilde{\mathbf{x}}$ of the same tidal unknowns $\mathbf{x}$ in (1) but a set of estimates $\tilde{\mathbf{b}}_1, \tilde{\mathbf{b}}_2, \ldots \tilde{\mathbf{b}}_N$ of the regression coefficients $\mathbf{b}_1, \mathbf{b}_2, \ldots \mathbf{b}_N$. Since $\tilde{\mathbf{b}}_j$ is related with the epoch t_j we can consider $\tilde{\mathbf{b}}_j = \tilde{\mathbf{b}}(t_j)$ as a discrete function of the time that describes the time variations of the regression coefficients.

If the number N of the segments is high, the number of the unknowns may become too high which can embarrass the computations. Due to this it is convenient to use the classical algorithm for the separation of the unknowns. In our case it consists in the following way to obtain the estimates.

We transform the matrices $\mathbf{A}_j$ into $\mathbf{C}_j$ through

$$\mathbf{C}_j = \mathbf{A}_j - \mathbf{V}_j(\mathbf{V}_j{}^{\mathrm{T}}\mathbf{V})^{-1}\mathbf{V}_j{}^{\mathrm{T}}\mathbf{A}_j \text{ and create the matrix } \mathbf{C} = \begin{pmatrix} \mathbf{C}_1 \\ \mathbf{C}_2 \\ \vdots \\ \mathbf{C}_N \end{pmatrix} \tag{6}$$

Then the estimates of the tidal unknowns are directly obtained through

$$\tilde{\mathbf{x}} = (\mathbf{C}^{\mathrm{T}}\mathbf{C})^{-1}\mathbf{C}^{\mathrm{T}}\mathbf{U} \tag{7}$$

where

$$\mathbf{C}^{\mathrm{T}}\mathbf{C} = \sum_{j=1}^{N} \left(\mathbf{A}_j{}^{\mathrm{T}}\mathbf{A}_j - \mathbf{A}_j{}^{\mathrm{T}}\mathbf{V}_j(\mathbf{V}_j{}^{\mathrm{T}}\mathbf{V}_j)^{-1}\mathbf{V}_j{}^{\mathrm{T}}\mathbf{A}_j \right) \tag{8}$$

$$\mathbf{C}^{\mathrm{T}}\mathbf{U} = \sum_{j=1}^{N} \left(\mathbf{A}_j{}^{\mathrm{T}}\mathbf{U}_j - \mathbf{A}_j{}^{\mathrm{T}}\mathbf{V}_j(\mathbf{V}_j{}^{\mathrm{T}}\mathbf{V}_j)^{-1}\mathbf{V}_j{}^{\mathrm{T}}\mathbf{U}_j \right) \tag{9}$$

Afterwards, we can compute the estimates $\tilde{\mathbf{b}}_j$ through

$$\tilde{\mathbf{b}}_j = (\mathbf{V}_j{}^{\mathrm{T}}\mathbf{V}_j)^{-1}\mathbf{V}_j{}^{\mathrm{T}}(\mathbf{U}_j - \mathbf{A}_j\tilde{\mathbf{x}}) \tag{10}$$

The results in the following sections are obtained for a single auxiliary channel – the air-pressure - and a single regression coefficient for every segment. In this case the vectors $\tilde{b}_j$ become a scalar b, which is the cross-regression coefficient and the expressions above are considerably simplified.

3. Station Cantley

Figure 3, compared to Figure 2, shows the strong effect of the application of a usual multi-channel analysis, to take into account the effect of the air-pressure, with a constant in time cross-regression coefficient b. In addition to the evident decrease of the level of the residuals, there is a huge decrease of the AIC value

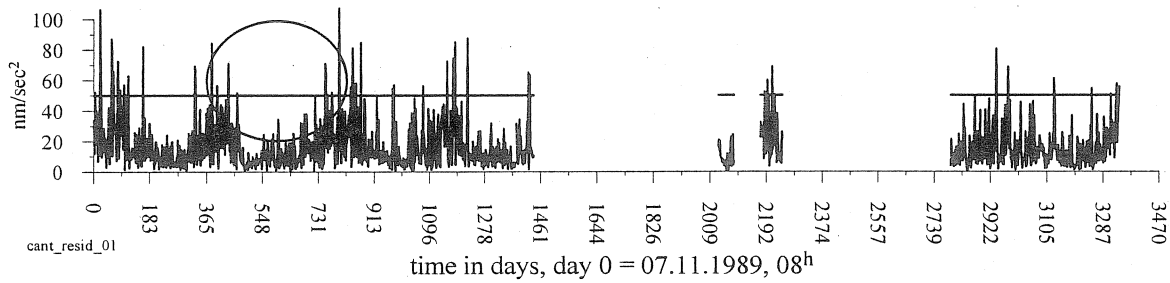

Figure 2. Cantley, modulus of residuals in the D-frequency domain; the effect of the air-pressure is ignored, i.e. no cross-regression. Akaike criterion for the analysis: AIC = 88,495.

A curious phenomenon is manifested at the place, indicated by a circle. In Figure 2 the residuals are relatively low. Surprisingly, in Figure 3, at the same place, they become relatively high. It looks like a noise, namely anomaly or non-tidal signal, generated by the reduction of the air-pressure effect.

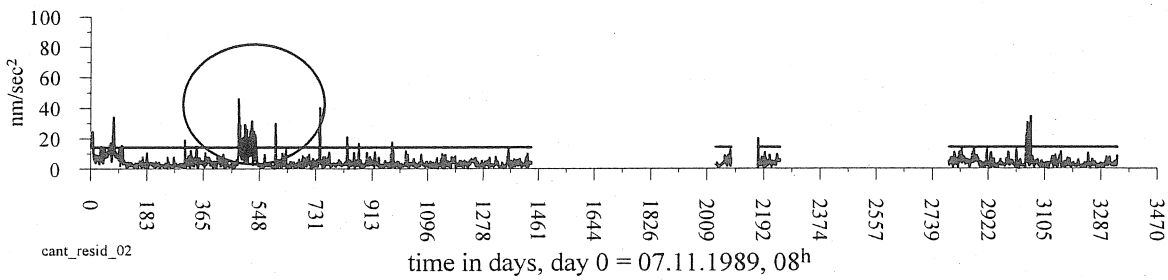

Figure 3. Cantley, modulus of residuals in the D-frequency domain; the effect of the air-pressure is taken into account, i.e. a cross-regression model is applied with a constant coefficient b; AIC= 60,201.

Figure 4 shows an attempt to check eventual time variations of b . There are 3 segments, defined by two large gaps. In parallel with the horizontal lines, giving the value of b in every segment, the 95% confidential intervals are given. These confidence intervals shows clearly that we have a significantly lower b value in the first segment.

It should be noticed that the m.s.d. (mean square deviations) of b are usually determined, e.g. by the ETERNA program (Wenzel,1996), on the basis of a white noise assumption. VAV computes the m.s.d. of b on the assumption of a colored noise, i.e. we get frequency dependent m.s.d. In the case when a single b coefficient is determined, the m.s.d. is determined by using the m.s.d. of the data at the lowest frequency, i.e. the highest possible m.s.d. Due to this VAV provides higher m.s.d. of b than other programs, e.g. than ETERNA. This gives us more confidence when a significant difference is observed. The significance of the time variation is also supported by a further decrease of AIC.

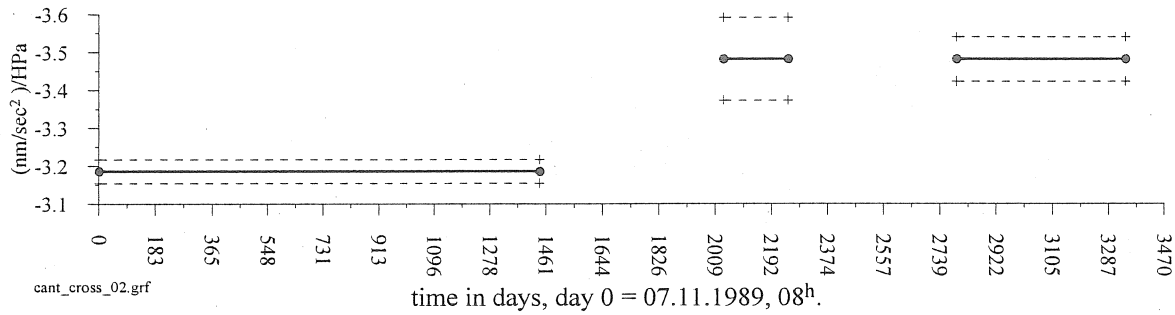

Figure 4. Cantley, time variations of the regression coefficient b. The data are partitioned into 3 segments, defined by two important gaps; AIC = 60,020.

The next Figure 5 shows a more detailed study of the time variations of b. There is an obviously significant decrease of b, around t = 548 days. A further decrease of AIC indicates the reality of this deviation.

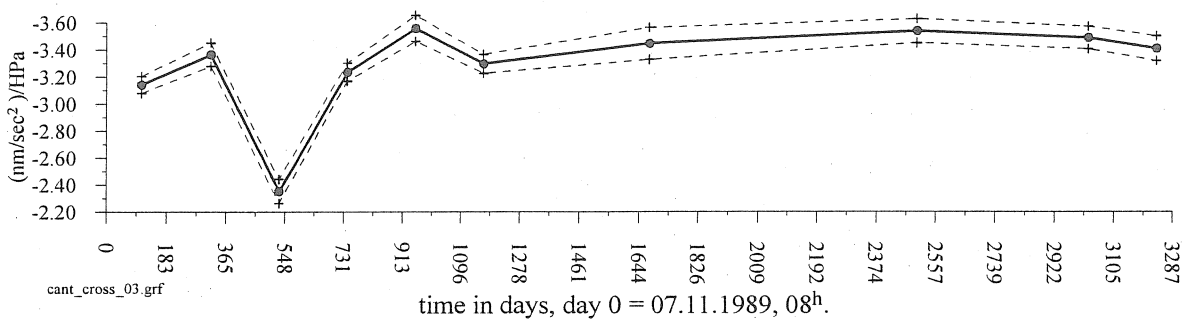

Figure 5. Cantley - time variations of the coefficient b. The data are partitioned into 10 segments, each segment including one and the same number of days; AIC = 59,151.

After several experiments we succeeded to isolate a segment in the interval of t (480, 540 days) (Figure 6) for which we have an extremely low coefficient $b \approx 0$. For this case we have got AIC considerably lower than in the other cases, which shows the reality of this strange value of b.

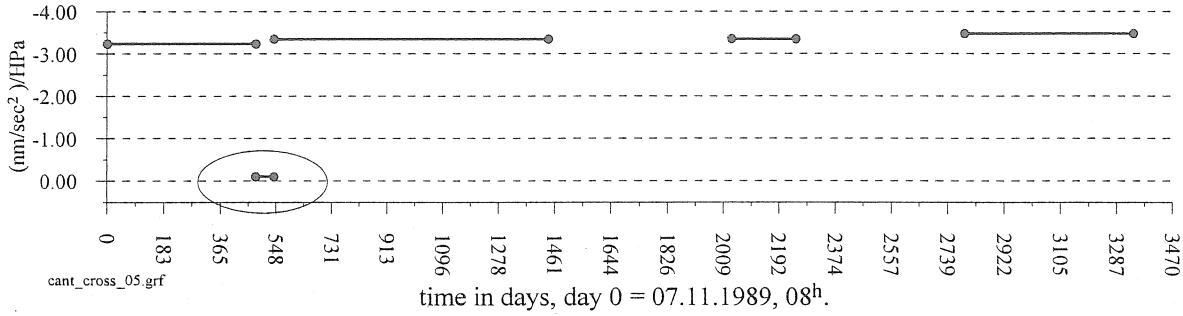

Figure 6. Cantley - time variations of the coefficient b; the segments are defined by two large gaps and the interval of (480, 540 days) of length 60 days; the regression coefficient in the interval is $b \approx 0$; AIC = 56,881.

As shown in Figure 7, when we accept the model of time variation of b shown in Figure 6, the anomalous residuals in Figure 3 have disappeared.

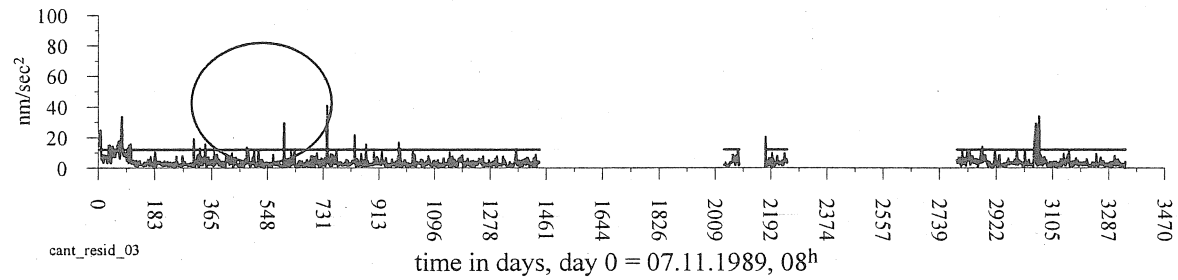

Figure 7. The D-residuals corresponding to the time variations of the b – coefficient given in Figure 6.

Unfortunately, this strange phenomenon cannot be any useful non-tidal signal. It is an example of what we have defined in section 1 as an anomaly and a serious one. Our supposition is that the data in the controversial interval have been repaired in one or another way, most likely through interpolation, but without restoring the atmospheric pressure effect. Thus, instead of finding an useful signal, we found an example showing how a careless intervention in the data, may be an unnecessary interpolation, can generate noise.

Table 2. Results of the analysis of a series of data 01.07.1990–1.11.1991 in variants: whole series without any gap and the series with a gap of 60 days, at the place of the controversial interval 02.03.1991 – 01.05.1991 (480-540 days).

Diurnal tides						
Data used	δ(Q1)	m.s.d.	δ(O1)	m.s.d.	δ(K1)	m.s.d.
Whole series	1.16568	±.00141	1.16648	±.00028	1.14836	±.00021
With gap 60 days	1.16474	±.00085	1.16657	±.00017	1.14823	±.00013
Semidiurnal tides						
Data used	δ(N2)	m.s.d.	δ(M2)	m.s.d.	δ(S2)	m.s.d.
Whole series	1.20961	±.00064	1.20429	±.00013	1.18396	±.00027
With gap 60 days	1.20964	±.00041	1.20429	±.00008	1.18369	±.00018
Cross-regression coefficient (admittance)						
Data used	*b*	m.s.d.				
Whole series	-2.8264	±0.0568				
With gap 60 days	-3.3201	±0.0358				

The results in Table 2 show that when such data are introduced, we get worse results instead of an improvement or, which is the same, that the exclusion of such data actually improves the results.

4. Station Boulder

Figures 8 and 9 are similar to Figures 2 and 3 in the previous section. They also demonstrate the strong effect of the cross-regression, with an important reduction of the AIC value.

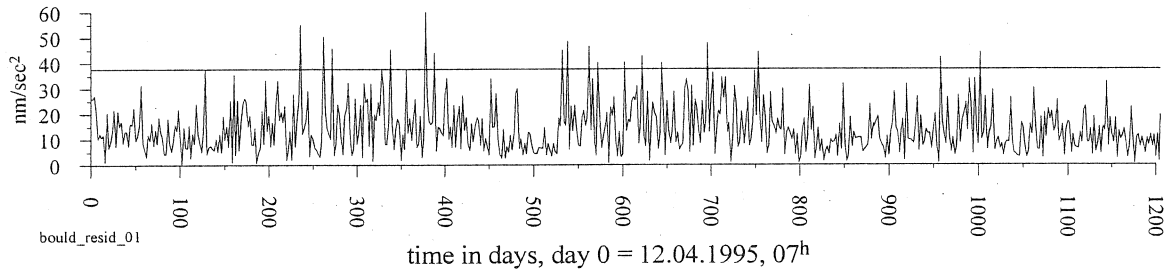

Figure 8. Boulder, residuals (modulus) in the D-frequency domain; the effect of the air-pressure is ignored, i.e. no cross-regression model; AIC = 46,504

Unlike the case of Figure 3, in Figure 9 we see very few residuals over the threshold level. The indicated case is interesting because it does not exist in Figure 8. It turned out, that this anomaly is due to some interpolated air-pressure data. It is again an example of anomaly, generated by an unnecessary data manipulation.

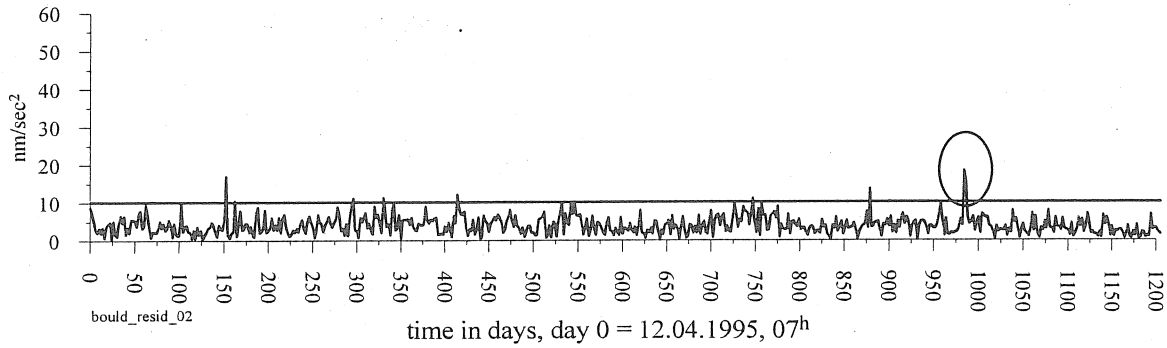

Figure 9. Boulder, residuals (modulus) in the D-frequency domain; the effect of the air-pressure is taken into account. A cross-regression model is applied with a constant coefficient *b*; AIC= 29,121.

Otherwise, Figure 9 shows data with very good general behavior that are certainly interesting to study for time variations of the air-pressure admittance.

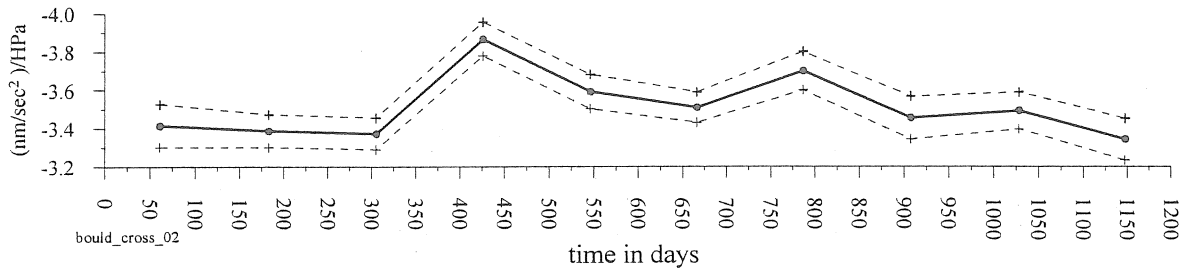

Figure 10. Time variations of the *b* coefficients; the data are partitioned into 10 equal segments; AIC = 28,913.

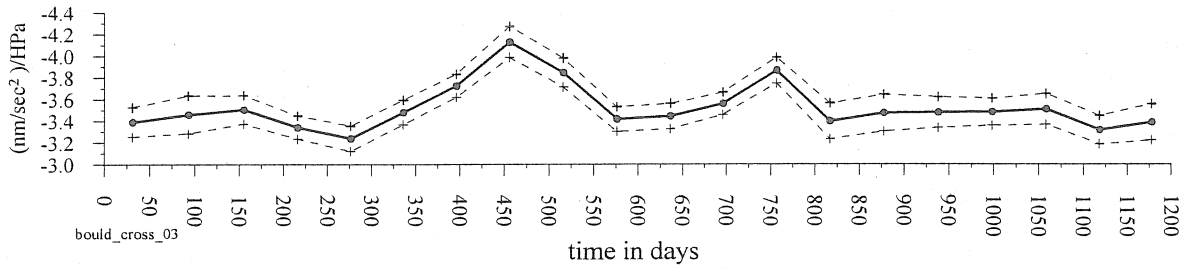

Figure 11. Time variations of the *b* coefficients; the data are partitioned into 20 equal segments; AIC = 28,809.

Figures 10 and 11 represent the time variations of the *b* coefficients, when the data are partitioned into 10 and 20 equal segments respectively. We have a reduction of the AIC value, compared to Figure 9. This means that we have really some variations of *b*. The two peaks are significant deviations from the general behavior of the observed curve. The distance between the peaks is close to one year. This is an indication about a possible yearly period, i.e. for some seasonal variations. We shall return to this point in section 6.

The attempts to find more details in the time variations of *b* were not successful. Moreover, the introduction of a time variable *b* has not seriously improved the analysis results.

5. Station Strasbourg

In Strasbourg two instruments were successively installed: T005 from 1987 to 1996 and CT26 later on (Table 1). Figures 12 and 13 are similar to the Figures 2 and 3 or Figures 8 and 9 in the previous sections 3 and 4. In figure 12 the noise level is very similar for both instruments and is mainly due to the atmospheric pressure effects. In Figure 13 we have again a large reduction of the level of the residuals, especially for CT26, and a corresponding considerable decrease of the AIC value. Nevertheless, in Figure 13 a considerable number of values are exceeding the threshold level for T005. It is obvious that the records of the new CT instrument are of much better quality.

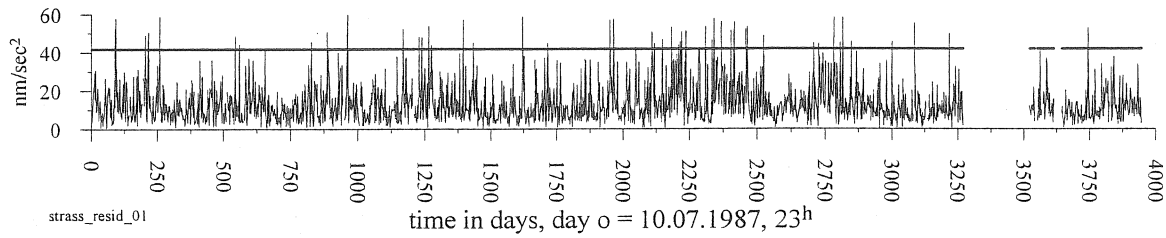

Figure 12. Strasbourg, residuals (modulus) in the D-frequency domain; the effect of the air-pressure is ignored, i.e. no cross-regression model; AIC = 145,247.

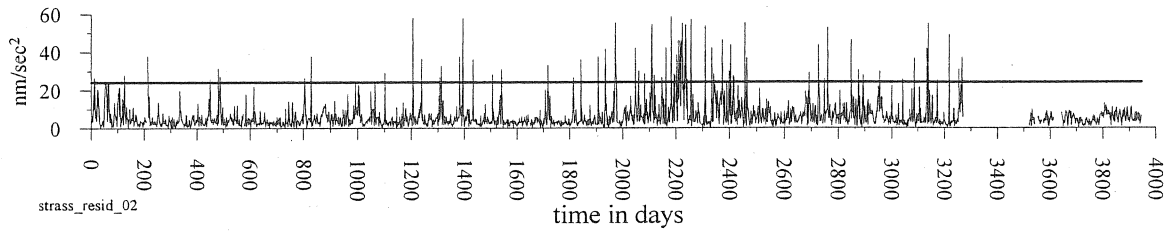

Figure 13. Strasbourg, residuals (modulus) in the D-frequency domain; the effect of the air-pressure is taken into account; a cross-regression model is applied with a constant coefficient *b*; AIC= 124,076.

The first attempt to study the time variations of *b* is shown in Figure 14. The data have been partitioned in two segments corresponding to the different instruments. The results are confirmed in Ducarme & al., 2002 (Table 1), where the authors got using ETERNA software (Wenzel, 1996):

For T005 (3,272days) $b = -3.128 \pm 0.010$ nm.s^{-2}/hPa

For CT26 (817days) $b = -3.394 \pm 0.007$ nm.s^{-2}/hPa

A premature conclusion is that we have different admittances for the two instruments. Such a conclusion could lead us to state that an important part of the air-pressure effect is instrumental.

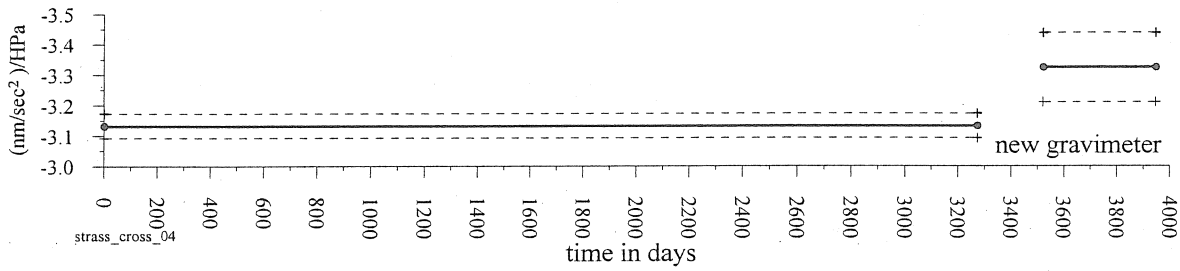

Figure 14. Strasbourg, time variations of *b* through partition of the data in two segments defined by a gap coinciding with the replacement of the gravimeters; AIC = 124 065.

Figure 15 shows an attempt to study in more details the time variations of *b*. According to the AIC value this case is more reliable and the premature conclusion made above is no more

so convincing. Now we can see several relatively low values, in particular at the very beginning, as well as at two points in the interval (1950, 2250 days).

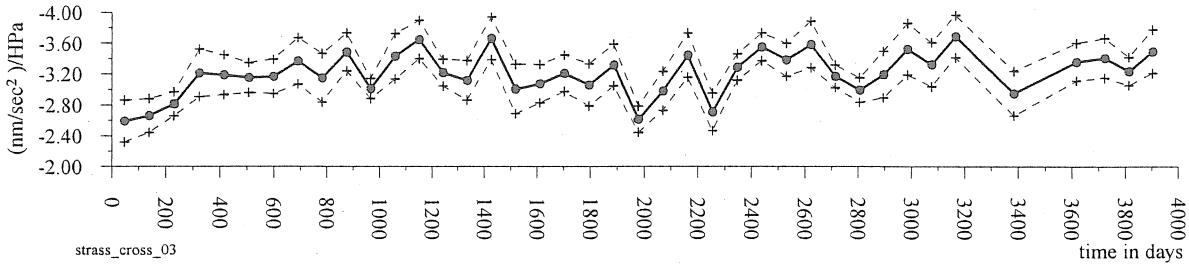

Figure 15. Strasbourg, time variations of b through partition of the data in 30 equal segments; AIC = 123,872.

The next Figures 16 and 17 are samples showing more details in these areas. We have namely four segments of length between 10 and 24 days in which we have practically $b = 0$. The confidential intervals of b are not shown, but actually in all these cases of low b they cover the zero. The further decrease of AIC is in support of this result. In both Figures the AIC has one and the same value because the graphics are obtained through one and the same analysis.

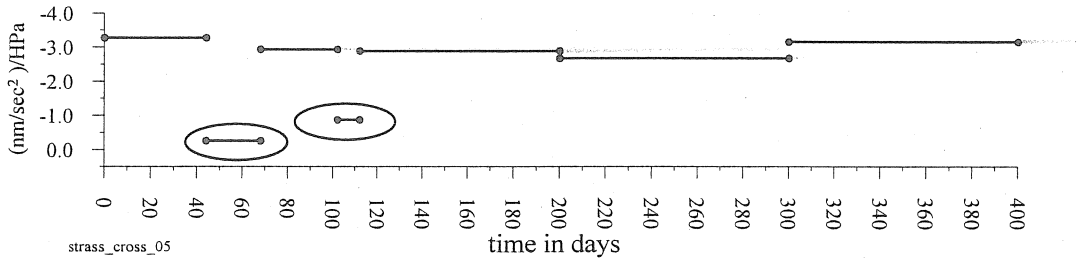

Figure 16. Strasbourg, location of two segments, (44, 68 days) and (102, 112 days), with values of b, which do not differ significantly from the zero; AIC = 123,345.

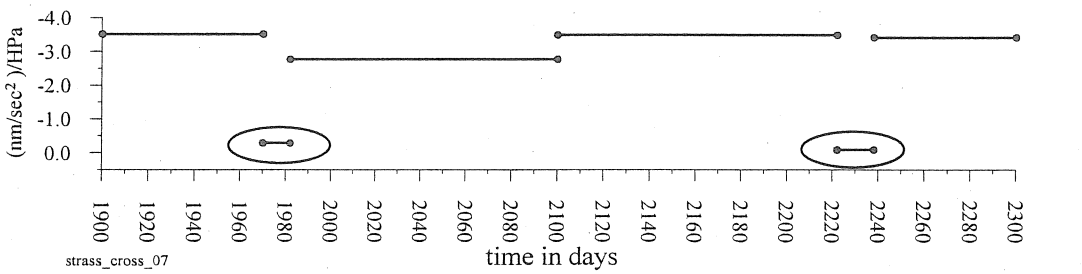

Figure 17. Strasbourg, location of two segments, (1970, 1982 days) and (2222, 2238 days), with values of b which do not differ significantly from the zero; AIC = 123,345.

In (Hinderer et al., 2002) the authors are in favor of the use of interpolated data, as well as of "repaired data". Due to this we can suppose that the segments with zero admittance are actually interpolated data. Normally the air pressure effect should be artificially introduced in the interpolated sections, using its nominal admittance. Perhaps it was not done properly. We can thus suppose that there are other parts in this series with interpolated data without introduction of

the air pressure correction. The result is the introduction of additional noise in the residues of Figure 13, which exceed the threshold level.

It is too difficult to find all places with interpolations and repairs. We have thus simply applied the option of VAV for automatic elimination of the doubtful data, which are of course not only interpolated data. Table 3 shows the results of this procedure, applied in 4 iterations. Although this option resulted in a massive elimination of data, till 23.6% of all data as well as it introduced a huge number of gaps, we have got a fair diminution of the associated RMS errors.

The cases of ETERNA and VAV without any elimination, i.e. in the 0-iteration, are practically identical. However, when we apply VAV possibility to check and eliminate the doubtful data, which is also based on the VAV capacity to deal with a great number of gaps, we get considerable deviations from ETERNA. The precision for the D tides is raised more than twice and, for the SD tides, nearly twice.

Table 3. Station Strasbourg (T005 and CT26): analysis by ETERNA on the whole series and by the VAV program in an iteration procedure, eliminating data with too big residuals.

Software	Nr of iteration	Elim. Data	Amplitude δ factor(diurnal tides)		
			Q1 m.s.d.	O1 m.s.d.	K1 m.s.d.
ETERNA		0%	1.14598 ±.00073	1.14733 ±.00014	1.13540 ±.00010
VAV	0	0%	1.14571 ±.00069	1.14726 ±.00013	1.13541 ±.00009
VAV	1	7.8%	1.14577 ±.00041	1.14748 ±.00008	1.13554 ±.00005
VAV	2	15.0%	1.14572 ±.00032	1.14757 ±.00006	1.13569 ±.00004
VAV	3	20.3%	1.14578 ±.00030	1.14756 ±.00006	1.13569 ±.00004
VAV	4	23.6%	1.14586 ±.00029	1.14756 ±.00005	1.13573 ±.00004

Software	Nr of iteration	Elim. Data	Amplitude δ factor(semidiurnal tides)		
			N2 m.s.d.	M2 m.s.d.	S2 m.s.d.
ETERNA		0%	1.17173 ±.00040	1.18520 ±.00008	1.18784 ±.00017
VAV	0	0%	1.17173 ±.00039	1.18518 ±.00007	1.18784 ±.00015
VAV	1	7.8%	1.17231 ±.00026	1.18537 ±.00005	1.18795 ±.00010
VAV	2	15.0%	1.17211 ±.00023	1.18547 ±.00004	1.18787 ±.00009
VAV	3	20.3%	1.17214 ±.00022	1.18547 ±.00004	1.18782 ±.00009
VAV	4	23.6%	1.17220 ±.00021	1.18548 ±.00004	1.18786 ±.00009

It is interesting to see how the iterations affect the picture on Figure 14 and the possible conclusion that the air-pressure admittance is significantly different for the different instrument.

In Figure 18 the iteration 0 is a reproduction of Figure 14. After iteration 1, with a moderate quantity of eliminated data, we have still a difference between the two segments, i.e.

the two gravimeters. Nevertheless, the difference is smaller and the confidence intervals are overlapping, although they are narrower than in Figure 14. Hence the difference becomes statistically not significant. We can give a sigh of relief, because the instruments are not responsible for the difference and they cannot be accused to have a different admittance. The other iterations in Figure 18 follow the tendency to decrease the difference, so that after iteration 4 we get practically identical admittance for the two segments.

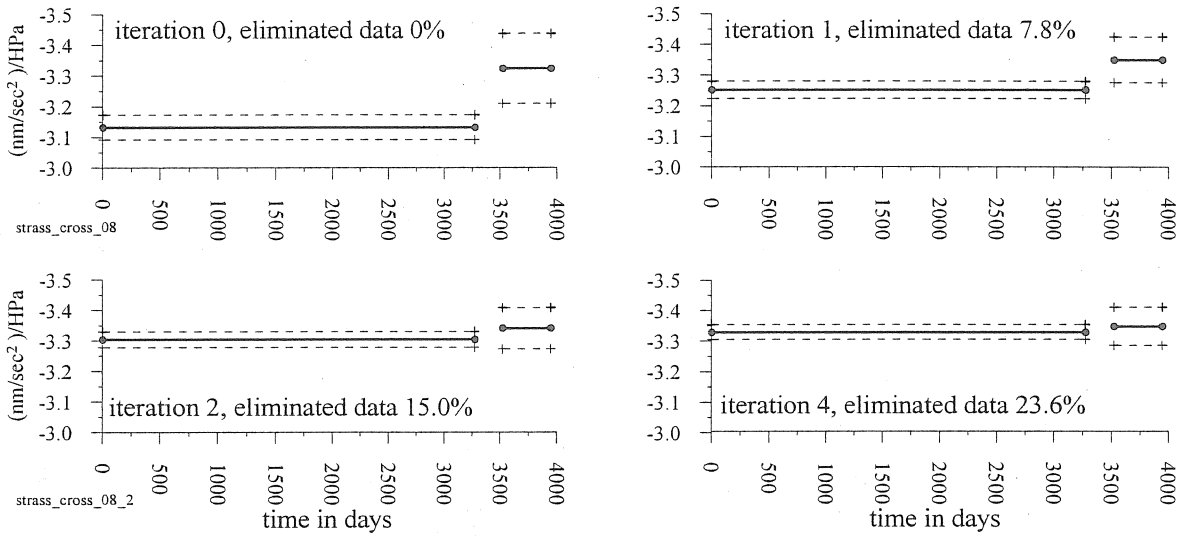

Figure 18. Strasbourg, time variations of *b* through partition of the data in two segments with elimination of data in an iteration procedure.

6. Seasonal variations of the air-pressure admittance

As said in section 4, in the series of Boulder, there are some indications of a seasonal variation of the air pressure admittance *b* with a yearly period. As far as such a supposition is correct, the time variations we can see in Figures 10 and 11 may be considered as a useful non-tidal signal. To check this hypothesis we have used a specific way. The data have been split into segments, which are defined as sets of data, instead of segments, which are data intervals. More concretely, in Figure 19, segment 1 includes all data in all years during the month of January, segment 2 – all data during February, and so on. Then the global analysis provides us the *b* coefficients for every segment. It is possible to say that we partition the data into seasons and get *b* estimated for every season – in Figure 19 for every month.

The curves in Figure 19, in particular the confidence intervals, indicate the reality of a seasonal dependence, characterized by an increase of the *b* values during the warmer seasons.

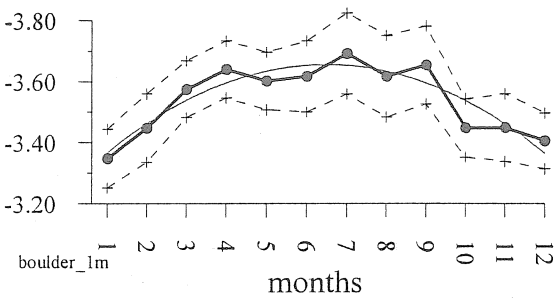

Figure 19. Seasonal variations of the cross-regression coefficient *b* with confidential interval, a season being chosen as a month.

Other variants of choosing the seasons are shown in Figure 20. Both cases **A** and **B** of this Figure confirm the inference for higher *b* during the warmer seasons.

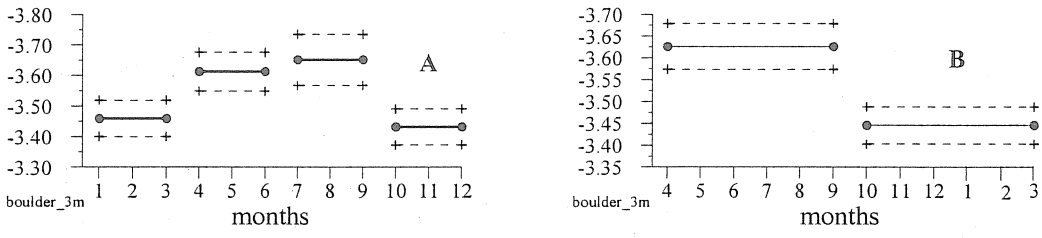

Figure 20. Seasonal variations of the cross-regression coefficient *b*; in case **A** we have 4 seasons, every season involving 3 months and in case **B** we have only two seasons, every one of them involving 6 months.

We confirm here the results obtained by T.van Dam & O.Francis (1998) who gave a meteorological explanation of this phenomenon.

In other series of data we have observed only very slight similarity to the picture in Figure 19. Obviously, the problem is very sophisticated as it depends essentially of the regional meteorological conditions. It should be investigated in more details. One of the necessary conditions for such investigation, is a careful check of the data and the elimination of all artificially introduced anomalies.

7. Conclusions

The initial purpose of this paper was to check the existing conception about the air pressure admittance and, eventually, to encourage the research of more sophisticated models. In this sense, the only result, which may be considered as moderately successful, is the observation of time variations in Boulder.

In the other examples, considered here, our computing technique turned out to be helpful only for finding some anomalies in the data. Thus the first conclusion is a trivial one: it is impossible or too difficult to find useful non-tidal signals, when the data still contain gross errors, i.e. non-useful non-tidal signals. It is traditionally the goal of the preprocessing of the tidal data to "repair" the data by eliminating the spikes and jumps and to fill small gaps in the series. Ideally abnormal data should always be eliminated, but the different tidal analysis methods had and still have different requirements on the preprocessed data, even if the term of "repaired data" may sound to a specialist on data processing no better than "false money" to a

cashier. In any case another conclusion of our investigation is that non-careful interpolations can generate very bad, non-stationary noise in data series of very good quality.

The fear of gaps is linked to the classical Fourier methods as they have been applied in the early times, the epoch without computers or with very slow computers. When such methods are applied on evenly data without gaps we get fine results and the computational work is very simple. If there are gaps, the computations become considerably more complicated. If the gaps are simply ignored and replaced by zeros, we get spikes and all possible deformations of the results.

The situation is completely different when the method of the least squares (MLSQ) is used. MLSQ is a more general method than the Fourier methods. There is not any condition of evenly spaced data. We have only to correctly create the observation equations about the data at the time moments at which they exist. The equations take into account all interrelations or interactions between the unknown parameters and the functions in which the parameters take part. Then the solution of the equations provides the estimates of the parameters without any spikes.

Of course, it is better when the data are without gaps, by the simple reason that higher quantity of data provides a higher precision. Nevertheless, it is a bad illusion to believe that, if a gap is fulfilled by artificially created data, this operation will improve the accuracy. In the best case, it is possible to get an apparent reduction of the m.s.d. Moreover, if the model used for interpolation is different from the real tidal factors of the series, interpolation will bias the results. Actually, the interpolated and repaired data are often source of additional noise. It is much more useful to work with longer series including gaps, to improve the resolution, than with shorter series without gaps. It is better to use a series of 12 month with a two months gap inside, than a series of 10 months without gaps.

Actually, we think that the interpolation is imposed by purely practical reasons. The methods of analysis like ETERNA (Wenzel, 1996), based on the general scheme of Chojnicki (1972), use high-pass filters like the filter of Pertsev. Such filters have a low signal-to-noise ratio, of the order of 1. Due to this they need a moving filtration, which replaces one original data by one filtered data (nearly). In the same time the moving filtration cannot support a great number of gaps, because they may produce losses of a great number of data. To obtain filters with better signal to noise and cut-off characteristics it is necessary to increase the length of application and thus to increase the loss of data at each gap. One cannot avoid these sharp filters when decimating the data from the original sampling rate to minutes or hourly data. Moreover the direct analysis without filtering, which is used for the determination of the long period tides including the so called "pole" tides, requires to model the drift in each data section. A large number of gaps or jumps will ends up with an unrealistic number of unknowns.

The methods like VAV use narrow band-pass filters, which have considerably higher signal-to-noise ratio. For example, if the time window is 48 hours, these filters provide, for each tidal family, a pair of filtered numbers, everyone with a signal-to-noise ratio very close to 48/2=24. Due to this we can apply the filters without overlapping, with all gaps remaining between the filtered intervals, with a very small quantity of lost data. Some people consider such a filtration as a decimation of the data with a step equal to the time window. Actually, this operation is a transformation of the data from the time domain in a time/frequency domain, which keeps the whole useful information.

The problem of spikes and tares is more delicate. If non-harmonic perturbations are left in the original sampling of the data, they will produce biased data after decimation to lower sampling rates, minutes or hours. In tidal analysis methods such as ETERNA, which can be applied to any sampling rate without decimation, spikes and tares have nevertheless to be "repaired" as their simple elimination will create a large numbers of small gaps. Other classical analysis methods such as VEN66 (Venedikov, 1966) or NSV98 (Venedikov & al., 1997) still

require uninterrupted data sets of let's say 48h and it was the usual practice to interpolate missing data up to a few hours to complete blocks and to smooth out small perturbations. Only VAV accepts unevenly spaced data and will no more require interpolations or data smoothing, as abnormal data can be directly eliminated in the original sampling.

References

Chojnicki, T., 1972. Détermination des paramètres de marée par la compensation des observations au moyen de la méthode des moindres carrés, *Institute of Geophysics, Polish Academy of Sciences, Marées Terrestres, 55, 48-80.*

Crossley, D., 2000. Report on the status of GGP, *Cahiers Centre Européen Geodyn. Seism.*, 17, 1-7.

Ducarme, B., Vandercoilden, L., 2000. First results of the GGP data Bank at ICET, *Cahiers Centre Européen Geodyn. Seism.*, 17, 117-124; Bull. d'Inform. Marées Terrestres, 132, 10291-10298.

Ducarme B., Sun, H.P., Xu, J.Q., 2002. New investigation of tidal gravity results from GGP network, *Third WORKSHOP of the Global Geodynamics Project (GGP) on Superconducting Gravimetry, Jena, March 11-14, 2002, Bull. Obs. Marées Terrestres, 135,...*

Hinderer, J., Rosat, S., Crossley, D., 2002. Influence of different processing methods on the retrieval of gravity signals from GGP data, *Third WORKSHOP of the Global Geodynamics Project (GGP) on Superconducting Gravimetry, Jena, March 11-14, 2002, Bull. Obs. Marées Terrestres, 135,...*

van Dam, T., Francis, O., 1998. Two years of continuous measurements of tidal and non-tidal variations of gravity in Boulder, Colorado, *Geophys. Research Letters, 25, 3, 393-396.*

Venedikov, A.P., 1966, Une méthode d'analyse des marées terrestres à partir d'enregistrements de longueurs arbitraires, *Observatoire Royal de Belgique, Série Géophysique, 71, 463-485.*

Venedikov, A.P., Vieira, R., de Toro, C., Arnoso, J., 1997. A new program developed in Madrid for tidal data processing, *Bull. Obs. Marées Terrestres, 126, 9969-9704.*

Venedikov, A.P., Arnoso, J., Vieira, R., 2001, Program VAV/2000 for tidal analysis of unevenly spaced data with irregular drift and colored noise, *Journal Geodetic Society of Japan*, 47, 1, 281-286.

Wenzel, H.G., 1996, The nanogal software: data processing package ETERNA 3.3, *Bull. Inf. Marées Terrestres, 124, 9425-9439.*

Using Atmosphere-Gravity Correlation to Derive a Time-Dependent Admittance

by

David Crossley[1], Jacques Hinderer[2], and Severine Rosat[2]

[1]Earth and Atmospheric Sciences, Saint Louis University,
[2]Institut de Physique du Globe / EOST Strasbourg, France
crossley@eas.slu.edu

Abstract

The purpose of this paper is to investigate the role of the correlation between atmospheric pressure and gravity in the context of a single scalar admittance. We consider two GGP data sets from Boulder and Strasbourg, both of which we processed from the raw data before decimating to 1minute files. The cross correlation and scalar admittance between gravity and pressure were determined for 3 averaging windows of 1 hour, 6 hours and 1 day. The data clearly show that cross correlation and admittance are related; furthermore, the shorter the averaging window the more the scatter in both quantities. We found that when the correlation was high the admittance tended towards a value that was higher for shorter windows and higher frequencies. Our attempts to use the correlation to improve the traditional assumption of a single scalar factor (e.g. -0.3 μgal mbar^{-1}) were unsuccessful, probably due to the inherent noise in the gravity residuals.

Introduction

The use of a single scalar admittance has been well established in computing the influence of atmospheric pressure fluctuations on gravity (e.g. Warburton and Goodkind, 1977; Merriam, 1992; Crossley et al. 1995). The assumption is that when atmospheric pressure p (mbar) is recorded with relative or absolute gravity g (μgal) at a single station, the gravity can be corrected by using the relation

$$g_c = g - \alpha\,(p - p_0), \qquad (1)$$

where α is taken to be either a nominal - 0.3 μgal mbar^{-1} or determined by a least squares fit of p to g, thus minimising the residual gravity g_c. The effectiveness and simplicity of this method has led to its widespread use in gravity studies for many purposes. This loading correction can amount to 10 μgal or more during extreme weather (e.g. Rabbel and Zschau, 1985) and typically accounts for some 90% of the total atmospheric effect. It has been known for a long time, however, that this local correction can be improved, especially for monthly and seasonal periods, by including global atmospheric data available through the worldwide atmospheric data services, (e.g. Boy et al., 1998). Unfortunately this computation requires a fair amount of work to collect the data and convert it into a useful time series for each station at a certain epoch. Although the use of global atmospheric pressure is gradually gaining popularity for high precision studies, a single admittance still predominates most residual gravity computations.

Several approaches to using the local pressure more effectively have been attempted, particularly in using a frequency dependent admittance (e.g. Crossley et al. 1995; Neumeyer

et al., 1997, 1998; Kroner, 1998). These studies show that improvements, in the form of lower residuals, are possible with additional work, but the methods have never achieved regular use. It has also been noticed that the admittance shows some variation with time (e.g. Richter, 1987; Van Dam and Francis, 1998), usually on seasonal time scales. Our concern here is with the possible variations of α on time scales of hours to days. The reason for this is that the atmosphere is certainly variable on these short time scales, and local weather systems can move rapidly over a station in a few hours (Müller and Zürn, 1983). There is no guarantee that the correlation implied by (1) is satisfied over all length and time scales.

In addition to the admittance α, we also need to define the general cross-correlation between pressure p_i and gravity g_i

$$r_{pg} = \sum_i [p_i g_i] \Big/ \sqrt{\sum_i p_i^2 \sum_i g_i^2} \qquad (2)$$

The summation in (2) is over a subset of the whole data, called here the averaging window; it is varied from 1 hour to 1 day. We also note in both (1) and (2) that the local mean values have been subtracted from both subsets before the calculations. It should be obvious that the correlation in (2) is computed from the same subset of the data as (1).

We used two superconducting gravimeter (SG) data sets in which we analysed the cross correlation between pressure and gravity, as well as the admittance. We will show there is a strong connection between these two quantities that implies the frequency dependence of α noted above. Secondly, we will attempt to use this connection to improve the standard admittance correction based on (1). Our motivation is clearly to reduce the residual gravity even further, assuming the correction is related to pressure, in gravity studies. Noting that the local effect also dominates the global corrections, any improvement in the former is worthwhile.

Admittance for Two Data Sets

We begin with 1 year of data (days 96001 - 96366) from the Boulder GGP station at Table Mountain Gravity Observatory, Colorado. It is important for this study that all (most) known signals, other than pressure, are first subtracted from gravity, because the calculation of (1)

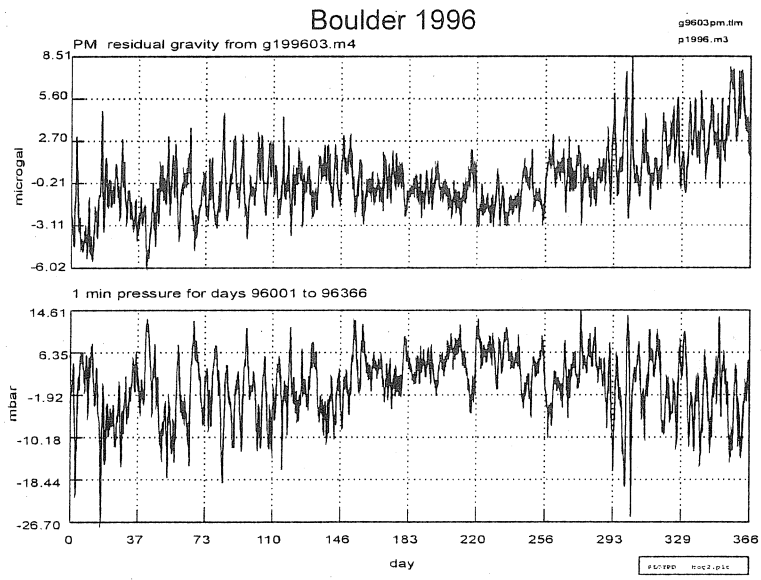

Figure 1. Residual gravity and pressure for BO.

and (2) is significantly affected by noisy data. We therefore fixed all obvious problems (gaps, spikes, offsets, earthquakes) in the pressure and gravity files, using the raw 5 second gravity and 1 minute pressure files. The gravity was then decimated to 1 minute and a local tide was subtracted using predetermined local tidal (delta, kappa) factors (see Crossley and Xu, 1998). Finally, we subtracted the IERS polar motion from the gravity. We show in Figure 1 the gravity residuals and pressure signals; it is clear that there is a large anti-correlation between the two series. This correlation can be seen more clearly in Figure 2 which shows the first 10 days of 1996.

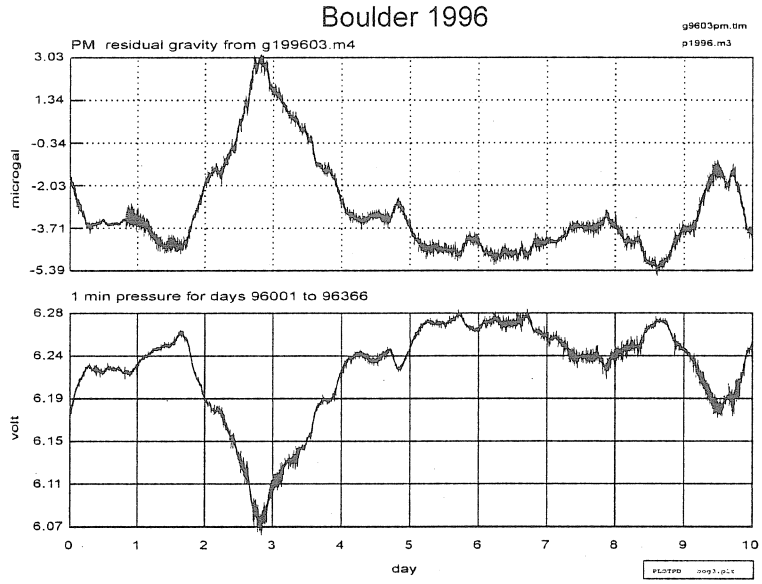

Figure 2. Residual gravity and pressure, 10 days.

Figure 3 shows identical treatment of data from the GGP station ST in Strasbourg (days 97113 - 97365). In this case both gravity and pressure are sampled every 2 sec, and the tidal parameters are of course different for this station.

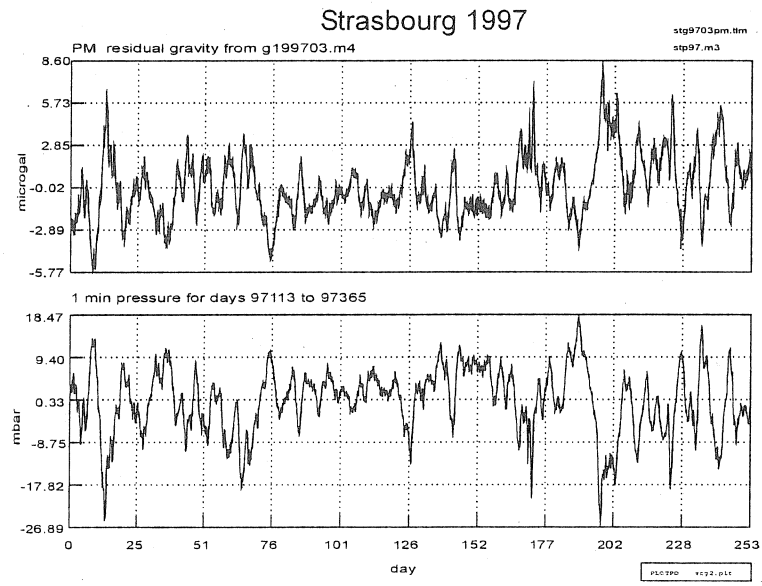

Figure 3. Residual gravity and pressure for Strasbourg

Despite the good correlation in these data sets, there are clearly times when the gravity does not respond directly to the pressure. An example can be seen in Figure 4, from Boulder in which the correlation is relatively poor, especially between minutes 2080 and 2140.

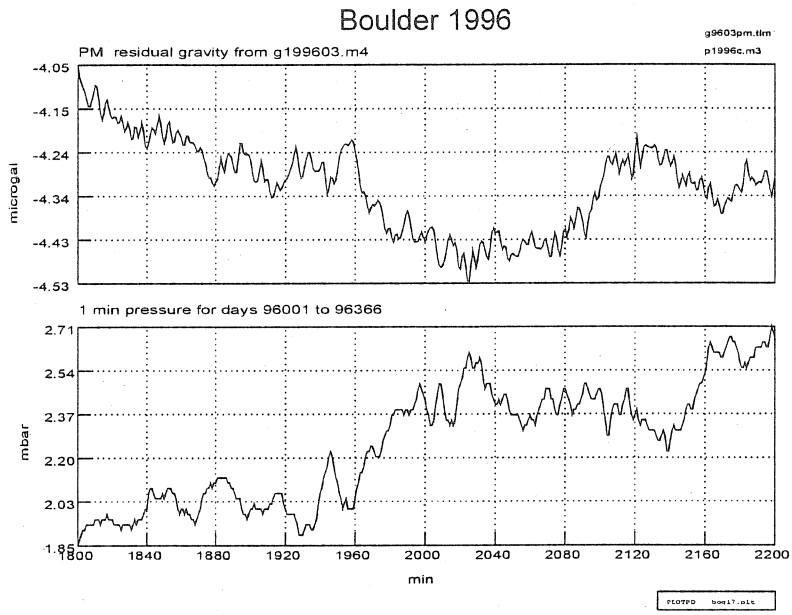

Figure 4. Residual gravity and pressure, detail showing poor correlation.

The question therefore arises - will the simple application of (1) sometimes inject an artificial and erroneous pressure signal into the gravity, instead of correcting for it?

We show the residual gravity (1) for BO for two standard calculations, one assuming that α is - 0.3 μgal mbar^{-1} and the second for a best fit of the whole of the series (Figure 5). In the latter case α = - 0.239 and the overall r_{pg} = - 0.666, which is only a modest correlation.

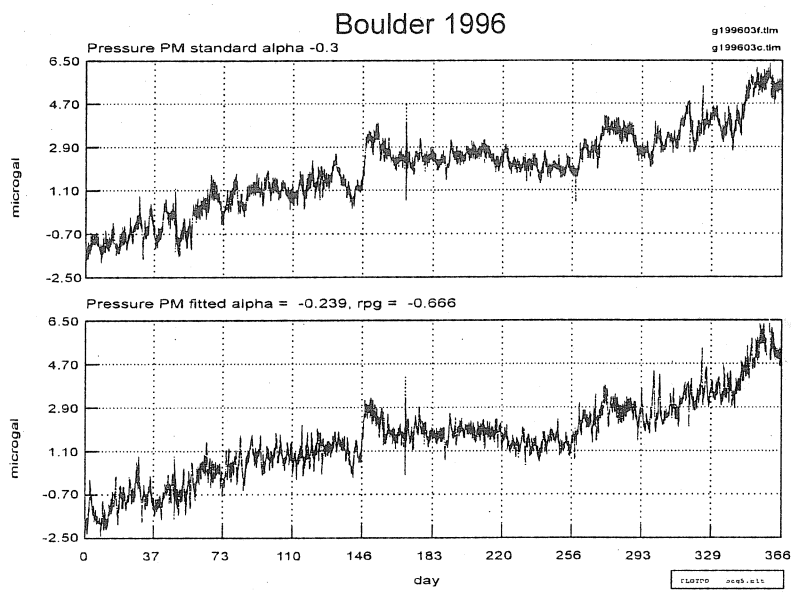

Figure 5. Corrected gravity for BO: nominal α (upper), fitted α (lower).

We repeat this for the ST series and obtain for the fitted case $\alpha = -0.270$ μgal mbar^{-1} and the overall correlation is very high, $r_{pg} = -0.910$ (Figure 6). Note the both the admittance and the cross correlation are higher for ST than for BO.

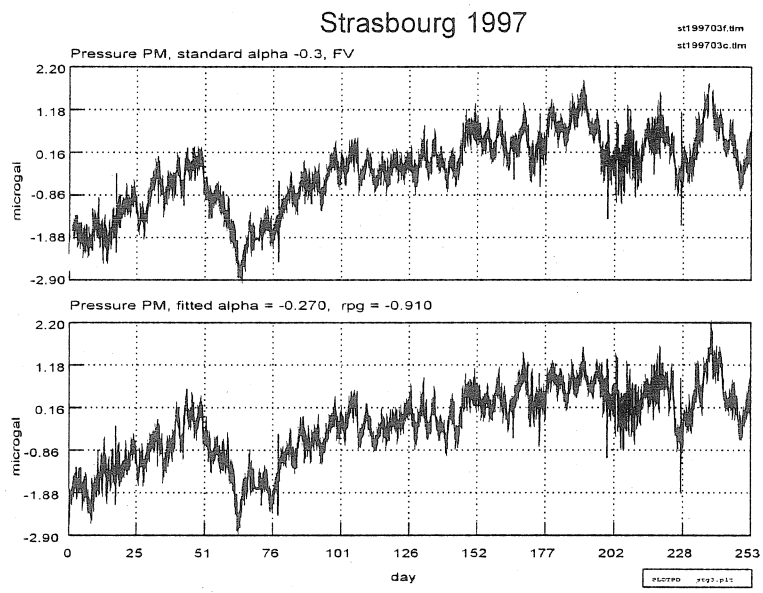

Figure 6. Corrected gravity for ST: nominal alpha (upper), fitted alpha (lower).

Relation Between Cross Correlation and Admittance

We now compute (1) and (2) for various subsets of the data:

- using the raw 5 or 2 sec data, with an averaging window of 1 hour (non-overlapping)
- the same for 6 hour and 1 day averages
- using the 1 minute data for each station, with an averaging window of 1 hour (non-overlapping)
- the same for 6 hour and 1 day averages.

Any non-pressure related signals in the gravity residuals obviously will corrupt the determination of correlation and admittance, especially for short averaging windows. Data spikes and instrumental disturbances should have no correlation with pressure. The period during the large surface waves of large earthquakes, for example, is one in which the correlation will be particularly bad. This is why a thorough cleaning of the data necessary.

For each experiment we produce a scatter plot of the cross correlation and admittance. Figure 7 shows the result for BO with a 1 hour averaging of the raw 5 sec data. Although the correlation coefficient must lie between -1 and 1 by definition, the values for the admittance of each block can be large; we show only those admittances between -2 and 2. There are some extreme values lying outside this plot.

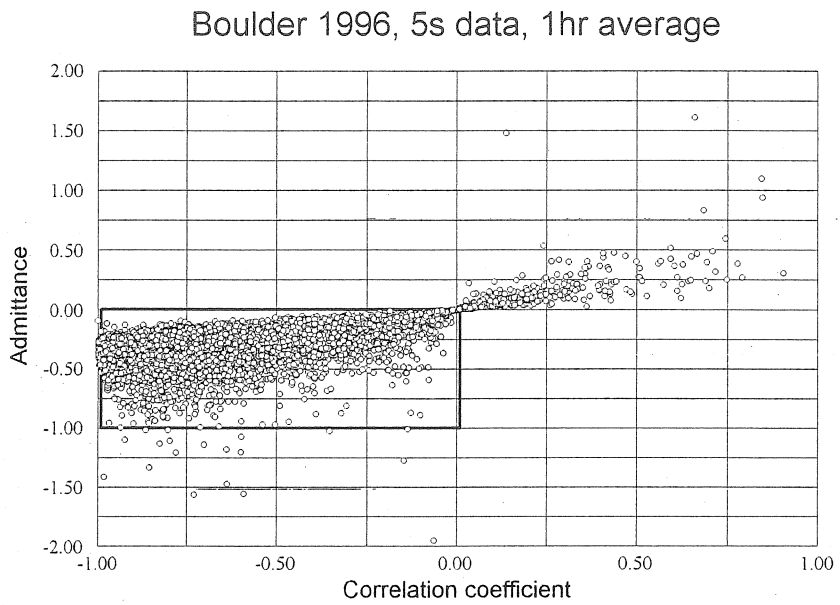

Figure 7. Scatter plot of Admittance vs Cross Correlation

There is clearly a well-defined pattern to the scatter plot, with a strong suggestion of a linear relation between α and r_{pg} extending from negative to positive correlations. Also obvious is the concentration of values around (0,0), indicating that where there is no correlation the admittance is also very small. For the rest of the study we concentrate on the portion of the plot between (-1,0) for both the correlation and also for α (in the heavy box).

We now quantify the above assumption and fit a straight line to the plot (Figure 8); in fact we show two fits, one for the L_1 norm (black) and the other for the L_2 norm (white). The slope of the two lines is 0.400 and 0.429 respectively. Of the 8784 hourly values for this year, 397 lie outside the acceptable limits for α .

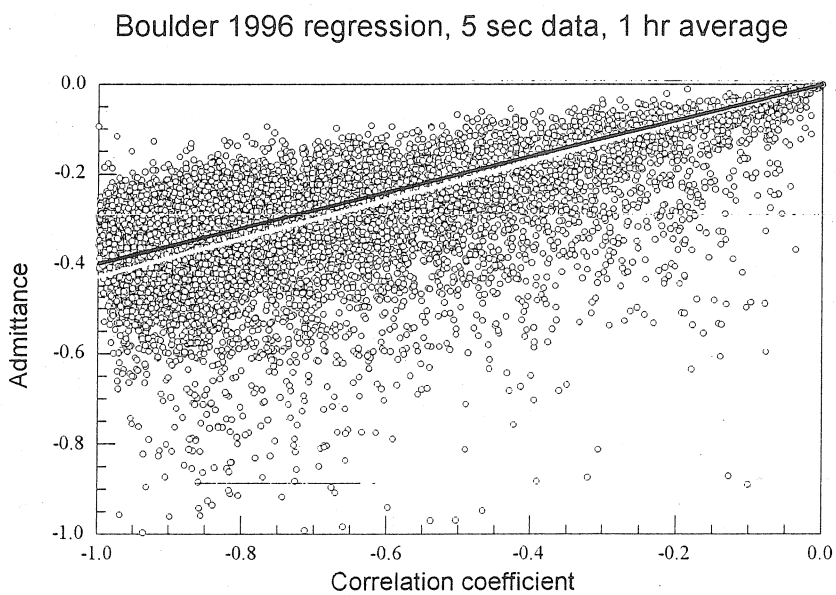

Figure 8. Admittance - correlation regression, 1 hour averaging.

Bearing in mind that the L_1 norm is more robust to outliers, we take its slope of 0.400 as indicative of the (α, r_{pg}) relationship. Note this value is also the intercept on the admittance axis when the pressure is perfectly anti-correlated with the gravity. Let us call this intercept the admittance factor α_0 for this data set.

As a contrast, we show in Figure 9 the same scatter plot, with fitted lines (almost coincident), for a 1 day averaging window of the same data. This time all 366 points lie within the acceptable limits for α.

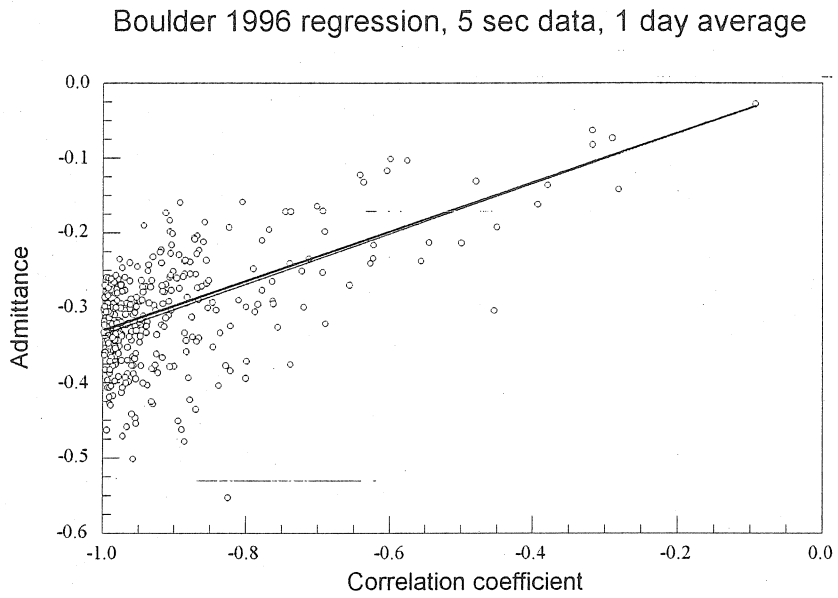

Figure 9. Admittance - correlation regression, 1 day averaging.

The admittance factors α_0 for the L_1 and L_2 lines are 0.330 and 0.336 respectively. Obviously, as the averaging window lengthens, the value of α_0 decreases because the lower frequencies have more influence in the data.

We performed a variety of similar experiments for averaging windows of 1 hour, 6 hours and 1 day on the Boulder data decimated to 1 min, and also on the ST data at 2 sec and 1 minute. Space does not permit all the plots to be shown, but they show the same characteristics as Figures 8 and 9, i.e. a linear trend with a well defined slope. These slopes, the admittance factors, are shown in summary form in Figure 10.

The symbols in Figure 10 refer to the station and year of the data (e.g. BO96, ST97) and the averaging window (e.g. -1hr), plotted against the data sampling. Note that we have added results from another year of BO data – 1997 - to compare the stability of the admittance with 1996; this data set is not otherwise discussed here.

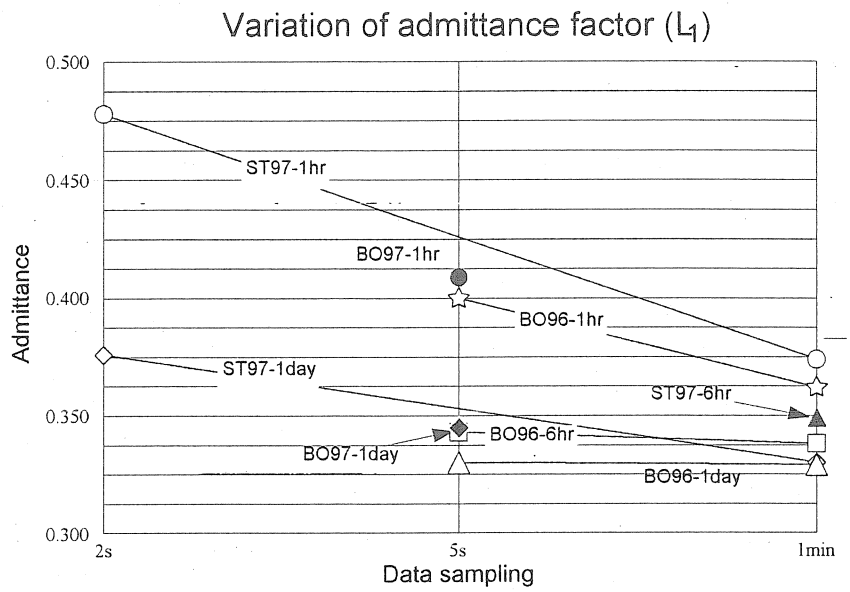

Figure 10. Admittance factors for a variety of data sets and averaging windows.

Our conclusions from Figure 10 are consistent with the variation of admittance with period (or frequency). We know that at high frequencies (periods of hours – minutes) the admittance approach a constant value of approximately –0.4 (e.g. Merriam, 1992; Crossley et al., 1995). At low frequencies (periods of months) the large scale atmospheric variations become important and the admittance decreases to values between -0.2 and -0.3. The data for Strasbourg in Figure 10 shows a high value of α (-0.478) probably because of the very high sampling periods and short averaging window.

Correcting Residual Gravity

One possible way to use the variables is to use the time dependent admittances (Figures 8 and 9) directly. The high scatter, however, includes a substantial number of values greater than 0.4, and these are not physically realistic. No doubt they would serve to reduce the residual gravity, but this would be an artificial reduction, much like that found in the frequency dependent treatment when the averaging window is reduced (Crossley et al., 1995).

Instead we make an assumption that the cross correlation can be used to derive an admittance from the straight line L_1 fits in the above figures. Thus, for each averaging window, we compute the admittance

$$\alpha = \alpha_0 r_{pg}, \tag{3}$$

assuming a linear relationship. The constant α_0 is the admittance factor which is just the slope (intercept) of the L_1 line. With this approach the admittance α is reasonably constrained in value. Even so, we also decide that for values of the cross correlation outside (-1,0) we will take the admittance to be zero.

We now apply a version of (1) to correct the gravity at each sample point (2s, 5s, 1 min ...).

$$g_{ci} = g_i - \alpha_i (p - p_{ref}), \tag{4}$$

where p_{ref} is a reference pressure and α_i is the admittance computed from (3). We can take p_{ref} typically either as a fixed nominal value for the station (as in absolute gravity pressure corrections), the first value (FV) of the series, or the series mean value. Figure 11 shows the results of taking the reference pressure to be the FV and computing (4) for the BO 1 minute data using a 1 hour averaging window.

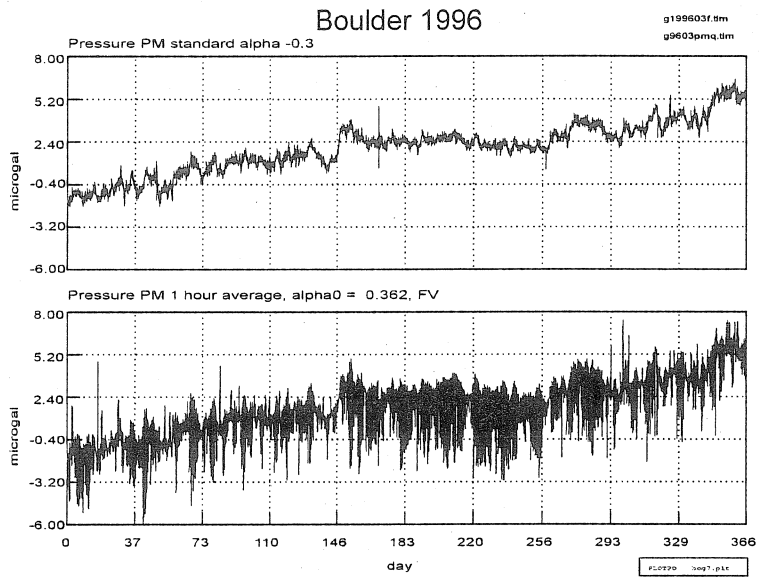

Figure 11. Gravity correction: fixed admittance (upper), variable alpha (lower). Note both plots are shown at the same scale.

The result is not encouraging. The lower curve shows large spikes that on closer inspection are coincident with places where the cross correlation falls to low values for some of the reasons given above. The spikes occur because a fixed reference is being used; identical results are found when using a mean pressure value as reference. If we extend the averaging window to 1 day the situation improves noticeably (Figure 12), basically because both the cross correlation and the admittance are much more stable in time.

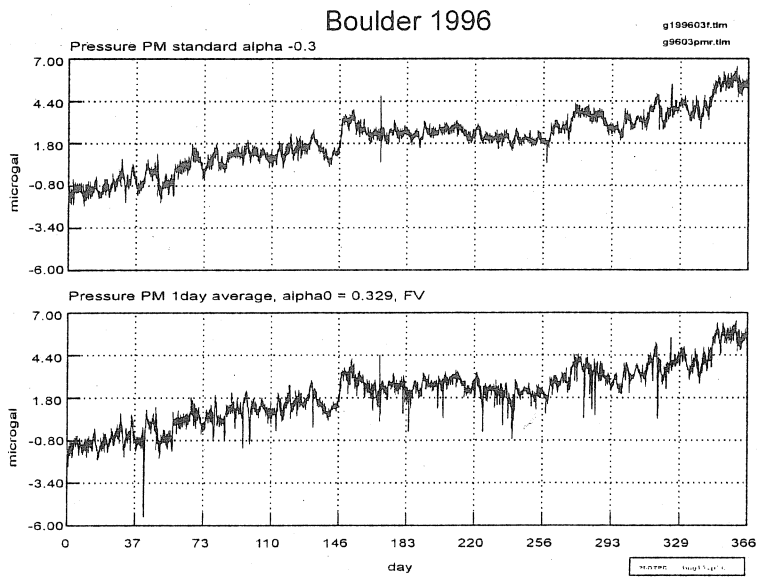

Figure 12. As Figure 11 but for 1 day averaging window.

We admit, however, that the gravity residuals for variable α, even for 1 day averaging, are still noisier than the standard correction. We can suggest two remedies, either restrict the value of α to a narrower range than permitted through (3), or change the pressure reference. In the latter case we need to ensure that when α is small (or even zero if r_{pg} is out of bounds) the correction is referred to the previous gravity and pressure values rather than a fixed reference. This latter idea can be implemented by using a moving pressure reference in the gravity correction:

$$\begin{aligned} \Delta g_i &= 0 && ,i=1 \\ \Delta g_i &= \Delta g_{i-1} - \alpha_i \,(p_i - p_{i-1}) && ,i>1 \\ g_{ci} &= g_i - \Delta g_i \end{aligned} \qquad (5)$$

This is slightly more complicated than (4), but ensures that the accumulated gravity corrected always refers only to the previous value. It can easily be shown that (5) reduces to (4) when α is constant, so that the choice of pressure reference is not critical in this latter case.

In Figure (13) we show the effect of implementing (5) on the Boulder data set. It is evident that the spikiness in the residual has gone (one might even say it is a little smoother), but instead we now see a slow drift of the signal away from the level when the admittance is constant.

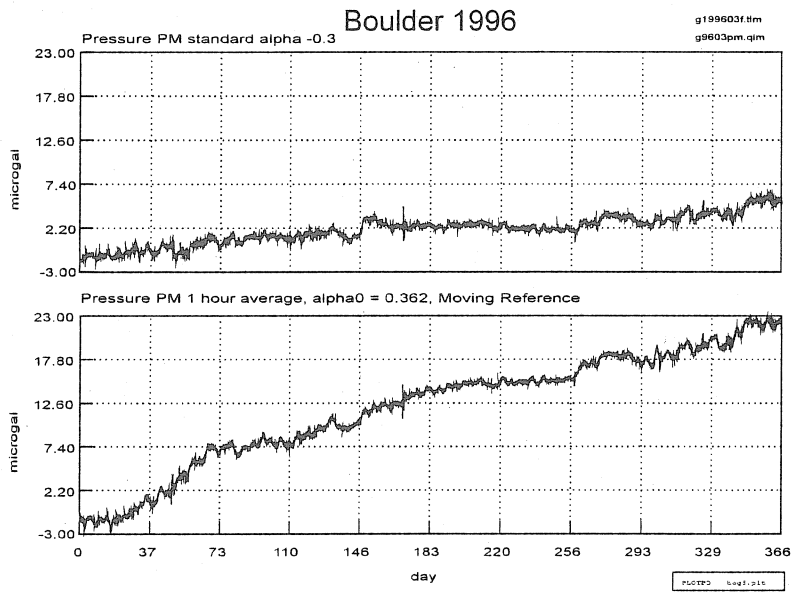

Figure 13. Corrected gravity using a variable admittance and moving average for the pressure reference.

The reason for this behavior is not hard to discover, as Figure 14 makes clear. We show a short section of the data, plotting the admittance and cross correlation, for a 1 hour average, showing the gravity corrections evolving according to (5). It can be seen that when the cross correlation becomes zero (or positive), then the admittance is zero and Δg does not evolve (it has a flat spot) and the gravity is not corrected at all for these points. The cumulative aspect of this method of correction then ensures that the gravity wanders away from its expected values.

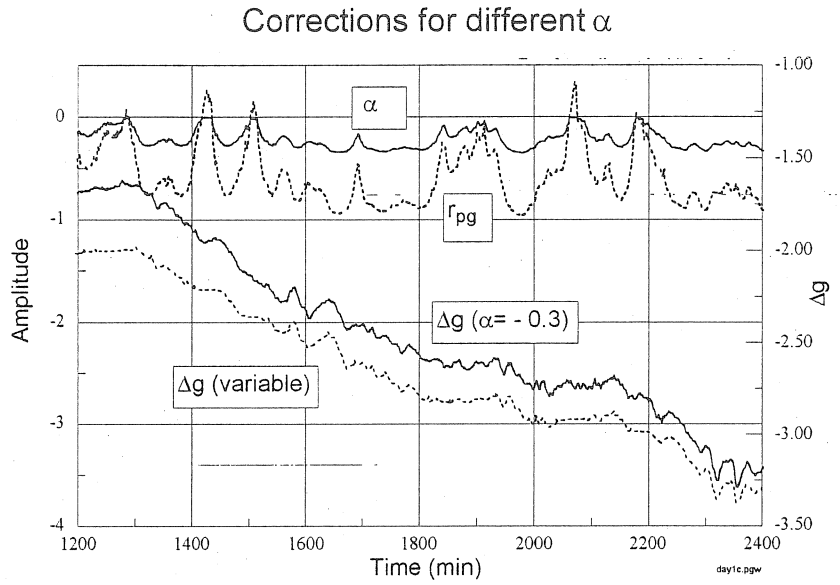

Figure 14. Detail on gravity correction using variable admittance.

Discussion and Conclusions

We have applied the corrections (4) and (5) to numerous other combinations of averaging windows and data sets, but were unable to find a case where there was a noticeable improvement over the use of a fixed α. We did however find that:

(a) the longer the averaging window, the closer we approached the solution for a constant α
(b) for both the FV and moving reference pressure models, the residuals improved when the averaging lengths were made longer
(c) the Strasbourg data set showed similar behavior to the examples shown above, even though the overall correlation was significantly higher than for BO.

We have also recently experimented on synthetic data sets and are able to shed some further insights on the pressure - gravity correlation and admittance. These and other findings will be discussed elsewhere.

Our principle conclusion is simply that the short term cross correlation appears too unreliable to serve as a basis for computing a time domain admittance. Long averaging windows are clearly more stable, but do not lead to superior results over a fixed admittance. We are thus reminded that it is fortunate in gravity studies that the simple local fixed admittance works so well for 90% of the atmospheric loading.

Acknowledgments

We thank CNRS for supporting this research. This is EOST contribution No. 2002-15-UMR 7516

References

Boy, J.-P. , J. Hinderer, and P. Gegout, 1998. Global atmospheric pressure loading and gravity, *Phys. Earth Planet. Int.*, **109**, 161-177.

Crossley, D. J., and S. Xu, 1998. Analysis of superconducting data from Table Mountain, Colorado, *Geophys. J. Int.*, **135**, 835-844.

Crossley, D. J., O. G. Jensen, and J. Hinderer, 1995. Effective barometric admittance and gravity residuals, *Phys. Earth Planet Int.*, **90**, 221-241.

Kroner, C. and G. Jentzsch, 1998. Comparison of air pressure reducing methods and discussion of other influences on gravity, *Proc. 13th Earth Tide Symposium, Brussels*, 423-430, Royal Observatory of Belgium, Brussels.

Merriam, J. B., 1992. Atmospheric pressure and gravity, *Geophys. J. Int.*, **109**, 488-500.

Müller, T., and W. Zürn, 1983. Observation of the gravity changes during the passage of cold fronts, *J. Geophys*. **53**, 155-162.

Neumeyer, J. and H.-J. Dittfeld, 1997. Frequency dependent atmospheric pressure corrections on gravity variations by means of cross spectral analysis, *Bull. Inf. Mar. Terr.*, **117**, 8649-8652.

Neumeyer, J., F. Barthelmes, and D. Wolf, 1998. Atmospheric pressure correction for gravity data using different methods, *Proc. 13th Earth Tide Symposium, Brussels*, 431-438, Royal Observatory of Belgium, Brussels.

Rabbel, W. and Zschau, J., 1985. Static deformations and gravity changes at the Earth's surface due to atmospheric loading, *J. Geophys*. **56**, 81-99.

Richter, B., 1987, Das supraleitende Gravimeter, Ph.D. Thesis, Deutsche Geodät. Komm., C 329, Frankfurt am Main, 124 pp.

Van Dam, T. and O. Francis, 1998. Two years of continuous gravity measurements of tidal and non-tidal variations of gravity in Boulder, Colorado, *Geophys. Res. Lett.*, **25**, 393-396.

Van Dam, T. and J. Wahr, 1987. Displacements of the Earth's surface due to atmospheric loading: effects on gravity and baseline measurements. *J. Geophys. Res.*, **92** B2, 1281-1286.

Warburton, R. J. and J. M. Goodkind, 1977. The influence of barometric pressure fluctuations on gravity. *Geophys. J. Roy. Astron. Soc.*, **48**, 281-292.

Workshop: Analysis of Environmental Data for the Interpretation of Gravity Measurements.
Institut für Geowissenschaften der Uni Jena, ,11.-15.03.2002.

Modelling of the field of gravity variations induced by the seasonal air mass warming during 1998- 2000

by Dietrich Simon*

Abstract
The paper informs about results of model calculations concerning the gravity variation component $g_c(t)$ induced by the seasonal warming of air masses. The modelling used the data of radio sounding launchings from eight Western European stations. The monograph of SIMON [2002] (Mitteil. des BKG, Band 23, in press) will contain an extended description of the model used for this purpose, the software AMACON and a test sample for its application. In the first step of modelling the air mass attraction functions A(t) have been calculated. Then, we correlated the A(t) functions with the corresponding time series of measured ground air pressure, p (t), to eliminate the components which are proportional to the local air pressure variations. The relative best elimination of this component was attained when using a value r_{AP} = 0,40 µGal/hPa for the coefficient of regression. This is valid for all the eight meteorological stations. The regression coefficients obtained from the correlation of gravimetric curves of measurement and local air pressure variations at ground level are known to be 25- 30% smaller as a consequence of the reducing influence of the loading effect.

The modelling work aimed at the determination of the component $A_c(t)$ of air mass attraction occurring with constant air pressure at ground level in the expression

$$A_c(t) = A(t) - r_{AP} * p(t).$$

So far, $A_c(t)$ has not been taken into account in routine evaluations of gravimetric series of measurement (SUN, DUCARME & DEHANT [1994], BOY, HINDERER & GEGOUT [1998]). For the change-over from the attraction component $A_c(t)$ to the gravity component $g_c(t)$ the relation

$$g_c(t) = - A_c(t)$$

is used.

The calculations showed that the main constituent of $A_c(t)$ is an annual wave, which reaches double amplitude of 1.6 µGal at 7 of the 8 stations mentioned. But at Ny Alesund (Spitsbergen) the double amplitude is about 2.0 µGal. The differences between the maximum and minimum values of $A_c(t)$ are 2,5 µGal at Medicina /Italy and 4,0 µGal at Ny Alesund/ Spitsbergen island. The mean amplitude of the annual wave $A_c(t)$ is latitude dependent and the maxima and minima occur in January and July, respectively. AMACON calculates the attraction of a cylindrical body of air masses at its ground (earth surface). The 10 mb pressure level is the upper boundary surface of the cylinder, which has the constant radius of 113 km. Assuming a varying air volume of time-constant mass (air pressure at ground level being constant!), the seasonal warming will primarily result in a volume expansion in the vertical direction. The centre of gravity of this volume will shift in the same direction. In the area of the Stuttgart weather station, for example, the altitude of this centre of gravity of the air body was found to be 247 m higher in July 1983, as compared to December of the same year.

The annual waves induced by air mass warming can explain only part of the seasonal components measured by high-precision gravimeters. But the elimination of these components from the series of gravimeter measurements may improve the chance of identifying and modelling more precisely other annual components, for instance the effects of seasonal sea level variations (CHAMBERS, D. P., CHEN, J. L., NEREM, R.S., TAPLEY, B. D.: [2000]).

*Bundesamt für Kartographie und Geodäsie, Richard-Strauss-Allee 11, 60598 Frankfurt/ M.
e-mail: simon@ifag.de, Tel: 069-6333-274

1. Introduction

The task of the modelling work consisted in determining of the component $g_c(t)$ of gravity variations occurring as an effect of seasonal warming or cooling of the atmospherical air layers under the condition of a constant air pressure at ground level. The calculations are basing on the aerological data of eight Western European radio sounding stations: Stuttgart, München, Essen, Dresden, Meiningen, Lindenberg in Germany, Medicina in Northern Italy and Ny Alesund at the Spitsbergen island, Norway. The measuring period was 01.01.1998 – 31.12.2000. The 8 stations are located in an area which is influenced almost by the Atlantic climate. This area has a North- South extension of about 34 ° and an East West extension of about 7° only. This array of stations was intended to allow the determination of a possible dependence of the component $g_c(t)$ on the latitude.

Table 1 gives a sample of a complete aerological data record in the form required for the calculation of a single value of $g_c(t)$. The modelling was carried out by means of the software package AMACON (SIMON [2002]).

Pressure [hPa] Fixed levels	Geopotential height [gpm]	Station height [m]
980	315,3	315
925	774	
850	1439	
800	1912	
700	2933	
600	4099	
500	5440	
400	7000	
300	8910	
250	10060	
200	11420	
150	13190	
70	17900	
50	19960	
30	23080	
20	25540	
10	29840	

Table 1: Stuttgart station, 28.01.1998, 12 h GMT: Sample of an aerological data record

2. Proof of the existence of an air mass attraction component, which does not depend on the variations of the local air pressure

So far the routine correction work of gravimetric series of measurements concerning atmospherical influences has not taken into account the existence of vertical air mass displacements also in the case that the air pressure at the earth does not vary (DUCARME & DEHANT [1994], BOY, HINDERER & GEGOUT [1998]). Therefore, it was necessary to prove the existence of such an effect at the beginning of the modelling . For this purpose the aerologic data of the radio sounding station Hannover / Germany of 1972 – 1994 were used. The data were published by the DWD in a manner comparable with Table 1, but as monthly mean values.

To exclude the influence of air pressure variations on A(t) the modelling was carried out with the aerological data sets only where ground pressure values were 1010 hPa (31 sets) or 1008 hPa (27 sets). Table 2 shows the geopotential heights of the pressure level 30 mb and marks in this way the month the data set comes from. The geopotential heights of the 30 mb surface are in July / August about 1100 gpm higher than in December/ January.

Year	Jan	Feb	Mar	Apr	May	Jun	Jul	Aug	Sep	Oct	Nov	Dec
1972												
1973					24062				24061			
1974			23345	23680				24304				
1975							24368		24099		23571	
1976							24374					
1977					24131							
1978								24301				
1979					24075							
1980	23215			23804	24050						23461	
1981						24257			24048			
1982												
1983												
1984												
1985							24321					
1986							24307					
1987			23471									
1988									24058			
1989										23703		
1990												23329
1991				23716					24075	23851		
1992							24332					
1993						24154				23674		
1994										23673		

Table 2a: Hannover: Geopotential heights of the 30 mb surface (ground pressure: 1010 hPa)

Year	Jan	Feb	Mar	Apr	May	Jun	Jul	Aug	Sep	Oct	Nov	Dec
1972			23769			24276						
1973												
1974					24003							23265
1975	23444			23807								
1976									24055			
1977												
1978					23994		24403					
1980						24339						
1980								24351				
1981							24414					
1982											23450	
1983												
1984						24205						
1985								24282				
1986			23516									23258
1987		23356			23952		24375				23403	
1988					24017							
1989												
1990				23753								
1991												
1992												
1993							24305					
1994					23946			24274				

Table 2b: Hannover: Geopotential heights of the 30 mb surface (ground pressure: 1008 hPa)

Concerning the 1010 hPa set group there is no data set in February, and in the case of the 1008 hPa set group there is no data set in October. After the calculation of the corresponding air mass attraction values A(t) these gaps were closed by interpolation, and mean values were determined for months with more than one set of data.

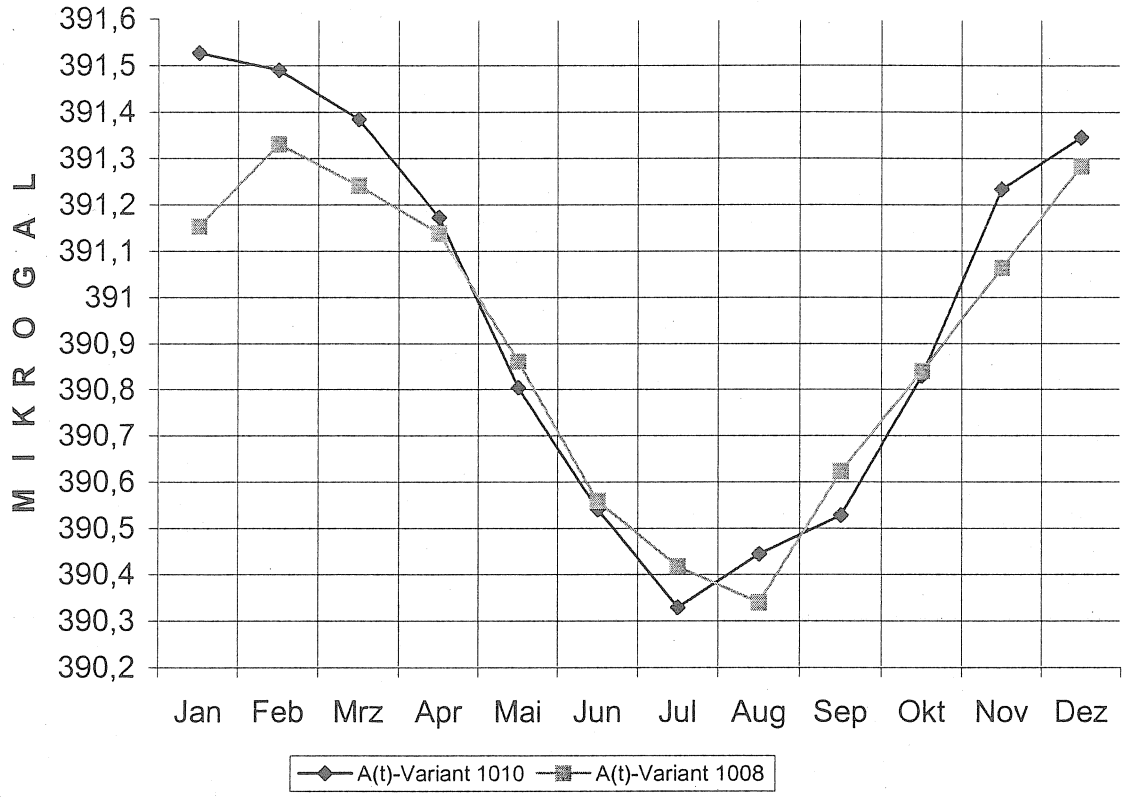

Fig.1: Hannover: Seasonal variation of the air mass attraction A(t) in the case of a constant ground air pressure (1010 hPa or 1008 hPa, respectively) during the year

Fig.1 shows the seasonal variation of the air mass attraction A(t) for this special case, in which there are not any variations of local air pressure at the earth's surface. The double amplitude of the seasonal wave reaches a measurable amount of about 1,2 µGal. The air mass attraction $A_c(t)$ reached maximum values in January/February and minimum ones in July /August. The corresponding component of gravity variation has the opposite sign:

$$g_c(t) = - A_c(t). \qquad (1)$$

3. Empirical determination of the coefficient r_{AP} for the regression between air mass attraction A(t) and the local air pressure variations p(t) at the ground

Differing from the situation represented by Fig.1 the component $A_c(t)$ of air mass attraction is generally small in relation to the second component $A_p(t)$ defined by (2):

$$A_c(t) = A(t) - A_p(t) = A(t) - r_{AP} * p(t). \qquad (2)$$

A(t) = air mass attraction, $A_p(t)$, $A_c(t)$ = components of A(t)
p (t) = air pressure at the ground, $r_{AP} = r_{AP}$ [µGal/ hPa] regression coefficient

To separate the component $A_c(t)$ from the total effect A(t) of air mass replacements we need a well- fitting numerical value of the regression coefficient r_{AP} . It is possible to determine such a value empirically by a stepwise change of r_{AP} and subtraction of the corresponding $A_p(t)$ from A(t) using the condition that the residual curve $A_c(t)$determined by this iteration method must be completely free from any components depending on the local air pressure variations p(t). An example of application of this method is shown in Fig.2:

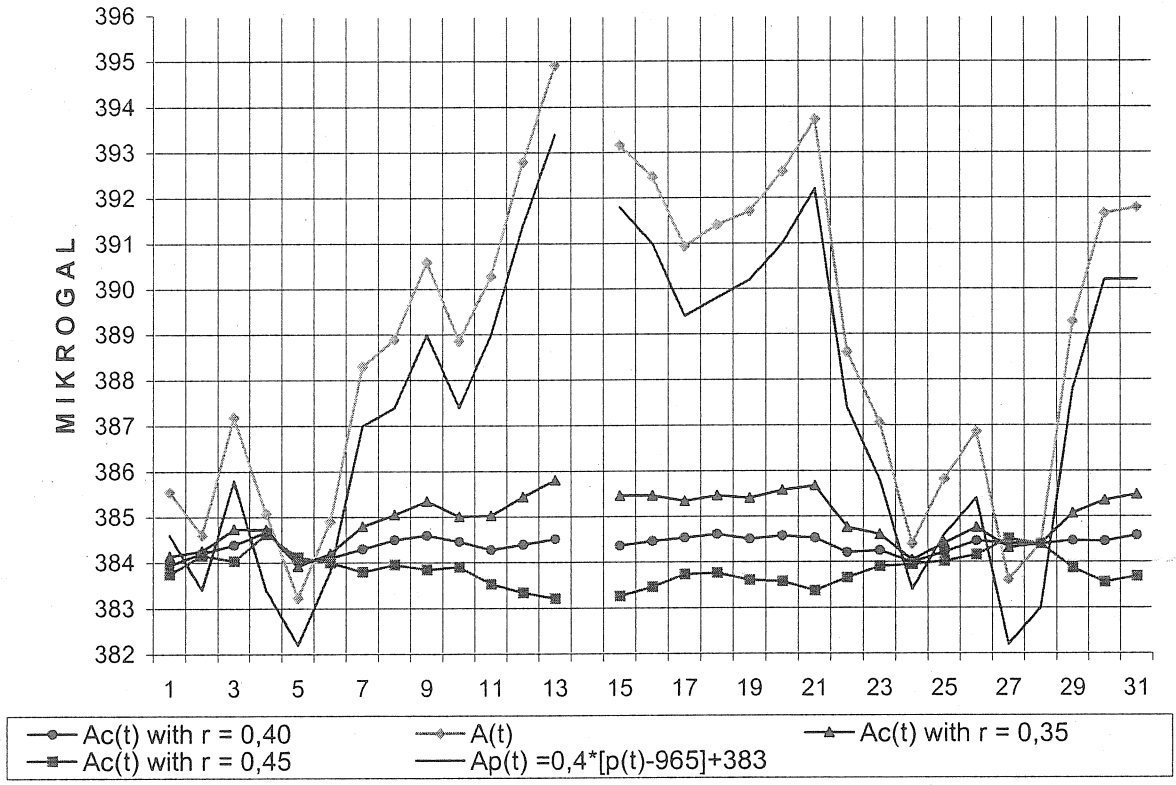

Fig.2: Stuttgart, 01. -31.01.2001: Air mass attraction A (t) and its components $A_p(t)$ and $A_c(t)$, determined with different numerical values of the coefficient r_{AP}

According to Fig. 2, there is a relative minimum of correlation between the model curves $A_c(t)$ and $A_p(t)$ in the case that the coefficient r_{AP} = 0,40 µGal/ hPa was used for the calculation of $A_p(t)$. Analogical tests with the data of other radio sounding stations, for instance Medicina, Hannover or Ny Alesund, respectively, led to the same result.

The numerical value of r_{AP} = 0,40 µGal/ hPa determined by this iteration method is in accordance with the results of modelling carried out by BOY, HINDERER & GEGOUT (1998, p.165, Fig. 2). The authors have calculated the atmospherical components of the gravity variations at the earth's surface for a spherical cap model body. In the case that the radius R of this model body is equal to 113 km or 1°, the numerical value of r_{AP} is equal to 0,40 µGal/ hPa .

4. Calculation of the components $A_c(t)$ of air mass attraction for 8 Western European stations during the period 1998 – 2000

Using the software AMACON (SIMON [2002]) the components $A_c(t)$ of the air mass attraction were calculated at 8 surface measuring points (radio sounding stations) located in Western Europe. The measuring period was 01.01.1998 – 31.12.2000. The raw data of the modelling are aerological data sets (like table 1) of the radio sounding launchings carried out

daily at 12 h GMT . The same pressure coefficient 0,40 µGal/ hPa was used for the separation of the attraction components $A_c(t)$ at all the 8 stations. A first look at the diagrams in Fig. 3 – 6 shows several common characteristics and also some deviations between the 8 model curves:

4.1 Dependence of $A_c(t)$ on phase and latitude

- The attraction components $A_c(t)$ reach their maximum values regularly in the winter months January and February, respectively, at all the 8 stations
- The time position of the summer minimum of attraction is shifting with decreasing latitude of the station from July (Ny Alesund) to August (Medicina)
- The double amplitude of the seasonal wave $A_c(t)$ or its width of variation, respectively, reaches its maximum values at the North (Ny Alesund) and at the North- East (Lindenberg, Dresden) of the area of investigation.

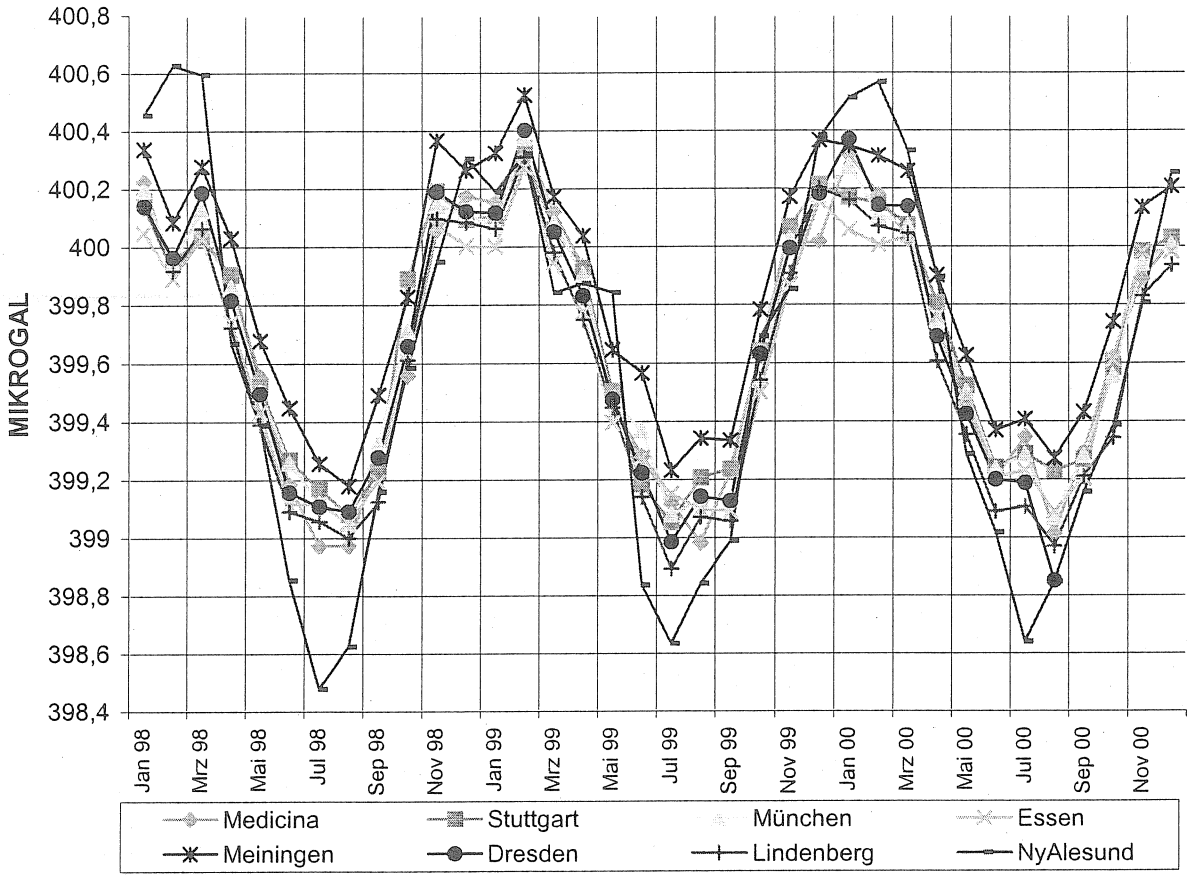

Fig. 3: Seasonal variations of $A_c(t)$ at 8 European weather stations. Consideration of the air masses from the earth's surface up to the height of the 10 mb pressure level

4.2 Deviations from the regular course induced by anomalies of the climate

- Samples for such anomalies: 1. Relative minimum in 1998, February; 2.Relative maximum in 1999, February; 3. Relative minimum in 2000, July. The effect number 3 may have been induced by a series of weeks spoilt by rain (July 2000) after a hot spring (May - June 2000). The July 2000 effect did not occur at Ny Alesund.

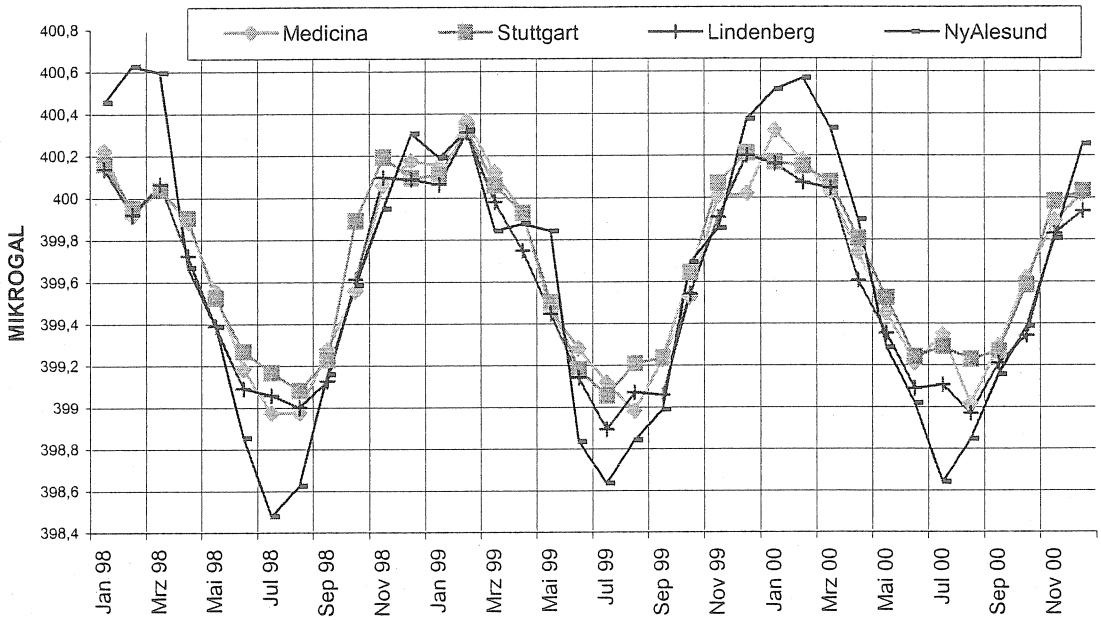

Fig.4: Model curves for the component A_c (t) of air mass attraction calculated for 4 Western European stations located at latitudes between 44°N and 78°N

4.3 Hints on influences of the Atlantic and continental climate

- "Atlantic climate influence zone": Stuttgart, Essen, Meiningen (winter month 1999, 2000)
- "Atlantic climate influence zone": Strong intermediate anticyclone during 2000, July.
- "Continental influence zone": München, Dresden (winter months 1999, 2000)

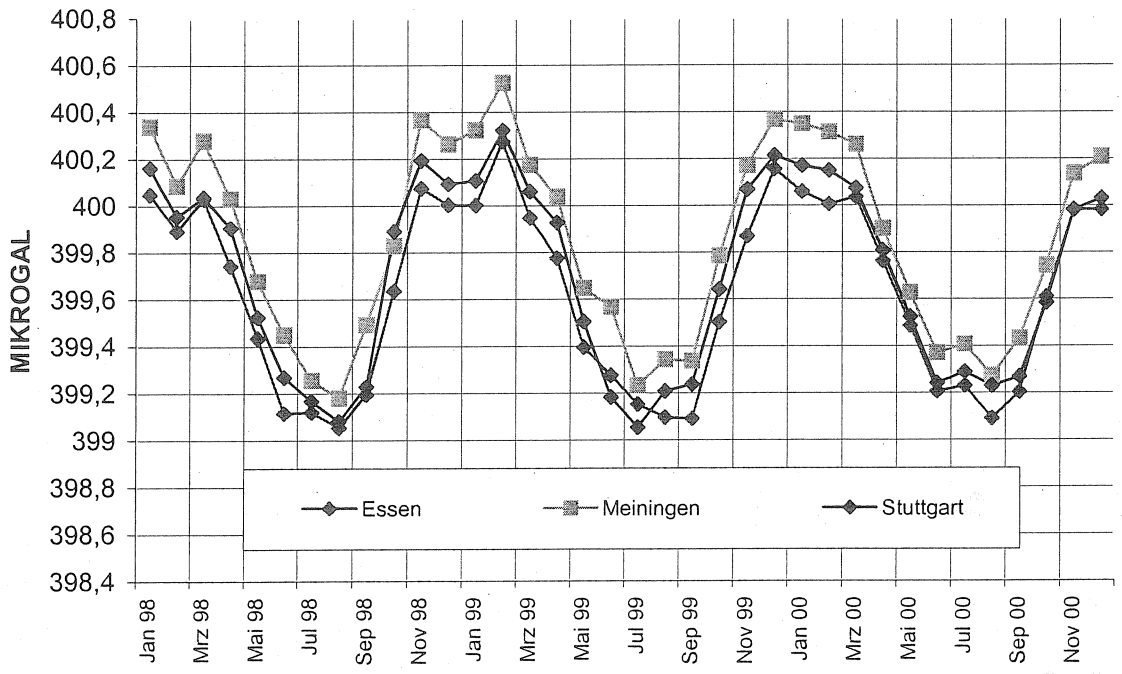

Fig.5: Model curves $A_c(t)$ of air mass attraction calculated for 3 stations located inside the Atlantic climate influence zone

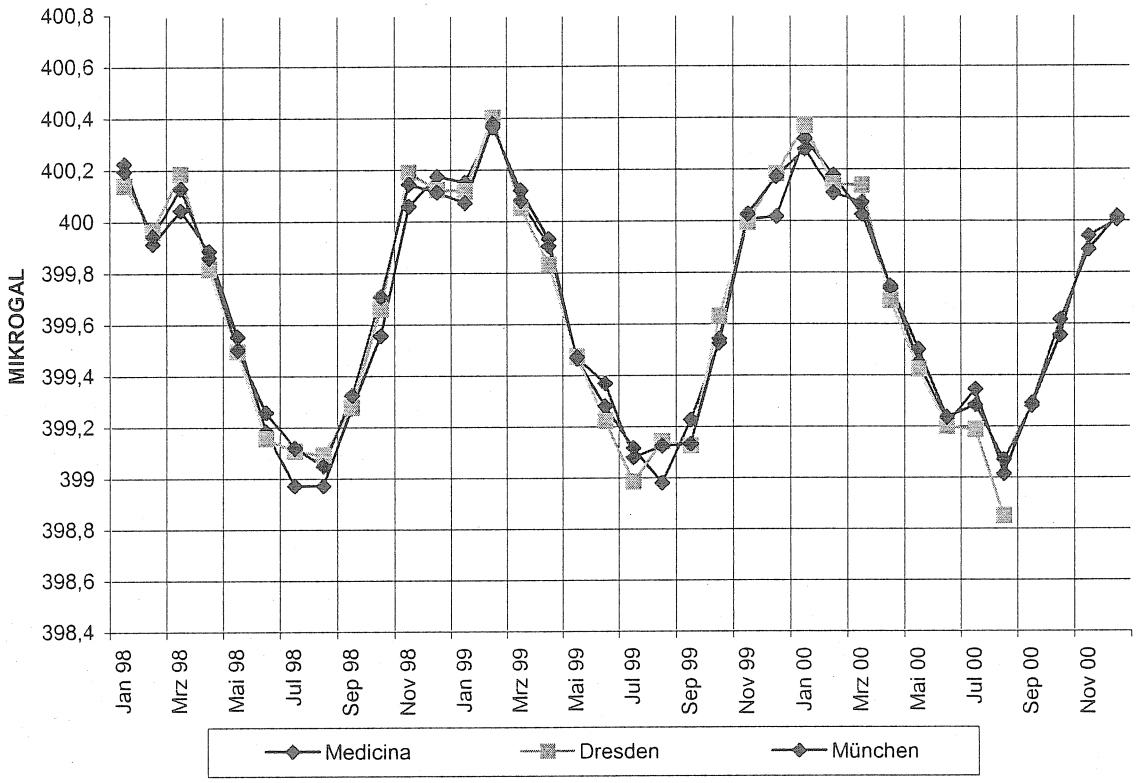

Fig.6: Model curves $A_c(t)$ of air mass attraction calculated for 3 stations located near the continental climate influence zone

5. Modelling of the gravity variations induced by the seasonal air mass warming at Bad Homburg during 1981- 1984

A first application of the new software AMACON was the calculation of the model function $g_c(t)$ for the gravimeter station Bad Homburg where a superconducting gravimeter installed by RICHTER [1987] had recorded continuously during 1 August 1981– 1 May 1984. Radio sounding measurements are not carried out at Bad Homburg. The next radio sounding stations were located at Stuttgart and Essen, respectively, during that period. Table 3 shows the coordinates of both the meteorological stations and their distances to Bad Homburg:

Station	Longitude	Latitude	Distance to Bad Homburg
Bad Homburg	8,611°	50,229°	
Essen	6,967°	51,400°	175 km
Stuttgart	9,200°	48,850°	163 km

Table 3: Distances of the next radio- sounding stations to Bad Homburg

To check the regional variability of the model curves the air mass attraction components $A_c(t)$ were calculated for both radio- sounding stations, Stuttgart and Essen. The result is shown in Fig. 7:

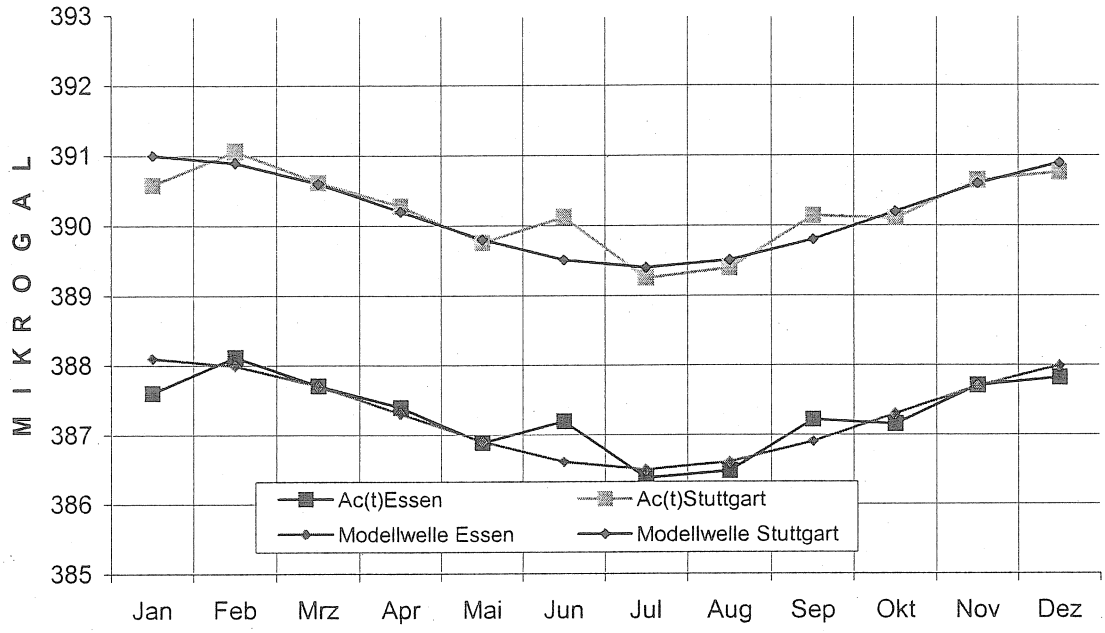

Fig. 7: Radio- sounding stations Stuttgart and Essen 1983: Attraction components $A_c(t)$ induced by the seasonal warming

The Bad Homburg gravimeter station is located about halfway between Essen and Stuttgart. As a consequence of the small differences between both $A_c(t)$- curves represented in Fig. 7 the modelling of the gravity variations of Bad Homburg was made by means of the radio sounding data of Stuttgart only. Fig. 8 shows the gravity component $g_c(t)$ at Bad Homburg together with a model cosinus function. The latter has an amplitude of 0,8 µGal and reaches its maximum value on 31 July. The evident deviations of $g_c(t)$ from the cosinus function during January/February 1982 and 1983, respectively, appeared during a time as the climate in Europe was influenced by the so-called Atlantic pendant of the "El Ninjo" phenomenon (LATIV & GRÖTZNER [2000]).

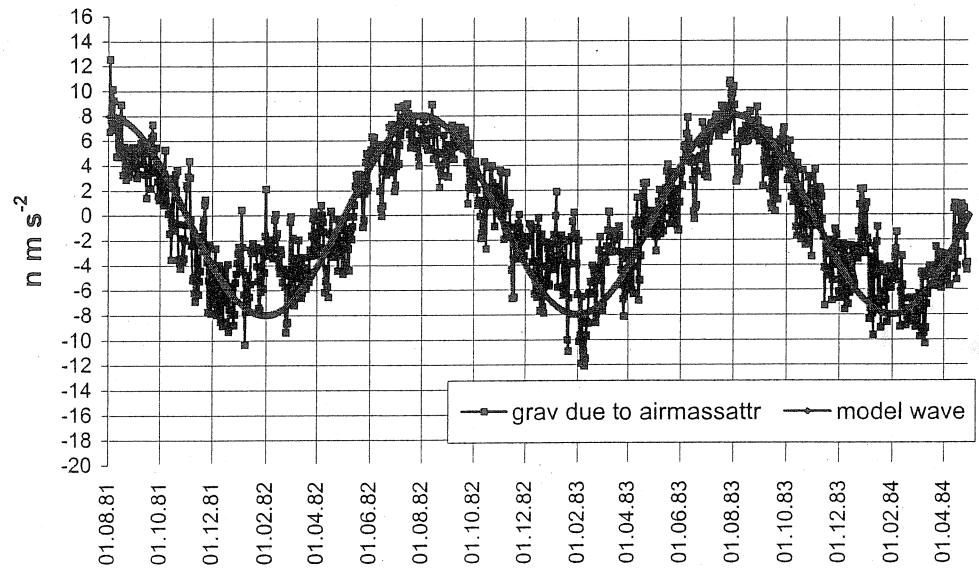

Fig.8: Model curves of the gravity variations $g_c(t)$ at Bad Homburg 1981-1984

The change-over from the attraction component $A_c(t)$ to the gravity component $g_c(t)$ was carried out using formula (1).

The model curve $g_c(t)$ varied during 1981-84 by 2,5 µGal. The maximum value was reached at August 1981, and the minimum ones at February 1983. In Fig. 9 the $g_c(t)$ curve was compared with a cosinus function having a double amplitude of 1,6 µGal. The relative maximum of this model function of gravity as on 31 July corresponds with a minimum of air mass attraction caused by the seasonal warming. Concerning the deviations from the model cosinus function the strongest anomalies were observed during the winter month, for instance in January- February 1982 or January- February 1984. Additionally, the gravity component induced by the polar motion was included in Fig. 9. The diagram gives an impression of the amplitude relation of both effects at Bad Homburg during 1981-84. The seasonal component of $g_c(t)$ reached about 1/6 of the maximum gravity variation induced by polar motion:

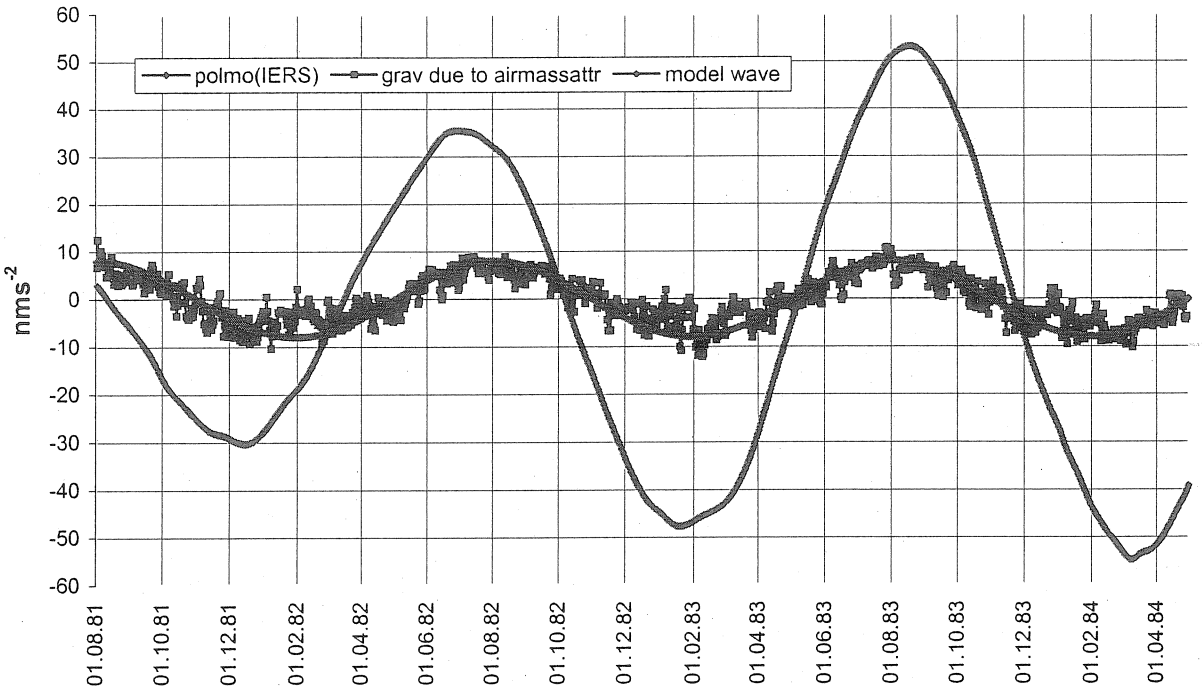

Fig. 9: Bad Homburg station: Gravity components induced by the seasonal warming of the atmospherical air masses and by the polar motions, respectively

The deviations of $g_c(t)$ from the model cosinus function referring to Jan./ Feb.1982, Jan./ Feb.1983 and Jan./ Feb.1998 (Fig. 3– 6) coincided with known El Ninjo (ENSO) events in the Southern Pacific. The effect of Jan./ Feb.1999 having the opposite sign could maybe correspond with the La Ninja event 1999. The directions of the deviations from the regular (Cosinus-) course of the $g_c(t)$ curve are compatible with such an interpretation (relative warming of air masses during Jan./ Feb.1998). In accordance with the results of investigations obtained by BARNETT, HURREL and LATIV (LATIV & GRÖTZNER [2000]) there is a pendant of the Southern Pacific ENSO phenomenon in the Atlantic. The Atlantic El Ninjo/ La Ninja effects are considered to be of considerable importance for the weather events in Europe.

The next step of investigation was to answer the question whether, e.g. the residual curve rk2 of the gravimetric measurements at Bad Homburg 1981-84 contains indeed an annual wave

with the harmonic constants of the calculated model curve $g_c(t)$. To determine the residual curve rk2 of the gravimetric TT40 series of measurements we had to subtract three additional components from the gravimetric measuring data. These components are induced by tidal influences, by atmospherical and by instrumental effects, respectively. For this purpose the following formulas were used in accordance with M. HARNISCH, G. HARNISCH, G. RICHTER und W. SCHWAHN [1998]:

$$rk2 = rk1 - \text{2nd degree polynomial} \quad (3)$$

$$rk1 = TT40 + 3{,}4 * airpr - tides\ (Ri) \quad (4)$$

TT40 [nms^{-2}] = measuring data of the TT40 gravimeter
2nd degr. polynomial = approximation of the instrumental drift of TT40
r_{TT40} = -3,4 nms^{-2}/hPa = air pressure coefficient (including the loading effect)
airpr = airpr [hPa] local air pressure variations p(t)
tides (Ri) = tidal model according to an analysis by RICHTER [1987, S.85].

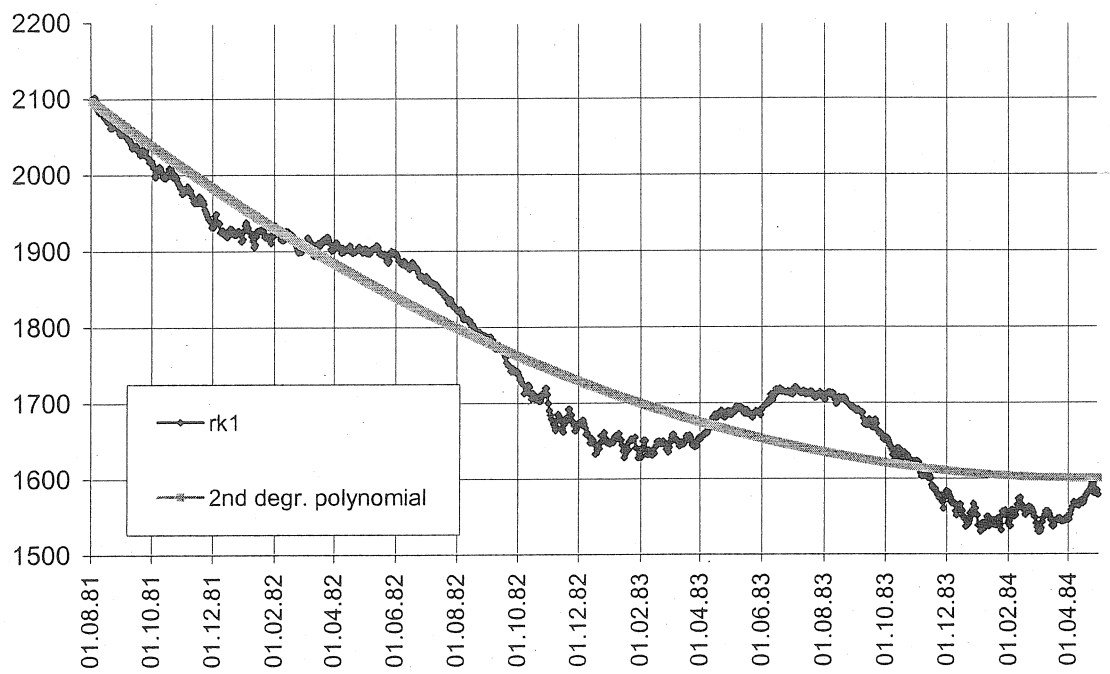

Fig. 10: Residual curve rk1 and the 2nd degr. polynomial (approximation of instrumental drift)

The regression coefficient r_{TT40} = -3,4 nms^{-2}/ hPa was determined by M. HARNISCH et al. [1998] using the ETERNA tidal analysis software. The negative sign of r_{TT40} is a consequence of formula (1).

Concerning the amount of the air pressure coefficient calculated for Bad Homburg 1981-84 it seems to be too large in comparison with those ones determined for other stations, to which values of about r_{TT40} = –3,0 nms^{-2}/hPa apply. Furthermore, M. & G. HARNISCH [2001] derived from the gravimetric data series 1999 –2001 of Bad Homburg a value of –2,95 nms^{-2}/ hPa. That means, it is probable that the residual curves rk1 and rk2 in Fig.s 10- 12 are not completely free of air pressure constituents.

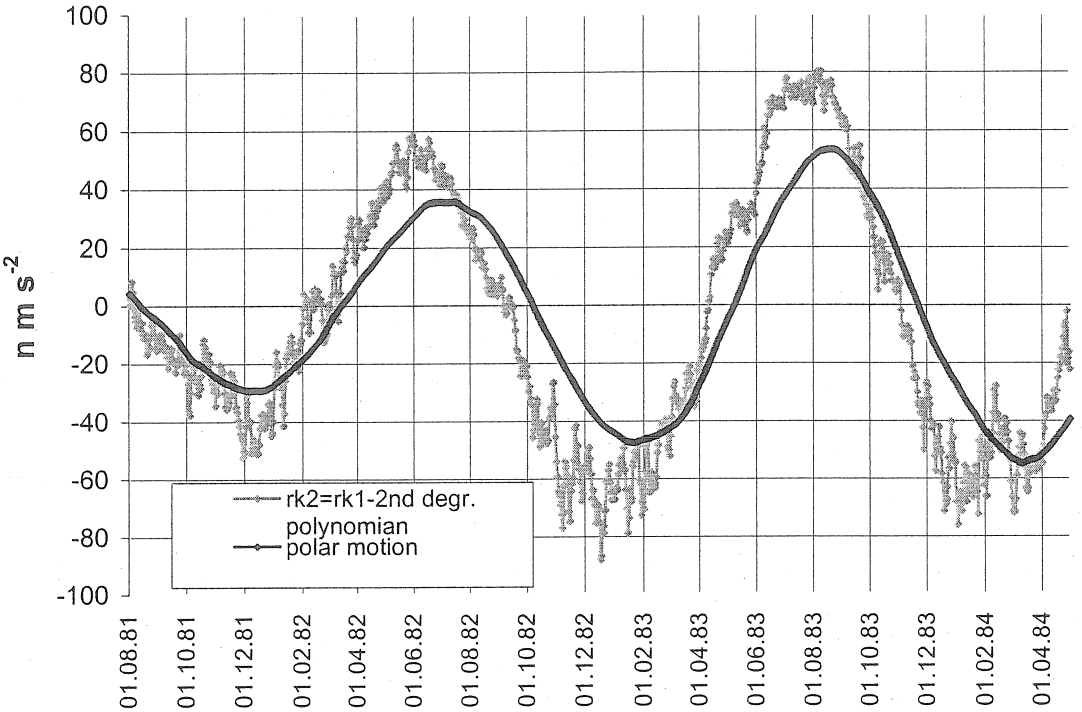

Fig.11: Residual curve rk2 of the TT40 measurements at Bad Homburg 1981 -84 in comparison with the local gravimetric component induced by polar motion

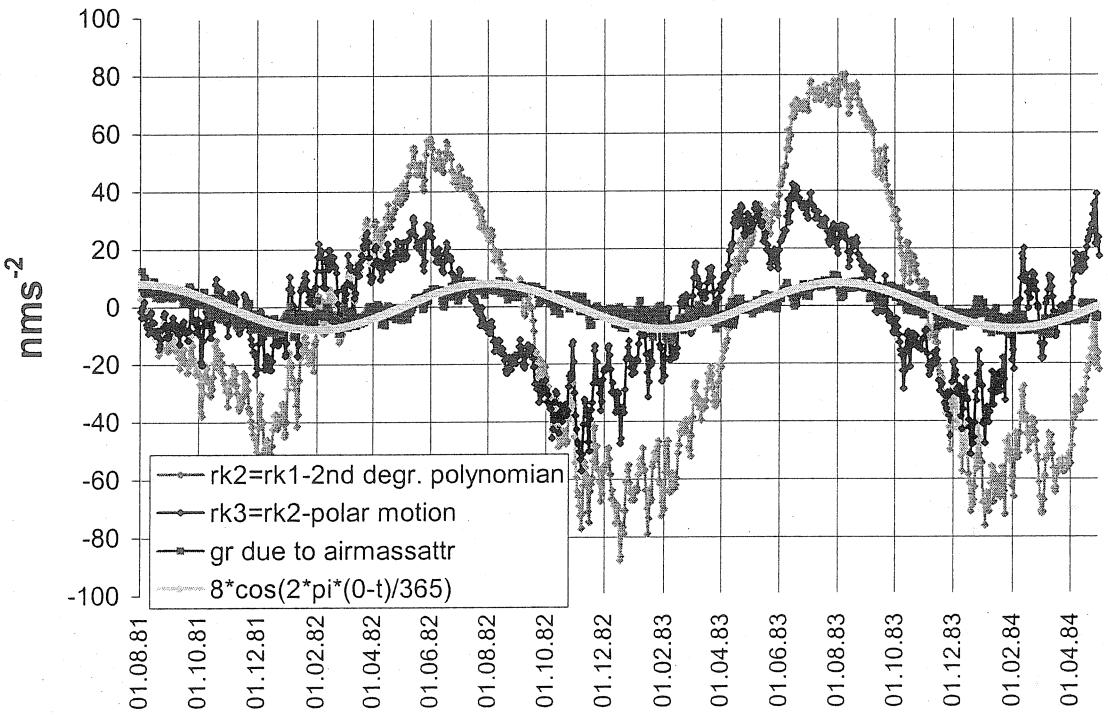

Fig.12: Bad Homburg, 1981-84: Residual curves rk2 and rk3 in comparison with the gravity components $g_c(t)$ induced by the seasonal warming of atmospherical air masses

In accordance with Fig. 12 an annual component with the double amplitude of 7– 8 µGal obviously predominates in the gravimetric residual curve rk3 of Bad Homburg 1981-84. This seasonal wave has its minimum values in November – January and its maximum values in June – July. The main constituent of the gravity variation $g_c(t)$ calculated from radio sounding data is an annual wave with about the same phase, too. But the double amplitude of the $g_c(t)$ wave reaches only 20 % of that one included in the gravimetric residuum rk3. However the residual curve rk3 of Bad Homburg 1981 – 1984 has not been corrected as yet concerning hydrological components.

7. Modelling of the gravity component $g_c(t)$ caused by air mass warming for Medicina 1998 – 2000 and comparison of the latter with the gravimetric residual curve

The gravity components induced by air mass attraction and by polar motion, respectively, were determined for Medicina 1998 – 2000 (Fig.13) and compared with an cosine function in an analogical manner as in the case of Bad Homburg 1981-84:

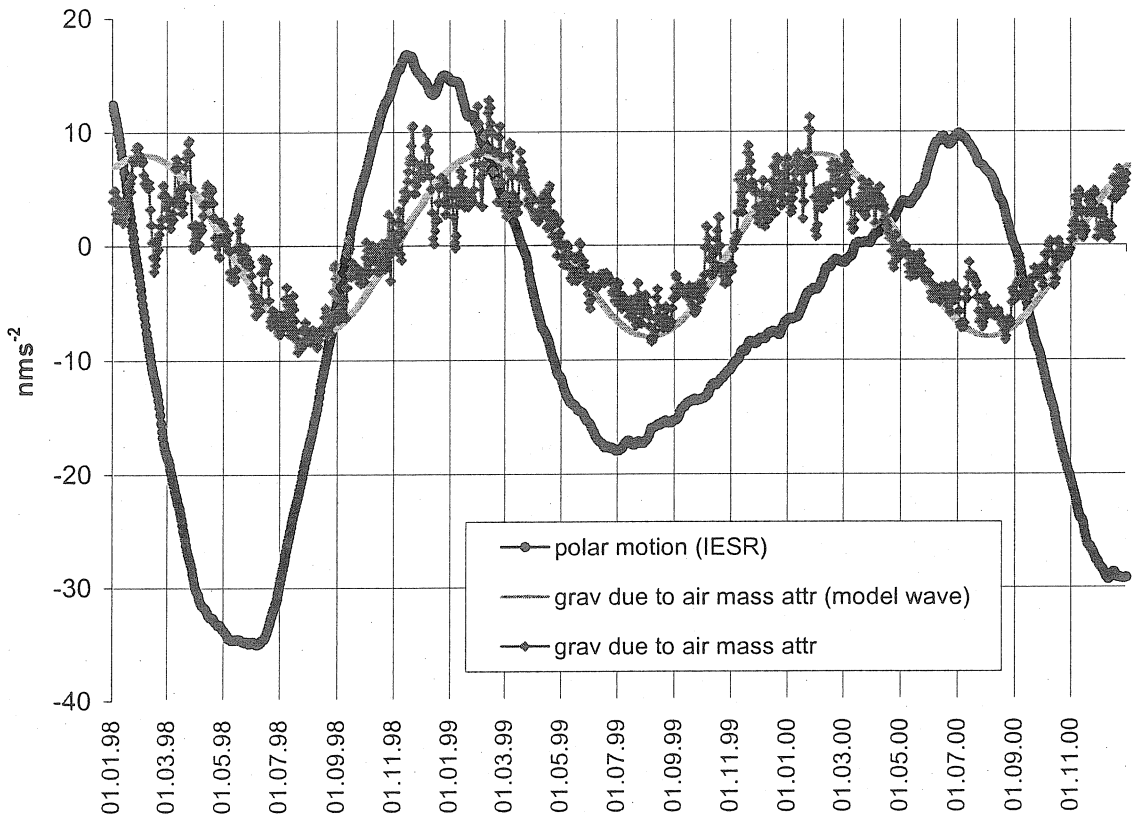

Fig.13: Medicina station: Gravity components induced by seasonal air mass warming and by polar motion, respectively

The component $g_c(t)$ was calculated for Fig.13 with a sampling rate of 24 hours. The same was performed for the polar motion effect. As a consequence, the fine structure of the regional anomalies as shown in Fig. 3- 6, was made perceptible. The polar motion component, which presented relatively small amplitudes during the period Sept. 98 – Sept. 99, allows a look on its fine structure for a short time, too. Here, the anomaly occurring during the La Ninja event at Jan/ Feb. 1999 is interesting. The $g_c(t)$ model curve of Fig.13 was used in Fig.14 for the

correction of both the time series of measurements received by means of the superconducting gravimeter SG023 and by 3 absolute gravimeters of the FG5 type:

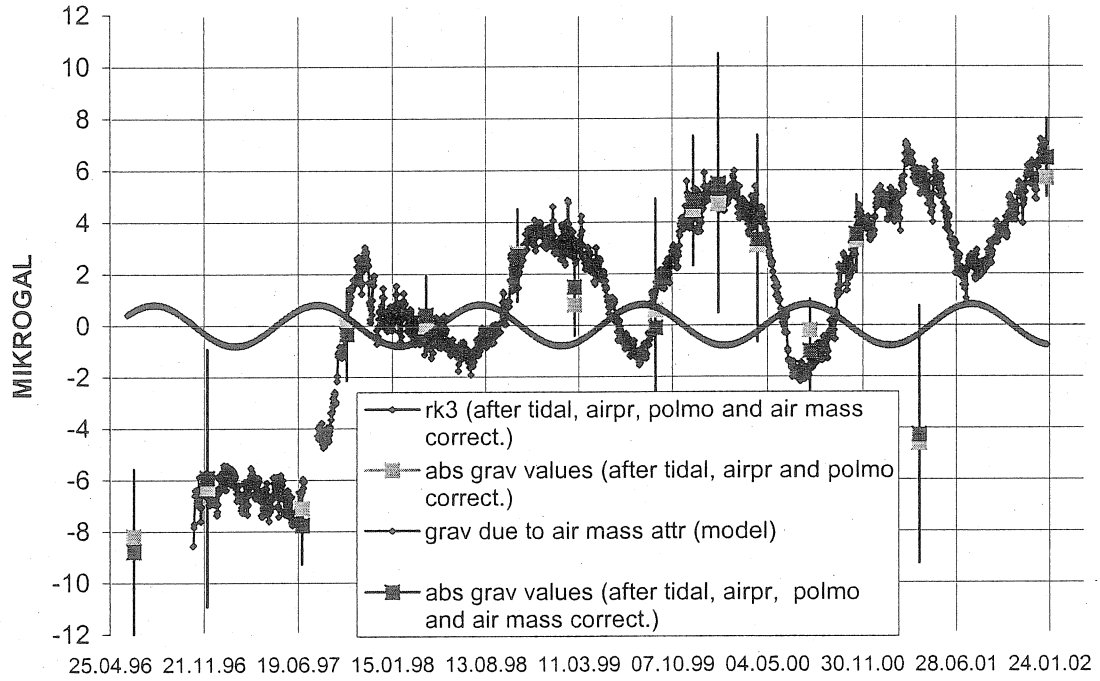

Fig.14: Medicina station: Residuals of the SG023 and FG5 measurement series 1996- 2000

8. Modelling of the gravity component $g_c(t)$ for Ny Alesund (Spitsbergen) 1998 – 2001

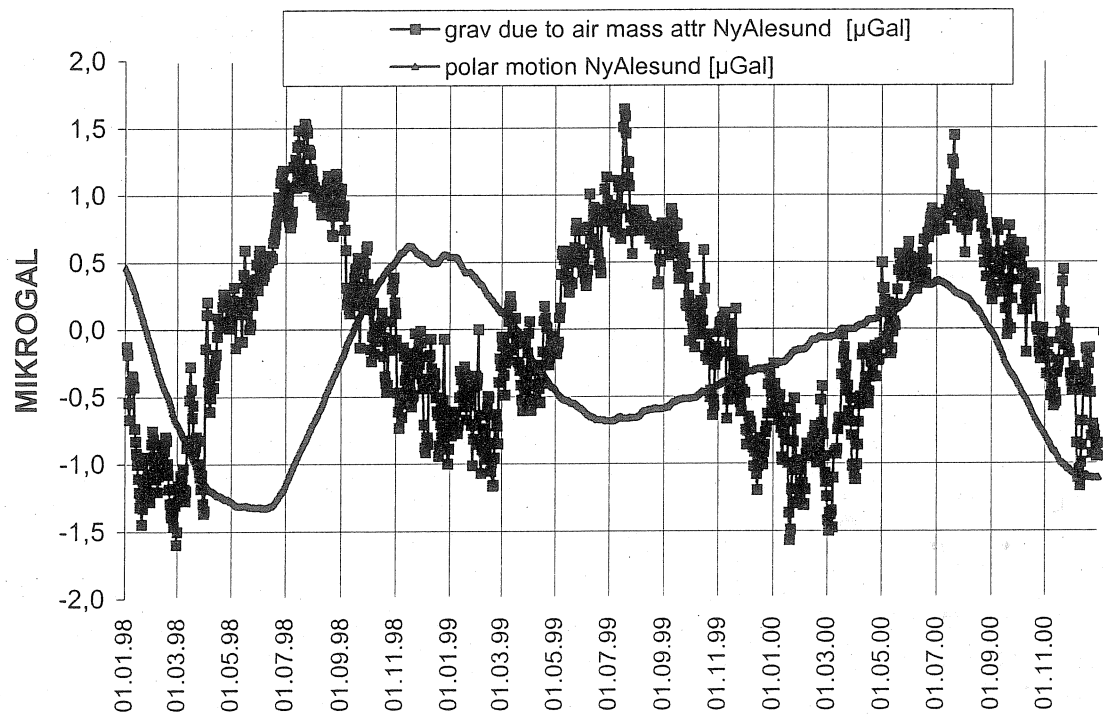

Fig.15: Ny Alesund station: Comparison of the gravity components induced by polar motion and by the seasonal warming of atmospherical air masses

In accordance to Fig.15 the effect of polar motion has the same order of magnitude at the Ny Alesund station as the $g_c(t)$ component of gravity variations caused by seasonal air mass warming. This phenomenon is induced by the high geographical latitude of the station.

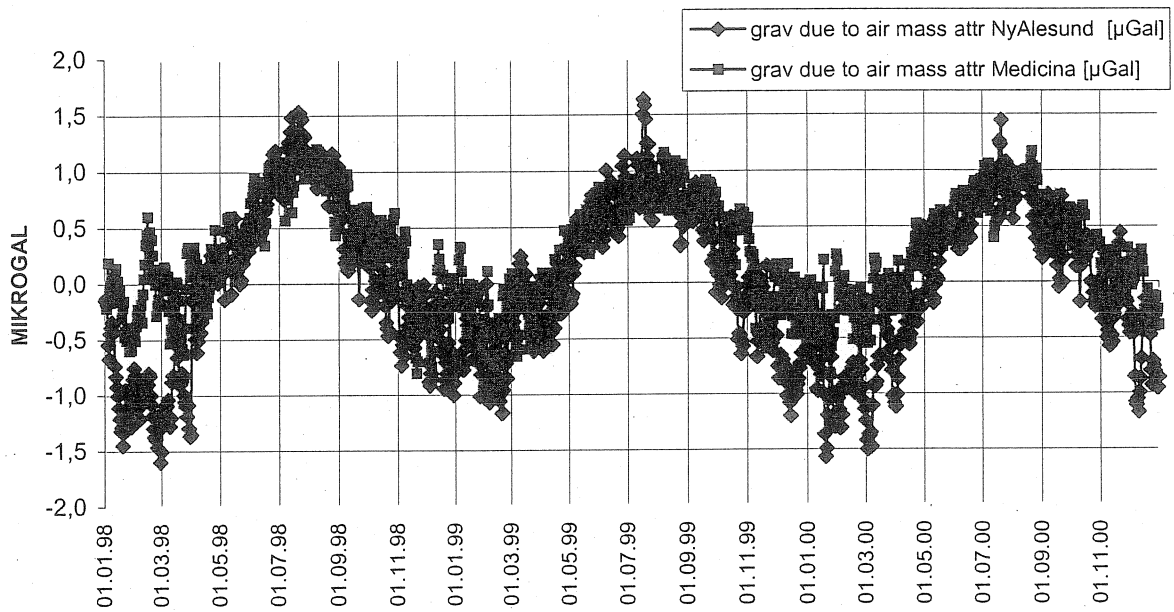

Fig.16: Ny Alesund and Medicina stations: Comparison of the gravity variations induced by the seasonal air mass warming

According to Fig.16 the maximal variation of the $g_c(t)$ component (sampling rate: 24 h) of Ny Alesund station is about 1,5 µGal larger than that of the Medicina station (Fig.16). But the polar motion effect of Ny Alesund reaches only 35 % of the corresponding effect observed at Medicina/ Italy (Fig.17):

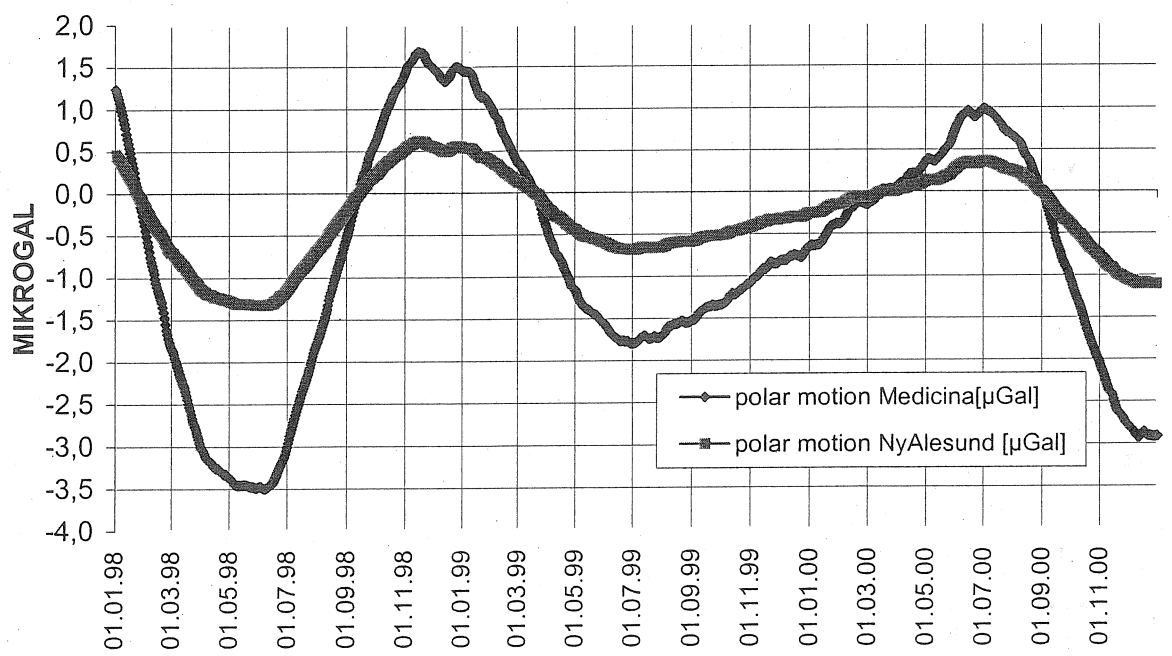

Fig.17: Comparison of the polar motion effects at Ny Alesund and Medicina

9. Conclusions and Outlook

- The seasonal warming/ cooling of the atmospherical air masses and special climatic anomalies, for instance the anomalies of Jan/Feb 19882, Jan/Feb 1983 and Jan/Feb 1998 comparable with El Ninjo effects or other anomalies, as for instance that of Jan/Feb 1999, produced in Western Europe gravity variations of at least 2,5 – 4,0 μGal (Fig.18). The effect could even be greater eventually at stations located in the influence zones of the continental climate, for instance at Warsaw, Budapest or Moscow.
- The modelling of the seasonal warming effect considered the effects of atmospheric air layers up to the height of the 10 mb pressure level. However, test calculations by SIMON [2002] have shown that the magnitude of the $g_c(t)$ variation increases with growing thickness of the model air layer packet. The radio soundings can seldom reach a ceiling which surpasses the height of the 10 mb surface by more than 2-3 km. The number of the model air layers considered could further increase if meteorological data of the CHAMP/ GRACE projects were available for this purpose. It was estimated that the $g_c(t)$ variation would increase by 20 % if the calculation was made on the basis of CHAMP/ GRACE data instead of radio sounding data.
- To obtain a first impression of the $g_c(t)$ field of gravity variations by means of radio sounding data we planned to perform a completion of the results presented here by the modelling of the effects at 2-3 inner- continental radio- sounding stations The results of these additional calculations should be included in the monograph of SIMON [2002], too.

My thanks are due to the Alfred– Wegener- Institut (Dr. König- Langlo), Bremerhaven, the ARPA Meteo Data (Dr. Zanoli), Medicina, and the German Meteorological Service (Dipl.-Met. Koelschtzky), Offenbach , for their kind provision of the data.

10. Literature

BOY, HINDERER & GEGOUT [1998]: Global atmospheric loading and gravity. Physics of the Earth and Planetary Interiors 109 (1998) 161 – 177. Elsevier Science B.V.

CHAMBERS, D. P., CHEN, J.L., NEREM, R.S., TAPLEY, B.D.: Global Mean Sea Level Change and the Earth's Water Mass Budget. Geophys. Res. Lett. (2000)

HARNISCH, M., HARNISCH, G., RICHTER, B., and SCHWAHN, W., SASAGAWA, G.: Estimation of Polar Motion Effects from Time Series Recorded by Superconducting gravimeters. Proc. of the 13th Int. Symp. on Earth Tides. Bruxelles 1997, pp

LATIV, M., GRÖTZNER, A. [2000]: The equatorial oscillation and its response to ENSO. Climate Dynamics (2000) 16; 213- 218

RICHTER, B. [1987]: Das supraleitende Gravimeter. Anwendung, Eichung und Überlegungen zur Weiterentwicklung. DGK. Reihe C: Dissertationen. Heft Nr.329

SIMON , D.[1998]: Jahresperiodische Schwerevariationen mit Amplituden von 1 - 2 μGal als Folge von saisonalen Dichteänderungen in der Atmosphäre (erste Rechenergebnisse) Paper pres. on the Working Group "High Precision Tidal Data Processing", 31.08. – 01.09.1998, Jena, Germany

SIMON, D. [2002]: Berechnung der saisonalen Änderungen der Luftmassenattraktion anhand von aerologischen Messdaten. Mitt. des BKG Frankfurt, Bd.23 (in press)

SUN, H. -P., DUCARME, B., & DEHANT, V. [1994]: Theoretical Calculation of the Atmospheric Gravity Green functions. Paper pres. on the Working Group "High Precision Tidal Data Processing", 30.08. – 02.09.1994, Bonn, Germany

DETECTING HYDROLOGICAL SIGNALS IN TIME SERIES OF IN-SITU GRAVITY MEASUREMENTS: A FIRST APPROACH

R IJpelaar (1), P. Troch (1), P. Warmerdam (1) , H. Stricker (1), B. Ducarme (2)
(1) Sub-department of Water Resources, Wageningen University, The Netherlands.
(2) Royal Observatory of Belgium.
ruben.ijpelaar@users.whh.wau.nl / Fax: +31-317-484885

A new generation of in-situ gravity meters and remote sensing techniques enable the detection of small variations (equivalent to less than 10 mm water layer) in mass at the Earth's surface, such as water storage in surface and subsurface reservoirs. The general aim of the research is to investigate the possibility to detect variations in river basin water storage from measurements of the time dependent gravity field, and to assess the accuracy of these estimations based on in-situ and satellite observations of the gravity field. This could be beneficial for water balance models and catchment water management in general

This poster describes a first approach to detect hydrological signals, caused by seasonal processes or sudden events, in time series of in-situ gravity measurements. Based on data from the Global Geodynamics Project (GGP), all available time series of gravity that are accompanied with hydrological measurements will be analysed. Other elements of the observed gravity field, such as tides, air pressure and instrumental drift are subtracted from the raw gravity signal to obtain the residual gravity. Precipitation and groundwater table data, are used to estimate the change of water storage in the direct vicinity of the in-situ gravity meter. A method is used to quantify correlation between the observed and expected residual gravity change at multiple measuring sites. A first order statistical analysis will be performed by splitting each time series in different time scales, based on spectral analysis, and comparing the observed gravity change in each time scale class with the expected gravity change. The expected gravity change is estimated from the change in water storage. The relative difference between observed and expected gravity for all time scales, can be compared for all stations of the gravity measurement network. A pattern of high and low correlation in the bias for certain time scales could reveal the relative influence of uncertainties in other geophysical factors like air pressure, snow, instrumental errors and subsurface geology. Some provisional results of this first order analysis will be shown at the poster.

Effect of groundwater changes on SG observations in Kyoto and Bandung

Shuzo Takemoto*, Yoichi Fukuda*, Toshihiro Higashi*, Maiko Abe*, Shihori Ogasawara*, Sjafra Dwipa**, Dendi Surya Kusuma**, and Achmad Andan**

* Department of Geophysics, Graduate School of Science, Kyoto University, Rigaku 4-Goukan, Sakyo-ku, Kyoto 606-8502, Japan

** Geothermal Division, Directorate of Mineral Resources Inventory, Indonesia, Lj. Soekarno-Hatta No. 444, Bandung 40254, West Java, Indonesia

Abstract

In order to estimate hydrological effect on gravity observations using Superconducting Gravimeters in Kyoto (TT-70#009) and Bandung (TT-70#008), we installed groundwater level-meters near the SG stations in Kyoto and Bandung, respectively, in 2000. At the Kyoto station, SG observation was often interrupted because of earthquake vibrations, and artificial noise caused by construction of new buildings in the University. Therefore, we cannot discuss in detail on relation between rainfall, groundwater level change and gravity residual in Kyoto at present stage. As the only significant evidence, the gravity residual at the Kyoto station changed about 9 μGal after heavy rainfalls of 210mm in total during the period of September 11-13, 2000. At that time, the groundwater level showed 2m upheavals at a well about 1.5km away from the SG station. At the Bandung station, time keeping of the SG observation system has not been so good, because the GPS receiver was often broken by the thunderbolt. After correcting time lags, we estimated hydrological effect on SG observation. As a result, gravity residual is closely correlated with groundwater change: 1m upheaval of groundwater level causes 4.2-4.4μGal increase in gravity residual with the time lag of about 13-20 days.

1. Introduction

Two Superconducting Gravimeters (Model TT-70: #008 and #009) were introduced into Kyoto University in 1988. Since then, continuous observation of gravity changes employing two Superconducting Gravimeters had been carried out in Kyoto until December 1997 (Takemoto et al., 1998a). During the period, we investigated instrumental noise (Higashi, 1996), atmospheric effect (Mukai et al., 1995a, 1995c) and the effect of ambient temperature change on gravity measurements (Mukai et al., 1995b). In December 1997, one (#008) of the two Superconducting Gravimeters in Kyoto was shifted to Bandung under the cooperation between the Graduate School of Science (GSS), Kyoto University and the Volcanological Survey of Indonesia (VSI), Directorate General of Geology and Mineral, Ministry of Mines and Energy of the Republic of Indonesia (Takemoto et al., 1998b). We installed the SG #008 in the underground observation room where Baron Melchior and his colleagues carried out gravity observation in 1987 by employing the LaCoste & Romberg gravimeter (L 336) (Melchior et al., 1995).

In this paper, we present a preliminary result about the effect of groundwater changes on SG observations in Kyoto and Bandung.

2. Hydrological effect on gravity observation in Kyoto

In Kyoto, we started observation of water level changes on June 15, 2000 at a well in a private house about 1.5km away from the SG station in Kyoto University by employing a water pressure sensor (KADEC-MIZU type) manufactured by KONA Co. Ltd. (Abe, 2002). **Fig. 1** shows observational results of gravity change obtained from SG#009 as well as atmospheric pressure change, water level change and precipitation during the period from June 15, 2000 to August 31, 2001. Unfortunately, SG observation in Kyoto has often been interrupted because of earthquake vibrations and artificial noise caused by construction of new buildings in the University. Therefore, we cannot discuss in detail on relation between rainfall, groundwater level change and gravity residual in Kyoto at present stage.

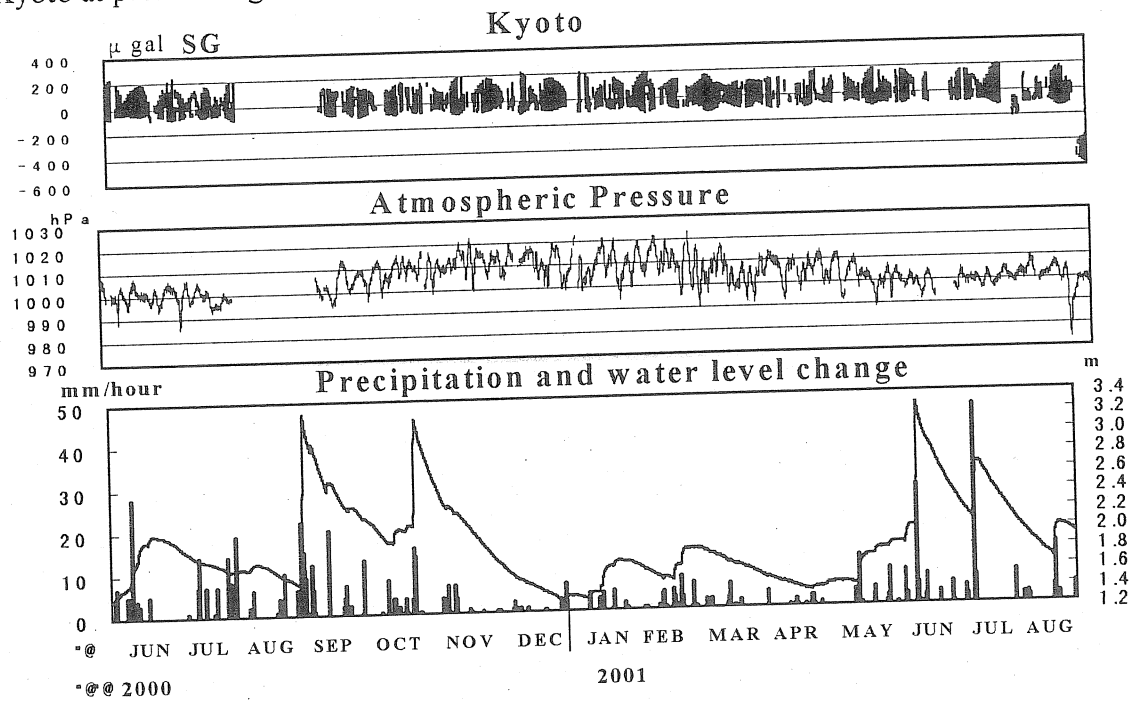

Fig. 1 Observational Result of gravity changes obtained from SG#009, atmospheric pressure changes, precipitation and water level changes in Kyoto during the period from June 15, 2000 to August 31, 2001.

Only significant evidence is shown in **Fig. 2**, in which the gravity residual at the Kyoto station changed about 9μGal after heavy rainfalls of 210mm in total during the period of September 11-13, 2000. This can be acceptable based on a simple calculation using a Bouguer model of water level changes in a semi-finite medium: 1m water level changes correspond to 4.2 μGal gravity changes in case of 10% porosity (Abe, 2002).

As appointed out by Makinen and Tattari (1988), Soil moisture changes will significantly affect on gravity changes in addition to water level changes near the gravity observation site. Accordingly, it is important to measure soil moisture changes in order to precisely interpret gravity residuals observed with SGs. We are now preparing to install soil moisture meters to monitor moisture content around the SG observation site.

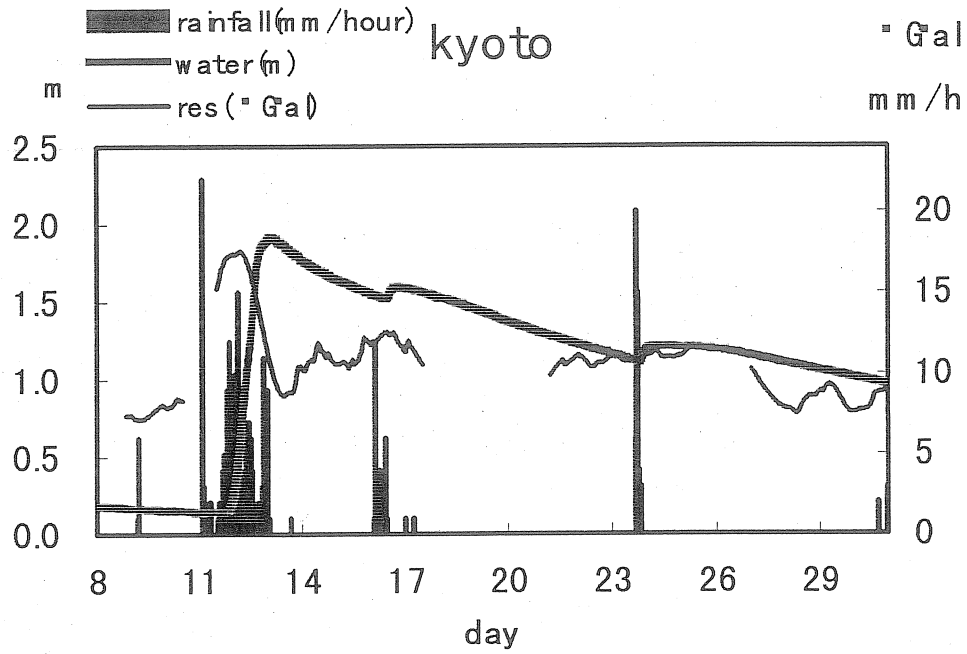

Fig. 2 Comparison of gravity changes and water level changes after the heavy rainfalls of 210mm in total during the period of September 11-13, 2000.

3. Hydrological effect on gravity observation in Bandung

The Bandung SG station (**Ba**) is the third station in the southern hemisphere and only one station existing near the equator in the GGP network. On this point of view, **Ba** is a very important station in GGP.

The observation room in Bandung is located at 06°53' 47" S, 107°37' 54" E, 713m above the sea level. The distance from the nearest sea is about 50 km. The SG #008 was installed on the concrete base of 1.2m x 1.2m, which was constructed 1 m below the floor in the underground room on the layer of very thick volcanic deposit of sand and other volcanic products (Takemoto et al., 1998b). Observation of gravity variation in Bandung using the SG #008 was smoothly started in December 1997, but interrupted by the unexpected falling of a thunderbolt in April 1998. We repaired the system and observation was restarted in December 1998. Thereafter, continuous record of gravity change has been obtained.

Observation of water level changes in Bandung was started in January 2000 at a well in the campus of VSI about 200m away from the SG station by employing a water pressure sensor of same type as that used in Kyoto.

Fig. 3 shows the observational result of gravity changes observed with the SG#008 and atmospheric pressure changes during the period from February 1999 to October 2001 as well as water level changes in Bandung during the period from January 2000 to October 2001.

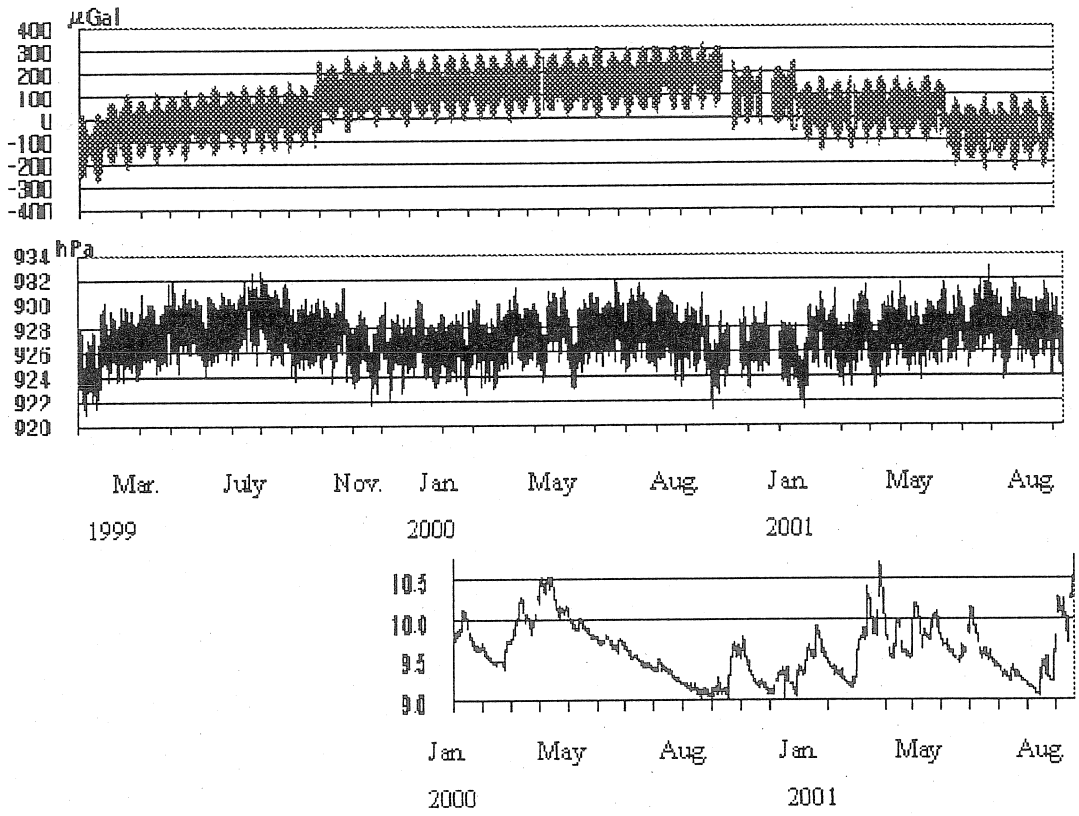

Fig. 3 Gravity changes observed with the SG#008 (upper), atmospheric pressure changes (middle) and water level changes (lower) in Bandung.

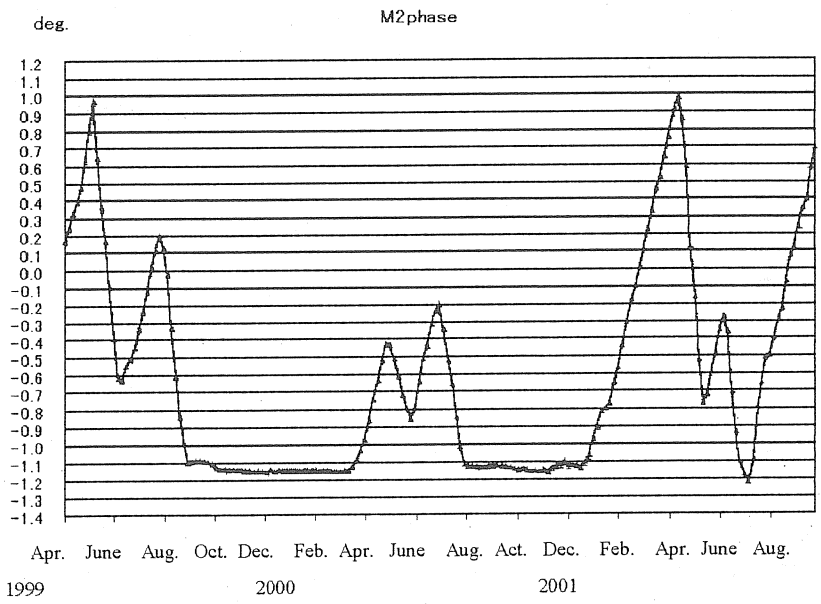

Fig. 4 Apparent phase change of M2 constituent observed with the SG#008 in Bandung.

One of the serious problems in Bandung, however, is the time keeping of SG record. We installed a GPS receiver to control the clock of the data acquisition system in Bandung. But the GPS receiver has often broken by thunderbolts and GPS data have been interrupted. **Fig.** 4 shows apparent phase change of M2 constituent without time correction. Based on this data, we corrected the "time" of the data acquisition system in Bandung.

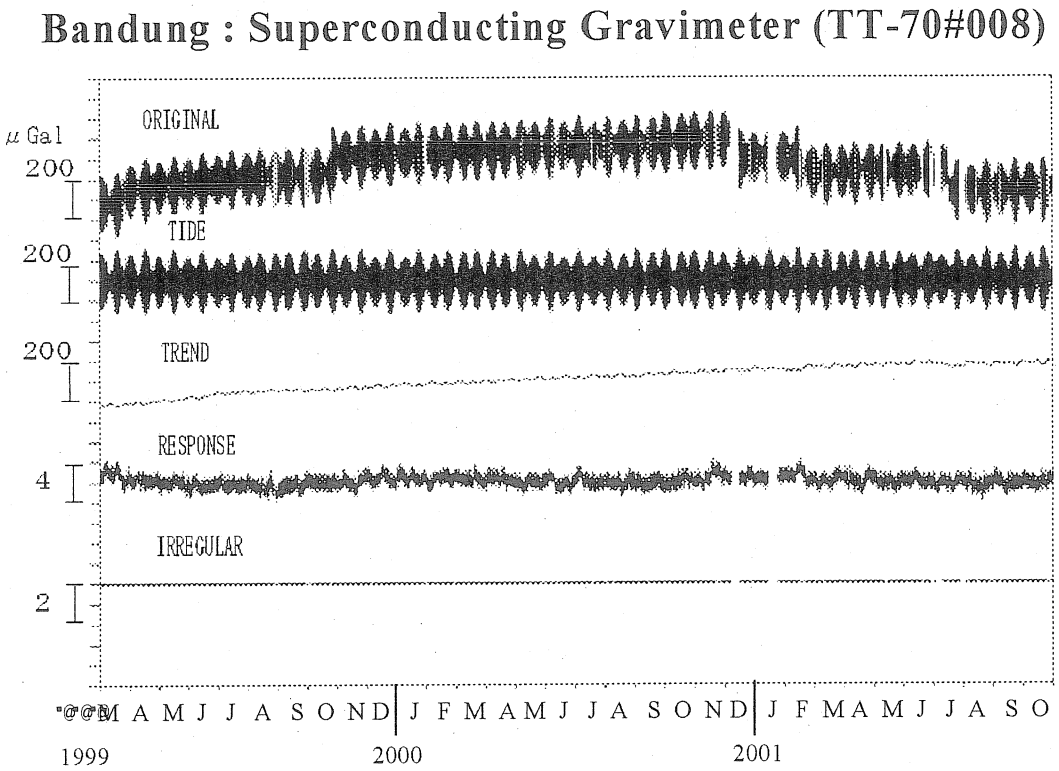

Fig.5 Observational result of SG#008 in Bandung during the period from March 1999 to October 2001.

Fig. 5 shows the observational result of SG#008 during the period from March 1999 to October 2001. Tidal analyses were made by applying the Baysian Tidal Analysis Program 'BAYTAP-G' (Tamura et al., 1996) to the observational data obtained in Bandung. In the tidal components ('TIDE'), it is obvious that semi-diurnal constituents are dominant in Bandung compared with those in Kyoto. In the trend component ('TREND'), we can also recognize that long period tidal constituents are dominant in Bandung.

After eliminating long period tides and the polar motion effect form the trend component shown in **Fig.** 5, we approximated long term gravity variation with the 3-degree polynomial, and then we estimated hydrological effect on gravity residual.

Fig. 6 shows the trend component, in which contributions from long period tides and polar motion are eliminated, as well as the 3-degree polynomial approximation curve during the period from March 1999 to October 2001.

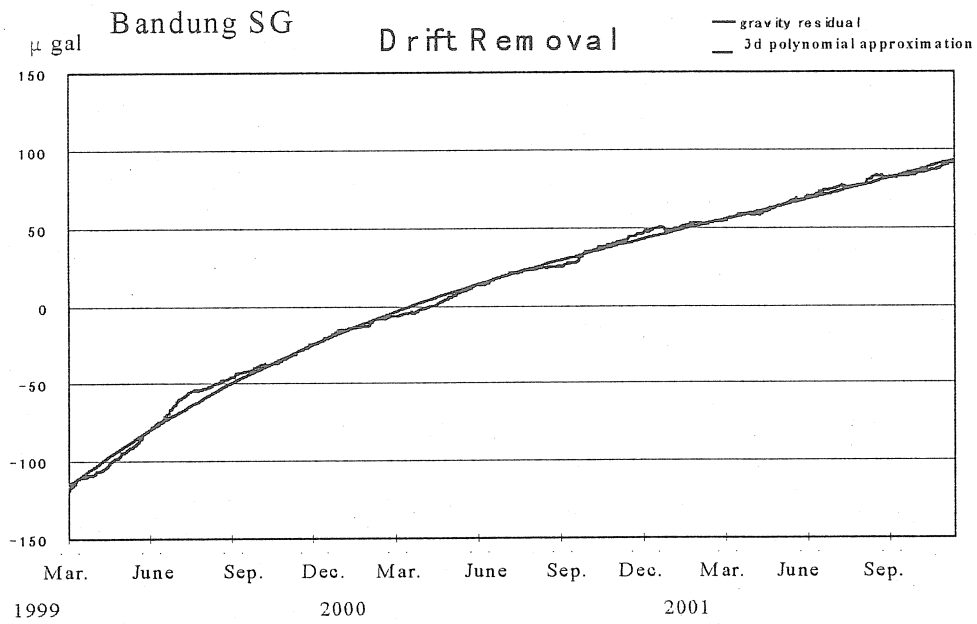

Fig. 6 Trend of gravity variations observed with the SG #008 during the period from March 1999 to October 2001 as well as the 3-degree polynomial approximation curve.

Fig. 7 shows the gravity residual obtained by subtracting the 3-D polynomial approximation from the trend curve, in which contributions from long period tides and polar motion are previously eliminated. Groundwater level change is also shown in **Fig.** 7. Comparing these two curves of gravity residual and groundwater level change, we found out three events in which it should be necessary to add minor correction (about 2μGal) in gravity residual. The first event is the earthquake of Mw = 7.9 in South Sumatra on June 04, 2000, which was the largest earthquake occurred in the area within 1000km from the SG station during the observation period. The second is the artificial noise on September 11-12, 2000 according to maintenance of GPS recorder system by Indonesian colleagues. The third is stop of the recording system continued for a week after the electronic power failure on January 8, 2001.

After correcting gravity residual at these three events mentioned above, we obtained a corrected gravity residual curve as shown in **Fig. 8**. In this figure, we can see that large part of gravity residual is correlating to groundwater level change with phase delay of about 10-20 days.

Although all of the gravity residual would not be related to groundwater level change, we investigated the relation between gravity residual and groundwater level change. **Fig. 9** shows these relations in cases with phase lags of 0-30days of the gravity residual relative to the groundwater level change. In this figure, we can see that the gravity residual is correlated with groundwater changes and the linearity is improved in cases of time lags of 13-20 days in gravity residuals. 1m upheaval of groundwater level causes 4.2-4.4μGal increase in gravity residual with the time lag of about 13-20 days. Since the precipitation data in Bandung are not yet available, we cannot discuss the relation between gravity change and rainfall quantitatively at this time.

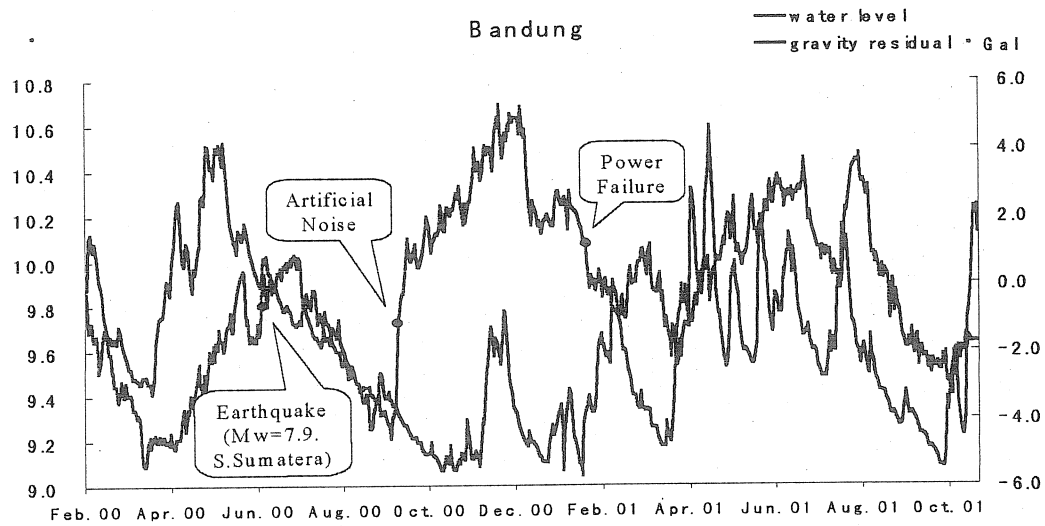

Fig. 7 Comparison of gravity residuals (thick line) and groundwater level change (thin line).

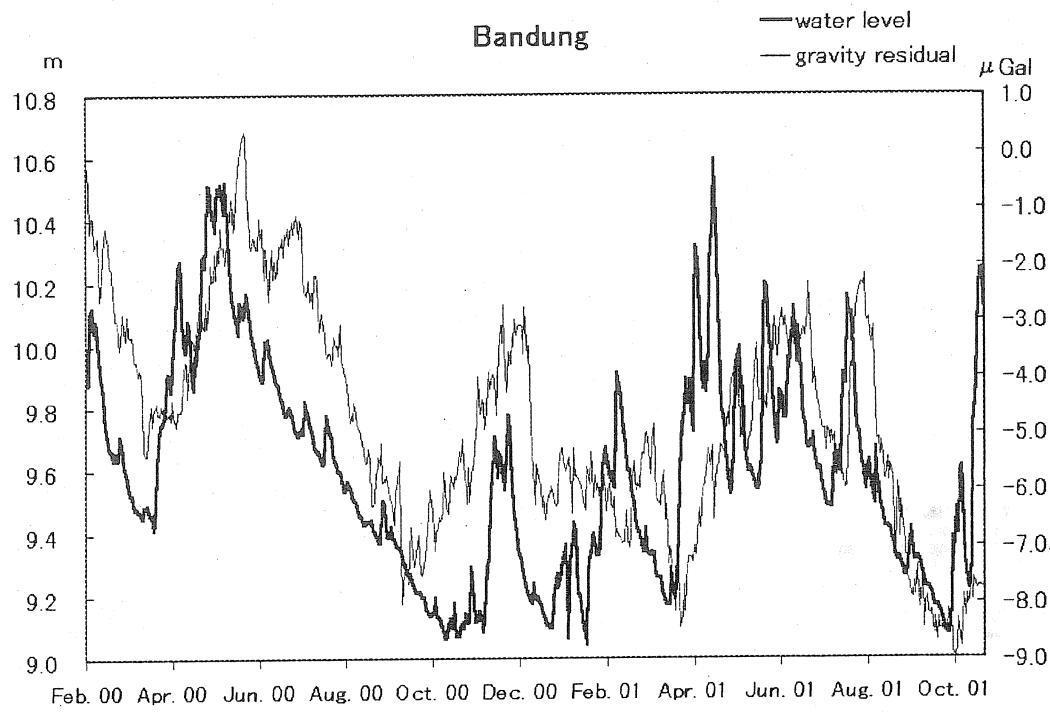

Fig.8 Comparison of gravity residuals (corrected) and groundwater level changes.

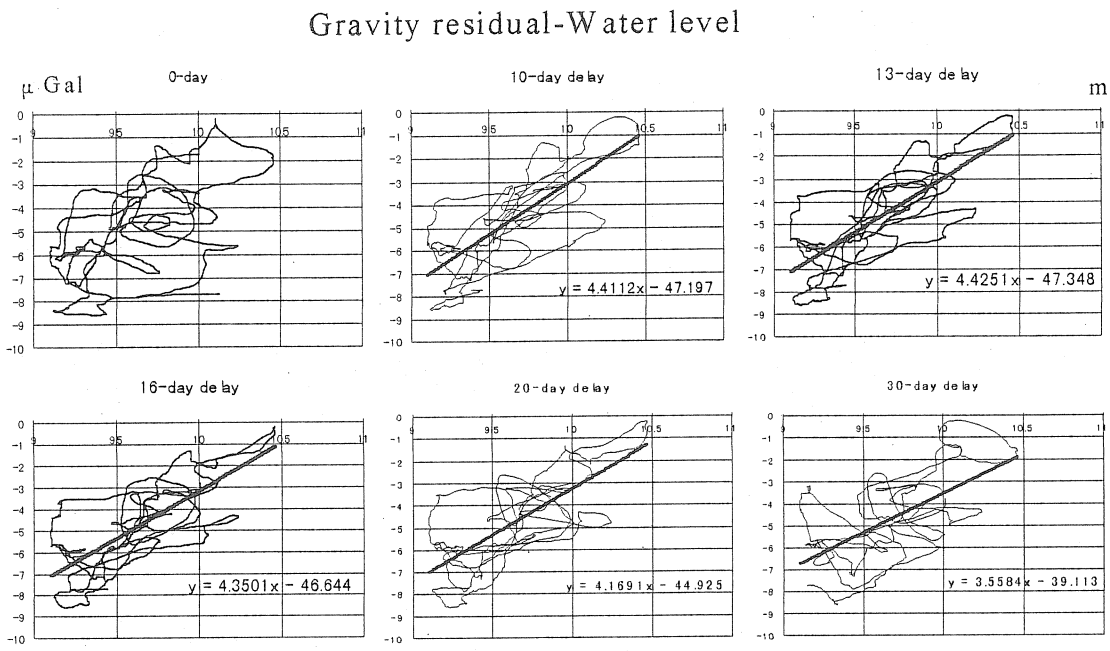

Fig. 9 Relation between the gravity residuals and the groundwater level changes.

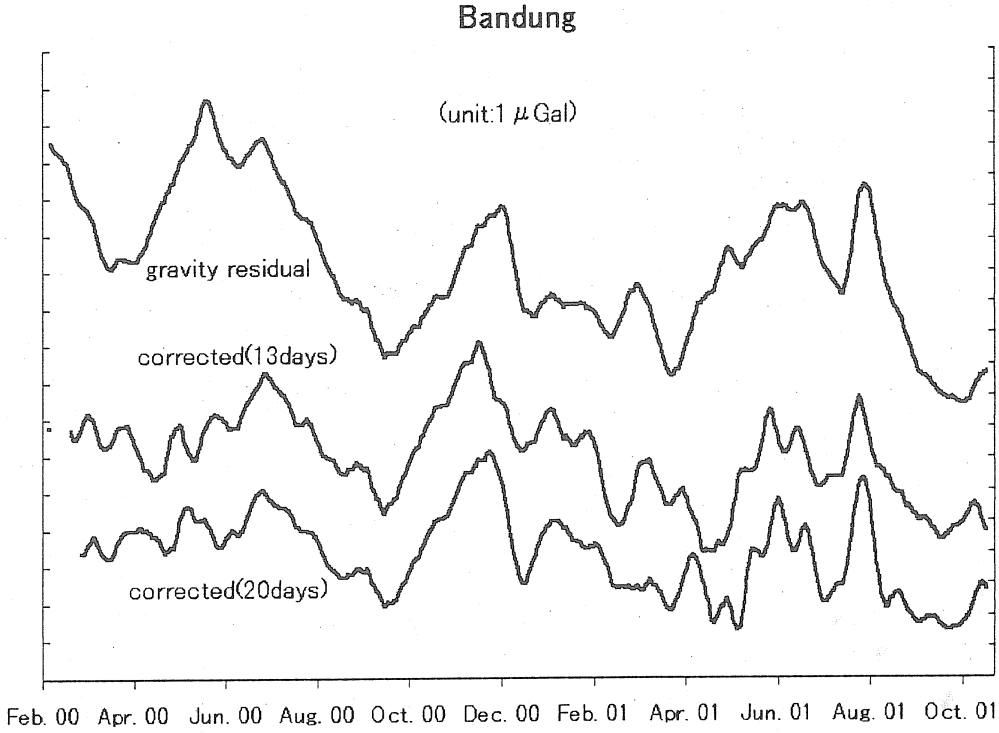

Fig. 10 Corrected curves of gravity residual.

We then attempted to eliminate the effect of groundwater level changes from the

gravity residual. **Fig. 10** shows the corrected curves for cases of time lags of 13 and 20days, respectively, together with 10-day running means of the gravity residual that is shown in **Fig. 8**. Each of corrected curves is obtained by applying each coefficient obtained from **Fig. 9**. Even if using these curves, gravity residual seems to be not so much improved. However, it is noticeable that the whole amplitude could be reduced to 5μGal from 8μGal in total.

4. Concluding Remarks

We installed groundwater level-meters near the SG stations in Kyoto and Bandung, respectively, in 2000 and started monitoring of hydrological effect on gravity observation. As a result, it was revealed in both Kyoto and Bandung that 1m upheaval of groundwater level causes about 4μGal increase in gravity residual. This can be acceptable based on a simple calculation using a Bouguer model of water level changes in a semi-finite medium: 1m water level changes correspond to 4.2μGal gravity changes in the case of 10% porosity. In Bandung, the gravity residual decreased to 5μGal from 8μGal by taking the effect of groundwater level change into consideration.

In order to discuss the hydrological effect on precise gravity observation in detail, we are preparing to install soil moisture meters in Kyoto and Bandung. Although precipitation data in Bandung are not available, we are now planning to install a rain gauge in Bandung. This will contribute to detailed interpretation of gravity residual and to search for meaningful gravity signals revealing dynamics of Earth's interior.

Acknowledgements

In order to carry out SG observation in Bandung, we have been indebted very much at the Volcanological Survey of Indonesia, Bandung and UNESCO Regional Office for Science and Technology for Southeast Asia, Jakarta. We would like to offer profound gratitude to Drs. Wimpy S. Tjetjep, R. Sukhyar, A. Djumarma Wirakusumah, M. Hashizume, Y. Aoshima and HAN Qunli.

This work was partially supported by the Grant-in-Aid for Creative Basic Research (No.08NP1101, Principal Investigator: Y. Fukao, University of Tokyo), Grant-in-Aid for Scientific Research(B) (No.09440158, P.I.: S. Takemoto), Grant-in-Aid for International Scientific Research (Field Research) (No.10041116, P.I.: S. Takemoto), Grant-in -Aid for Scientific Research(B) (No.11440132, P.I.: Y. Fukuda), and the 23rd Nissan Science Foundation (P.I.: S. Takemoto).

References

Abe, M. (2002): Hydrological Effect on Gravity Observations Using Superconducting Gravimeters – In case of Kyoto and Bandung, M.C. Thesis, Graduate school of Science, Kyoto Univ. pp. 46 (in Japanese).

Higashi, T. (1996): A Study on Characteristics of Tidal Gravity Observation by Employing Superconducting Gravity Meters at Kyoto, Japan, Memoirs of Fac. Sci., Kyoto Univ., Series A, **39**, No.3, 313-348.

Makinen J.and S. Tattari (1989): The infruence of varitation in subsurface water strage

on observed gravity, Proc. 11th Int. Symposium on Earth Tides, Hersinki, 1989, 457-471.

Melchior, P., O. Francis and B. Ducarme (1995): Tidal Gravity Measurements in Southeast Asia, Report for the IUGG General Assembly IAG Symposium "Geodesy in Southeast Asia" pp.28.

Mukai, A., T. Higashi, S. Takemoto, I. Nakagawa and I. Naito (1995a): Accurate Estimation of Atmospheric Effects on Gravity Observations Made with a Superconducting Gravity Meter at Kyoto, Phys. Earth Planet. Inter. **91**, 149-159

Mukai, A., T. Higashi, S. Takemoto, I. Naito and I. Nakagawa (1995b): Atmospheric Effects on Gravity Observations within the Diurnal Band, J. Geod. Soc. Japan, **41**, 365-378.

Mukai, A., S. Takemoto, Y. Fukuyama, I. Nakagawa (1995c): Effect of Room Temperature Changes on Gravity Observation with Superconducting Gravity Meters, J. Geod. Soc. Japan, **41**, 197-206 (in Japanese with English Abstract).

Takemoto, S., T. Higashi, A. Mukai, Y. Fukuda and T. Tanaka (1998a): Precise Observation of Gravity Changes with Superconducting Gravimeters in Kyoto (1988-1997), Annuals Disas. Prev. Res. Inst., Kyoto Univ., 41B-1, 77-85 (in Japanese with English Abstract).

Takemoto, S., S. Dwipa, Y. Fukuda, T. Higashi, A. Andan, D. S. Kusuma, R.Sukhyar, Wimpy S.Tjetjep, T. Tanaka and Leni S. Heliani (1998b): Precise Gravity Observation in Bandung Using a Superconducting Gravimeter, Proc. of Symposium on Japan-Indonesia IDNDR Project, September 21-23, 1998, Bandung, Indonesia, 223-230.

Tamura, Y., T. Sato, M. Ooe and M. Ishiguro (1997): A Procedure for Tidal Analysis with a Baysian Information Criterion, Geophys. J. Int., **64**, 507-516.